Title
Statistical Study of Lightning-Generated Whistler-Mode Waves Observed by Venus Express

Author
Hart, Richard A.

Publication Date
2022

Peer reviewed|Thesis/dissertation

UNIVERSITY OF CALIFORNIA
Los Angeles

Statistical Study of Lightning-Generated Whistler-Mode Waves Observed by Venus Express

A dissertation submitted in partial satisfaction
of the requirements for the degree
Doctor of Philosophy in Geophysics and Space Physics

by

Richard Allen Hart

2022

ABSTRACT OF THE DISSERTATION

Statistical Study of Lightning-Generated Whistler-Mode Waves Observed by Venus Express

by

Richard Allen Hart
Doctor of Philosophy in Geophysics and Space Physics
University of California, Los Angeles, 2022
Professor Christopher T. Russell, Chair

The existence of lightning on Venus has been a topic of debate for over four decades and arguably for centuries. The auroral-like phenomenon known as the Ashen Light was first reported in 1634 and lightning was one of the potential causes. Astronomers continued to report on sightings of the mysterious nightglow for hundreds of years with no conclusive explanation as to the source. In the late 20^{th} century, the USSR and the US began sending probes to our sister planet with the search for lightning as one of the objectives. Since then there have been numerous observations of lightning reported. The Venera landers detected electrical signals determined to be from lightning during their descents. The Venera 9 orbiter detected flashes of light with its visible spectrometer. Pioneer Venus Orbiter (PVO) observed very low frequency (VLF) radio waves on numerous occasions with the source determined to be lightning. An Earth-based campaign observed seven flashes of light on the nightside of Venus. During a gravity assist flyby of Venus, the Galileo spacecraft detected radio signals inferred to be from lightning. The Venus Express mission regularly detected whistler-mode waves as expected to be from lightning. These are the same type of waves detected by PVO. Most recently, the Akatsuki spacecraft has detected a flash in the clouds while in orbit

around Venus.

We use the Venus Express (VEX) 128 Hz fluxgate magnetometer data to search for lightning-generated whistler-mode waves in the ionosphere of Venus. Whistler-mode waves are right-hand circularly polarized, transverse plasma waves that are guided by the ambient magnetic field. Using these known properties of whistlers, we developed code to scan all mission data under 1000 km altitude and catalog any observed whistler-mode waves. Since the ionopause of Venus is at a relatively low altitude on the dayside, we restrict our statistical analysis to below 400 km altitude, a reasonable limit for the north polar observations of VEX. Although the detection rates were comparable for solar minimum and solar maximum (5.4% and 5.0%, respectively), the distribution of the waves was significantly different. During solar minimum, the waves were observed most often between 0600 LT and 1200 LT, while in solar maximum the waves were mostly observed near midnight. However, for both periods the peak observation rates occurred near periapsis $\sim$8% of the time, on average, throughout the mission. The median Poynting flux of the signals was 1.4×10^{-9} W m^{-2} and the peak values occurred at low altitudes, implying a lightning source from below the ionosphere. These results agree with previous studies from the PVO era. Because of the global greenhouse effect, the Venus atmospheric conditions do not vary greatly around the planet. Therefore, under the assumption that lightning near the north pole is not significantly different than any other location, we estimate the global rate of flashes to be 320 s^{-1}.

The dissertation of Richard Allen Hart is approved.

Marco Velli

Jacob Bortnik

Robert J. Strangeway

Christopher T. Russell, Committee Chair

University of California, Los Angeles

2022

For my mother, sister, and Michelle.

I would not be here without your unwavering support.

Table of Contents

List of Figures

ACKNOWLEDGMENTS

First and foremost I would like to thank my mother, Alicia. She has never stopped encouraging me. Her constant affirmation that there is nothing that I cannot do made it possible to get through some of the toughest times. Every accomplishment of mine is hers as well.

I would like to thank my sister Carla for being someone that I can lean on when I don't know where else to turn. We lived 400 miles apart for most of our adult lives, but that didn't create any distance in our relationship.

For my partner, Michelle, I have no words that I feel are sufficient to express the gratitude that I have. She has held my hand through some of the most trying times in my life. She has never shown anything but complete support and encouragement. I am genuinely not sure if I would have made it to the finish line of this PhD without her. I owe her everything.

I would like to thank all of the fellow graduate students that I have gotten to know along the way, many of whom have become some of my closest friends. Of all the resources that EPSS and UCLA have to offer, none is greater than fellow graduate students. Many of the most fruitful scientific conversations I had were simply casual talks with friends and colleagues. Aside from science conversations, I received invalueable emotional support and basic advice about graduate school at UCLA from them. I will not list names for fear of forgetting some, but they know who they are. Thank you so very much.

I thank Professor Jacob Bortnik and Professor Marco Velli for the interesting conversations that we have had over the years and for serving on my committee. I feel very fortunate to have your names on my dissertation.

I want thank Dr. Robert J. Strangeway for serving on my committee and for the nearly 15 years of guidance he has provided. Though he may not realize it, I have considered him a mentor since well before I started graduate school. I can always count on his support and his candor.

I thank the Venus Express project team for the development, cruise, orbit insertion and

operations of the spacecraft at Venus, as well as the magnetometer development group and data processing personnel at the Austrian Academy of Science, Space Research Institute in Graz, for the instrument and data delivery. The work at the University of California, Los Angeles, was supported by NASA under research grant 80NSSC19K0243.

Finally, I would like to thank my advisor, Professor Christopher T. Russell. I knew nothing of lightning on Venus before beginning this graduate program and it has proven to be an exciting endeavor.

VITA

2004–2005	Tutor, Math Lab, Antelope Valley College, Lancaster, CA.
2005	A.S. Mathematics, Antelope Valley College, Lancaster, CA.
2006–2007	Undergraduate Research Assistant, Physics and Astronomy, UCLA.
2008	B.S. Astrophysics with a minor in Mathematics, UCLA.
2008–2018	IT System Administrator, Institute for Geophysics and Planetary Physics, UCLA.
2019	M.S. Geophysics & Space Physics, UCLA.
2012–present	Graduate Student Researcher, Earth, Planetary, and Space Sciences, UCLA.

PUBLICATIONS AND PRESENTATIONS

Hart, R. A., C. T. Russell, T. L. Zhang (2022). Statistical study of lightning-generated whistler-mode waves observed by Venus Express. Icarus, *accepted*.

Russell, C. T., H. Leinweber, **R. A. Hart**, H. Y. Wei, R. J. Strangeway, T. L. Zhang (2013). Venus Express observations of ULF and ELF waves in the Venus ionosphere: Wave properties and sources. Icarus, 226(2), 1527–1537, doi: 10.1016/j.icarus.2013.08.019.

Russell, C. T., **R. A. Hart**, T. L. Zhang (2022). Venus Express Cleaned High-Resolution 128 Hz Magnetic Field Data Bundle. PDS Planetary Plasma Interactions Node, doi: 10.17189/1522415.

American Geophysical Union Fall Meeting: 2012, 2013, 2014, 2015, 2019, 2020, 2021

Asia Oceania Geosciences Society: 2015

Committee on Space Research: 2014, 2018

Division for Planetary Sciences: 2015, 2016

European Geosciences Union: 2013, 2014, 2015, 2018

European Planetary Science Congress : 2013, 2014, 2015, 2019, 2020

International Venus Conference: 2016, 2018

Joint JPL-UCLA Planetary Science Workshop: 2015

Lunar and Planetary Science Conference: 2013, 2015

Venus Exploration Analysis Group: 2021

Venus Express Science Team Meeting: 2015

Venus Science Conference: 2021

CHAPTER 1

Introduction

1.1 Motivation

On Earth, lightning is a fairly well-understood concept, given the abundance of data and observations, but there are still questions that remain unanswered. While there are good hypotheses that are widely accepted, we don't definitively understand certain mechanisms, like cloud charging or the breakdown process that triggers lightning. Sometimes it is necessary to step outside of one's box, or planet, to gain new insights into matters that remain a mystery. Each planet is its own natural laboratory that we occasionally step foot into via robotic missions. The conditions in the Venus atmosphere are unlike anything else known in our solar system. If we are able to characterize lightning in such a foreign environment, then we may be able to learn something new about terrestrial lightning that we did not fully grasp. A feedback loop develops as both the planetary and terrestrial communities learn from each other. Beyond lightning itself, the lightning-generated whistler-mode waves, as observed at Venus, are a well-studied phenomenon in the terrestrial space environment. Any new knowledge gained about their propagation in the Venus ionosphere would necessarily stimulate a feedback loop.

The topic of lightning on Venus has been of great interest to planetary scientists and

astronomers for centuries. Since the first report of a mysterious night glow on Venus in the 17^{th} century, scientists have been trying to determine whether lightning occurs on Venus and, if so, how similar is it to the terrestrial process with which we are familar? There have been numerous claims of detections as the dawn of the Space Age spawned a host of planetary missions, which will be discussed in section 1.4. Most of the detections were observations of radio waves produced by lightning with only a few visible observations. Lightning on Earth is easily observed with the naked eye while in orbit, so a similar expectation has been placed on Venus by some skeptics despite the significant differences in atmospheric composition and dynamics between the two planets. If there is lightning in the Venus clouds, then there must be some explanation as to why it is difficult for the light to escape. It is likely some combination of dimmer strokes than on Earth and the optical thickness of the clouds. We simply cannot know the true reason without characterizing the lightning by some other means or with observations within the clouds. Radio observations have proven fruitful over the last few decades, but they were limited by instrumentation or observation time. The data collected by the Venus Express mission (VEX) is plentiful enough to develop robust statistics of radio observations to settle the debate once and for all. The research presented here provides statistics of VEX observations to determine that not only does lightning occur on Venus, but it is a frequent occurrence.

1.2 Venus

1.2.1 Overview

As this study is entirely focused on observations made of and at Venus, we begin by providing some background on the planet. Venus is often referred to as "Earth's twin" because their volumes and densities are relatively similar. Venus is slightly smaller with a mean radius of 6051.8 km, ∼95% of Earth's 6371 km radius. The bulk density is also ∼95% the density of Earth. Earth orbits the Sun at a mean distance of 1 AU, while Venus orbits at 0.72 AU,

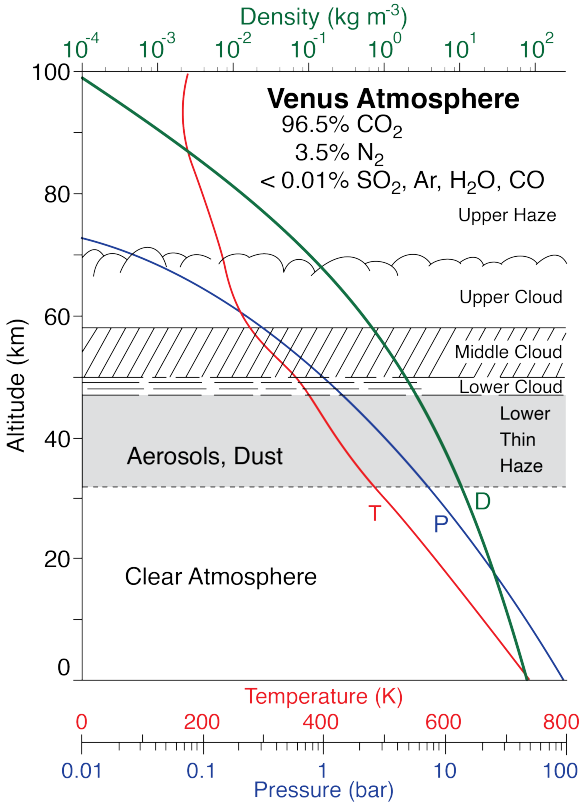

Figure 1.1: Profile of the Venus atmosphere. The temperatures and pressures in the cloud layers are similar to those on Earth. Adapted from *Rinnert* (1995) and *Lebonnois and Schubert* (2017).

just outside the inner boundary of the optimistic "habitable zone" (*Kopparapu et al.*, 2013). The axial tilt of the planet is 177.4°, or 2.6° while rotating in a retrograde sense (*Taylor*, 2006). It is the only planet in the solar system to rotate in such a way. It also happens to be such a slow rotator that 1 day (synodic) is equivalent to ∼117 Earth days. One sidereal orbit around the Sun is equivalent to ∼225 Earth days.

The atmosphere of Venus exhibits a global greenhouse effect, which leads to some extreme conditions. The surface of Venus is extremely hot and dry compared to Earth's surface, which inspires some people to modify its epithet to "Earth's evil twin". At the surface, the atmospheric pressure is 92 bar, equivalent to being nearly 1 km under water on Earth.

The surface temperature is 737 K, hot enough to melt some metals, such as lead and zinc (*Taylor*, 2006). The atmosphere on Venus is composed of 96.5% CO_2 and 3.5% N_2 with minor constituents of SO_2, Ar, H_2O, CO, He, and Ne (*von Zahn et al.*, 1983; *Taylor et al.*, 1997; *de Bergh et al.*, 2006; *Taylor*, 2006). Despite the hellish conditions on the surface of Venus, there exists a region in the cloud layers ($\sim$45 – 65 km) with temperatures and pressures comparable to the terrestrial atmosphere, about 300 K and 1 bar (Figure 1.1). Still inhospitable, the clouds are primarily composed of sulfuric acid (*Esposito et al.*, 1983). There are three main cloud layers bounded by hazes above and below. The upper haze extends up to the base of the ionosphere at approximately 120 km. The global greenhouse keeps the atmosphere of Venus from varying too greatly around much of the planet. The temperatures, pressures, and atmospheric constituents are relatively consistent barring certain geologic features, such as volcanoes. However, above the atmosphere in the plasma environment, the dynamics are dictated by the Sun.

1.2.2 Plasma environment

Venus has no intrinsic dipole field and there have been no measurements confirming a remanent field. *Luhmann et al.* (2015) reanalyzed low altitude magnetic field measurements from PVO and claimed that there is a subtle radial component at low latitudes in the western hemisphere. They suggest that this might be due to a crustal field that is too weak to measure properly from orbit. *O'Rourke et al.* (2019) support this hypothesis, suggesting that at low latitudes, a crust magnetized $> 1 - 5$ km below the surface could produce a field of $10 - 20$ nT at 50 km altitude. At orbital altitudes the detectability would diminish to $<$ 1 nT, explaining the current paradigm that Venus does not have a remanent crustal field. Further investigations with low altitude measurements are necessary to resolve this problem, but until then we are committed to working with the data that we have available.

In the absence of a global dynamo, the interaction with the interplanetary magnetic field (IMF) produces the global field geometry at Venus. The solar extreme ultraviolet (EUV)

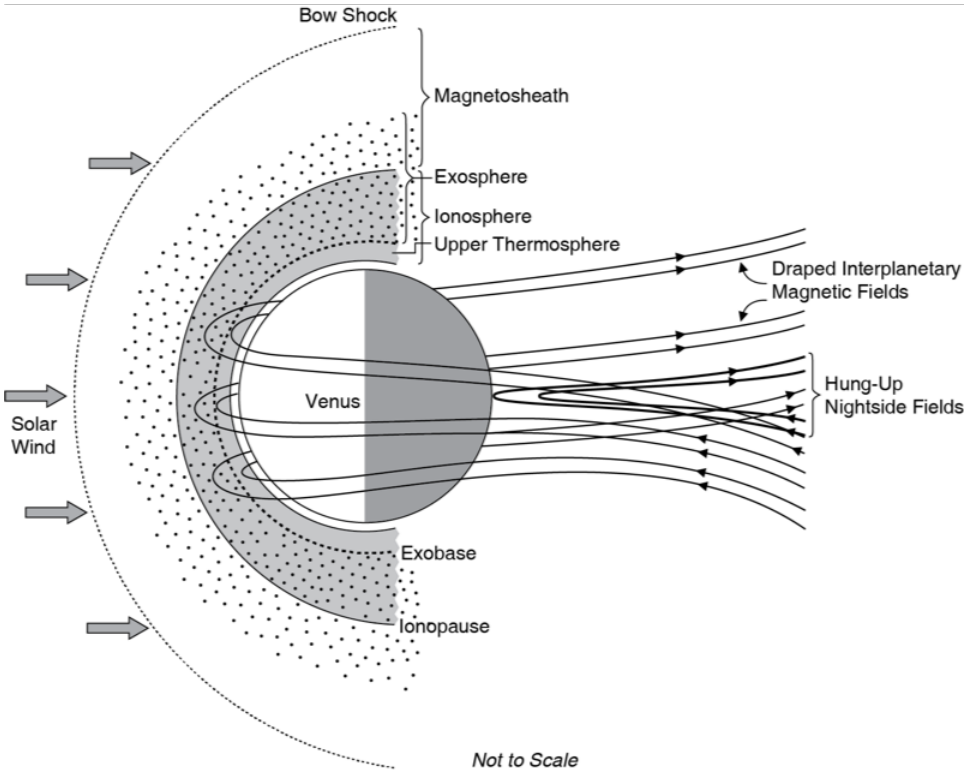

Figure 1.2: Schematic of the Venus plasma environment. The IMF encounters the obstacle of the Venus ionosphere and drapes around the planet.

radiation ionizes the upper layers of the Venusian atmosphere which creates the ionosphere. During high solar activity, when the ionosphere is especially conductive, the IMF will induce currents in the ionosphere which produce an opposing field. The IMF drapes around the conductive layer and diffuses into the ionosphere, magnetizing it parallel to the external field on the dayside and radially on the nightside (*Russell and Vaisberg*, 1983; *Luhmann and Cravens*, 1991) (Figure 1.2). When the ionosphere is weakly charged, as during solar minimum, it can become strongly magnetized as a result of the IMF diffusing into it. The ionopause boundary is formed where the solar wind dynamic pressure matches the ionospheric plasma pressure (*Luhmann*, 1986). This altitude of the ionopause is typically ∼350 km at the subsolar point depending on solar conditions. On rare occasions it can compress down to 200 km, and sometimes even below the exobase at which point the ionosphere be-

comes collisional. The ionopause flares outward with increasing solar zenith angles reaching up to 1000 km at solar zenith angles of ∼90°. Beyond the ionopause, the interaction with the solar wind is not much different than at Earth, although the magnetic obstacle is much smaller at Venus since it does not have the strong dipolar field that Earth does. The supersonic solar wind encounters an obstacle, Venus, and a bow shock is formed upstream to reduce the solar wind velocity. The nose of the bow shock is typically ∼2000 km above the ionosphere. On the nightside, the field can be radial at very low altitudes as evidenced by the ionospheric holes in the equatorial tail (*Luhmann and Russell*, 1983; *Luhmann*, 1986). During weak solar activity, magnetic flux tubes on the dayside ionosphere may descend into the planet and wrap around the conductive core, producing a radial field on the nightside that protrudes from the planet (*Brace et al.*, 1983; *Villarreal et al.*, 2015).

The overall result of the solar wind interaction with Venus is an ionosphere that extends several hundred kilometers on the dayside and over 1000 km beyond the terminators and the poles. The field draping that occurs around the planet results in a field that is parallel to the surface on the dayside and radial on the nightside, much like a comet.

1.3 Lightning and associated waves

1.3.1 Overview

Lightning is a common occurrence on Earth with 44 ± 5 flashes occurring somewhere on the planet every second (*Christian et al.*, 2003). Lightning on Earth is generally separated into three categories: cloud-to-ground (CG), cloud-to-cloud (CC), and intracloud (IC) lightning. CC and IC lightning are often grouped together as simply cloud lightning. By convention, CG lightning is negative if negative charge is transferred from the cloud to the ground, i.e. an upward positive current. 95% of all CG lightning is negative, occurring with typical currents of 30 kA and 10^9 J of energy (*Rakov and Uman*, 2003). Positive CG(+) lightning tends to be much more intense (∼120 kA) and more commonly associated with transient luminous events

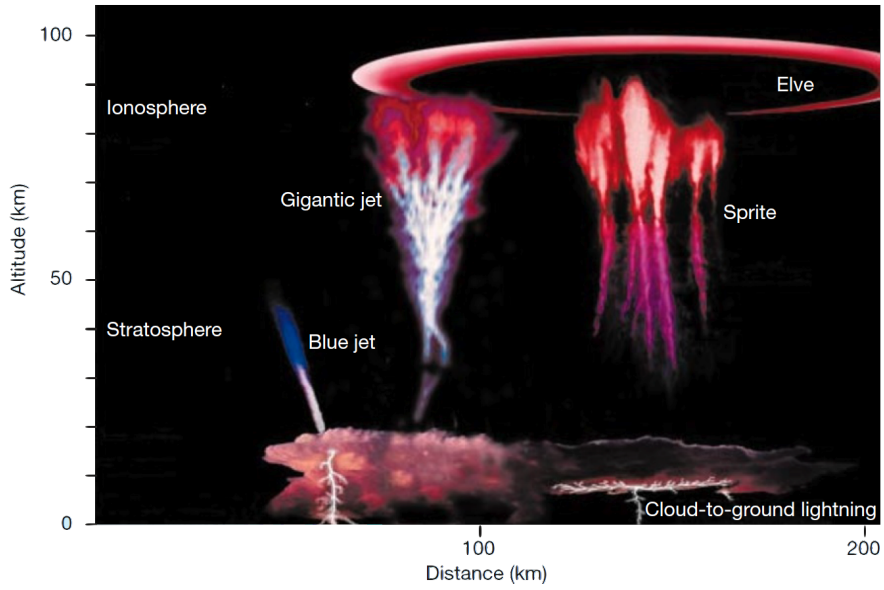

Figure 1.3: Artist's conception of transient luminous events from *Pasko* (2003, Fig. 1).

(TLE) (*Rakov and Uman*, 2003; *Dwyer and Uman*, 2014). TLEs are luminous phenomena that occur above the troposphere in response to intense lightning flashes. They consist of optical emissions known as Sprites, halos, Elves, blue jets, and gigantic jets as depicted in Figure 1.3. If such events occur on Venus, then there is a much greater likelihood of detecting optical signatures of lightning.

Lightning happens when a significant charge separation occurs in storm clouds producing an electric field that eventually reaches a threshold determined by the conditions of the local environment. This threshold is known as the breakdown electric field and once it is achieved a current flows from one charge domain to another, neutralizing the region. The lightning stroke creates a plasma channel with temperatures reaching up to 30,000 K. The extreme temperatures enable the production of certain compounds not readily produced otherwise in the atmosphere, such as NO and NO_2 (*Lawrence et al.*, 1995). According to *Rakov and Uman* (2003, and references therein), the charge separation process transpires as described below. The mechanism is predominantly a function of temperature and particle size. At high altitudes, where the temperature is below -15 °C, small ice crystals and graupel (soft

hail) interact and exchange charge. The larger graupel descends to lower altitudes, carrying with it a negative charge. The ice crystals are lofted and charge the upper portion of the cloud positively. At lower altitudes, where the temperature is above -15 °C, the charges are reversed, resulting in a cloud that is negatively charged in the middle with a thin layer of positive charge at the base. This process explains the typical tripolar cloud structure observed in electrical storms. A similar process is expected to occur in the clouds of Venus, but with sulfuric acid ice crystals as the main constituent instead of water ice (*McGouldrick et al.*, 2011).

1.3.2 Waves produced by lightning

The occurrence of lightning results in the production of three types of electromagnetic waves: sferics[1], Schumann resonances, and whistler-mode waves. Sferics propagate in all directions away from the source, undergoing multiple reflections in the surface-ionosphere wave guide. These reflections enable sferics to travel 1000's of kilometers before being detected. They are typically very low frequency (VLF) waves propagating in the frequency range of 3 kHz to 30 kHz on Earth (*Rakov and Uman*, 2003). Since Venus is approximately the same size as Earth and has a comparable atmospheric extent, sferics should propagate in about the same range. There is evidence from the Venera landers to suggest that this is correct (*Ksanfomaliti*, 1979; *Ksanfomaliti et al.*, 1982). Those observations will be discussed in subsection 1.4.2. Sferics cannot propagate much below the VLF range because there is a lower cutoff for the waveguide modes.

Schumann resonances are similar to sferics, but occur at lower frequencies, in the extremely low frequency (ELF) range (3 Hz to 3 kHz). Like sferics, they utilize the cavity between the two conductive boundaries of a planetary atmosphere. Resonant states develop as a result of lightning where the average equatorial circumference of the cavity is approxi-

[1]Short for atmospheric

mately equal to integral numbers of the signal wavelengths (*Simões et al.*, 2008). The size of the cavity is not simply the distance from the surface to the base of the ionosphere. Factors such as the composition and temperature of the boundary layers must be considered because, ultimately, the depth and height of the conductive layers that reflect waves at Schumann frequencies determine the size of the cavity. *Simões et al.* (2008) have calculated the resonant frequencies and size of the cavities for the seven planets from Venus to Neptune, as well as for Titan. The upper boundary for Earth is at 100 km altitude, the base of the ionosphere, and the lower boundary is near the surface of the planet because of the high water content. On Venus, a much drier environment, the lower boundary is estimated to be ∼40 km below the surface based on values of conductivity and temperature for similar ground compositions on Earth. The upper boundary is estimated to be at 130 km altitude, approximately the base of the ionosphere. Schumann resonances have not been observed on any body besides Earth, so the numbers quoted for Venus are purely theoretical, based on some assumptions about surface composition.

When a sferic propagates away from its source and reaches the base of the ionosphere, it reflects due to the increasing index of refraction of the plasma. However, some of its wave energy enters the ionosphere and propagates in the whistler-mode (*Helliwell*, 1965), described in detail in subsection 3.1.1. Whistler-mode waves propagate at frequencies between the local electron and ion gyrofrequencies and on Venus this extends up to several hundred Hertz. They are transverse electromagnetic waves that are typically ducted along the local magnetic field lines. This field ducting allows whistler-mode waves to travel great distances with little attenuation, but strong ducting is not always necessary at Venus. The relatively low field strengths in the ionosphere broaden the whistler-mode resonance cone, allowing the waves to propagate at more oblique angles to the ambient field. In the dipolar field at Earth, a whistler-mode wave can bounce numerous times between conjugate magnetic footpoints, but at Venus, the magnetic field geometry provides no opportunity for reflection of these waves. Waves that approach the ionosphere far from the their sources will be more horizontal

and do not require the field to be nearly as radial, so on the dayside it is less likely that the waves would be observed near their sources. The underlying physics of whistler-mode wave propagation will be discussed in subsection 3.1.1.

1.4 History

Lightning on Venus has been a controversial topic among researchers for hundreds of years. From the mysterious "Ashen Light" reported in the 17$^{\text{th}}$ century, through the US and USSR missions of the mid to late 20$^{\text{th}}$ century, to the current Japanese orbiter with a dedicated lightning camera, the existence of lightning on Venus has remained a topic of debate. There have been numerous observations of radio waves at Venus attributed to lightning, while only a handful of optical observations have been made. This seeming incongruity coupled with several unsuccessful attempts to observe lightning has fueled the debate for nearly half a century. In this section, we provide a brief summary of past observations of Venus lightning and the associated controversy. For more comprehensive reviews of Venus lightning, refer to the following articles: *Ksanfomaliti et al.* (1983), *Russell* (1991), *Grebowsky et al.* (1997), *Lorenz* (2018).

1.4.1 Ashen Light

The Ashen Light is a faint glow that appears on the night side of Venus and was first reported by Giovanni Riccioli in 1634 (*Moore*, 1957). While there have been many reported observations since then, the phenomenon is still shrouded in mystery. There does not seem to be any consistency regarding the observation conditions of successful viewings of the Ashen Light. *Goody and McCord* (1968) reported that the Ashen Light was most often observed near inferior conjunction. However, *Levine* (1968) found only 12% of their 125 observations occurred near conjunction. The observations occurring near conjunction were associated with an increase in the geomagnetic index A_p (*Levine*, 1968). This would suggest that the

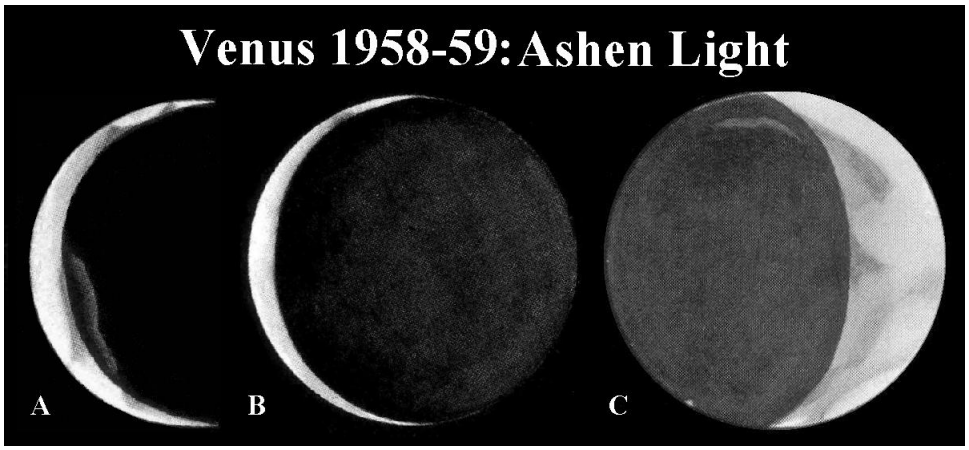

Figure 1.4: The Ashen Light of Venus as observed by *Firsoff* (1968). (*A*-*B*) The glow was visible while near inferior conjunction on 1958 Jan. 5 and 13, respectively. Ten observers of the British Astronomical Association reported observations of Ashen Light in the two weeks leading up to 1958 Jan. 13 (*McKim and Moore*, 2007). (*C*) Ashen Light observation on 1959 Oct. 8 during an elongation period with only one other sighting reported.

Ashen Light is some type of auroral emission, but the glow was only visible for 20% of the observation period with high geomagnetic activity while near conjunction.

Another possibility for the source of the Ashen Light is lightning. Only the most energetic lightning strokes would be able to optically penetrate the cloud tops of Venus with enough intensity to be seen from Earth. This limiting factor and the unpredictable nature of electrical storms would also explain the sporadic nature of the observations. However, optical observations of lightning are exceptionally scarce with only three confirmed reports to date (*Krasnopolsky*, 1980; *Hansell et al.*, 1995; *Takahashi et al.*, 2021). The increased geomagnetic activity associated with the Ashen Light could lead to enhanced electrification in the atmosphere of Venus, which would lead to an increase in lightning activity. This hypothesis gained traction with the detection of VLF waves by Pioneer Venus Orbiter (PVO) (*Scarf et al.*, 1980b; *Taylor et al.*, 1979). The VLF signals were attributed to lightning and were detected most often on the dusk side of Venus, the same side of the planet that offered

the most frequent observations of Ashen Light (*Russell et al.*, 1990). It should be noted that while the optical energy from a lightning flash will illuminate the clouds above, the energy committed to VLF wave propagation may be observed some distance away from the source.

McKim and Moore (2007) provide a summary of 108 years of Ashen Light observations by the British Astronomical Association (BAA). The records cover the tenures of two directors of the BAA Mercury and Venus Section, spanning from 1892 to 1999. Despite the abundance of sightings discussed, no definitive conclusions were drawn regarding the cause of the Ashen Light. It has been suggested that it could be a trick of the human eye (*Baum*, 2000). By the very nature of Venus observations from Earth, the darkest sky with which one can observe Venus is near the horizon while at maximum elongation, which means the observer must view through a much greater air mass. To reduce any optical effects due to air mass, one would need to observe Venus further from the horizon, but with that comes increased sunlight. It is possible that optical illusions from consistent observations in less than ideal conditions could play a role. While the observing community has yet to settle on a verdict for this centuries old mystery, nothing has been entirely ruled out. The Ashen Light continues to inspire researchers to investigate the optical phenomena at Venus.

1.4.2 Radio observations

In the 1960s and 1970s, both the Soviet Union and the United States began in situ exploration of Venus with the Venera series space probes and the Pioneer Venus project, respectively. In December of 1978, VLF radio measurements were taken during the descent of the Venera 11 and 12 landers. The onboard Groza (Thunderstorm) instrument suite was equipped with an acoustic sensor and an electric loop antenna with four narrowband channels centered at 10, 18, 36, and 80 kHz as well as a wideband channel (*Ksanfomaliti*, 1979, 1980). The acoustic sensor was saturated from the noise during the descent, so it was unable to detect any evidence of thunder. The electric antenna on each lander detected electrical impulses while descending to the surface, which were determined to be from a temporarily varying source

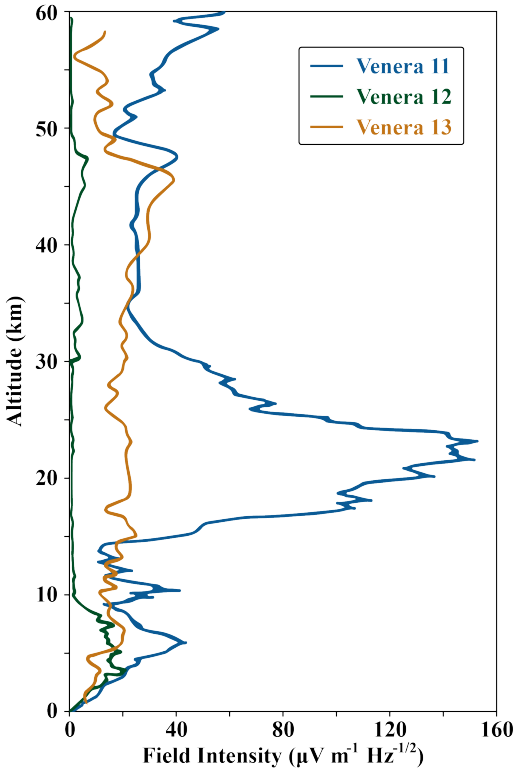

Figure 1.5: Altitude profiles of electrical activity observed by the Venera landers' Groza instruments. The data are 20 second averages of electrical impulses observed at 10 kHz. The profiles are adapted from *Ksanfomaliti et al.* (1982, Fig. 1).

(*Ksanfomaliti et al.*, 1979). Most notably, each lander exhibited different descent profiles despite relatively similar landing trajectories (Figure 1.5). In March of 1982, the Venera 13 and 14 landers arrived at Venus. They were built much the same as their predecessors, but with an improved Groza experiment, Groza-2 (*Ksanfomaliti et al.*, 1982). Figure 1.5 shows profiles of the electrical activity observed during the descents of Venera 11, 12, and 13. Venera 11 detected the strongest electric fields of the four landers, while the rest recorded signals of comparable intensities, albeit with Venera 12's most significant observations at low altitudes. Venera 11 observed the most intense fields at 15 – 30 km altitude, but was otherwise in agreement with the other landers. The interpretation of this mid-altitude peak is that Venera 11 had line-of-sight to a distant electrical storm, but as the lander

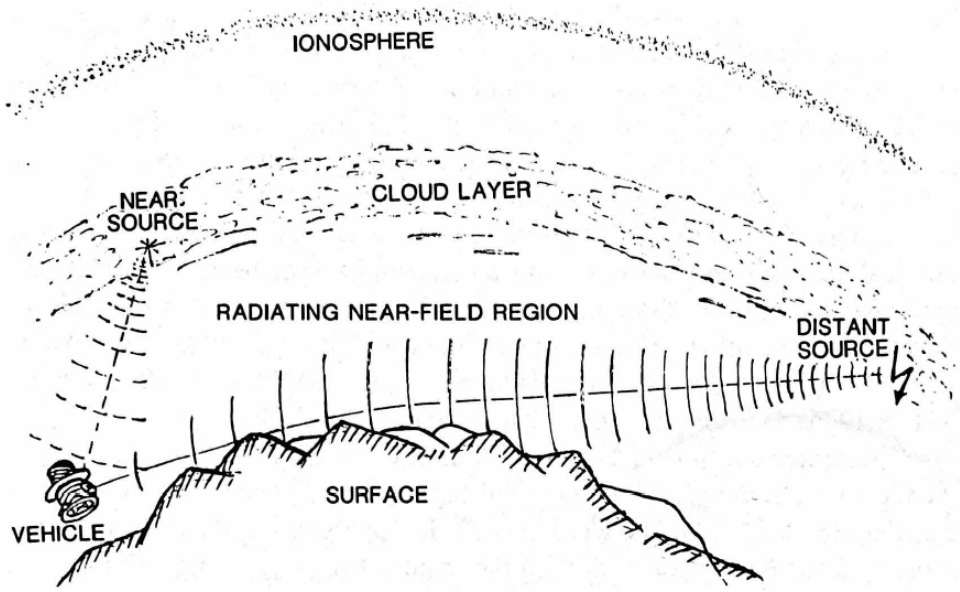

Figure 1.6: Diagram illustrating the difference in signals received by near and distant sources within the atmosphere of Venus. Venera 11 was likely blocked from its strongest source at low altitudes due to the curvature of the planet. (*Ksanfomaliti et al.*, 1983, Fig. 11).

approached the surface, the signal was blocked by the curvature of the planet Figure 1.6. *Croft and Price* (1983) plotted the ray propagation paths for atmospheric waves generated by lightning (sferics). They found that beyond a 1000 km range, lightning occurring below 33 km altitude would produce the electric field profile observed by Venera 11. Lightning within 100 km of the landers would be observed without any considerable defocusing of the rays. Therefore, Venera 11 was likely the only lander to observe such a distant source, but all four detected signals within relatively close proximity. Venera 12 appears to have only observed an intense storm while at very low altitudes, and it also happens to be the only vehicle that observed a signal after landing. Although it was only one burst, the detection on the surface supports the hypothesis that Venera 12 observed enhanced electric fields from a close source.

In 1978, Pioneer Venus Orbiter (PVO) arrived at Venus and was placed into an elliptical polar orbit with its periapsis near the equator. The orbit was fixed in inertial space, so

the periapsis passed through all local times in one Venus year, about 225 Earth days. The spacecraft was equipped with an electric field sensor (OEFD) that sampled in four narrow frequency bands spanning 30% of the central frequencies at 100 Hz, 730 Hz, 5.4 kHz, and 30 kHz (*Scarf et al.*, 1980b). Within the first month of observations, impulsive signals were observed in each frequency band (*Taylor et al.*, 1979). The impulses could only be observed on the nightside because the instrument was susceptible to increased noise while in sunlight. Signals should not be able to propagate through a collisionless plasma above the electron gyrofrequency, so *Scarf et al.* (1980a) decided on a new definition for impulses due to lightning events. Only signals occurring below the electron gryofrequency without being accompanied by signals at higher frequencies would be counted. This essentially limits the observations to the 100 Hz band and occasionally the 730 Hz band. The magnetic field had to be strong enough that the gyrofrequency well-exceeded the 100 Hz band (> 4 nT).

Scarf and Russell (1983) examined a larger sample of data and attempted to correlate the observations with surface topography. From the 14% of the Venus surface that was analyzed, they found that 65% of the signals were associated with elevated regions on the surface, possibly connecting the events to active volcanism. They were able to calculate a flash rate of 2.4 bursts km^{-2} yr^{-1}, which is equivalent to 35 bursts s^{-1} globally. However, a burst may contain multiple flashes because samples were only collected every 0.5 s due to the decay time of the instrument. There were also many signals not considered in the calculation because of the conservative selection criteria. Therefore, the burst rate calculated is a lower limit of the flash rate. *Taylor Jr. et al.* (1985) rejected the lightning hypothesis and dismissed the geolocation of the signals as simply being coincident with the orbiter path. This began a long series debates spanning dozens of articles, which is briefly summarize here. *Taylor Jr. et al.* (1985) suggested that the events often occurred simultaneously with ion troughs and can be attributed to typical dynamic processes in such an environment. They propose that the waves cannot be electromagnetic, as would be necessary for the lightning hypothesis to be correct, because their wavelengths are much larger than the associated ion troughs. *Taylor*

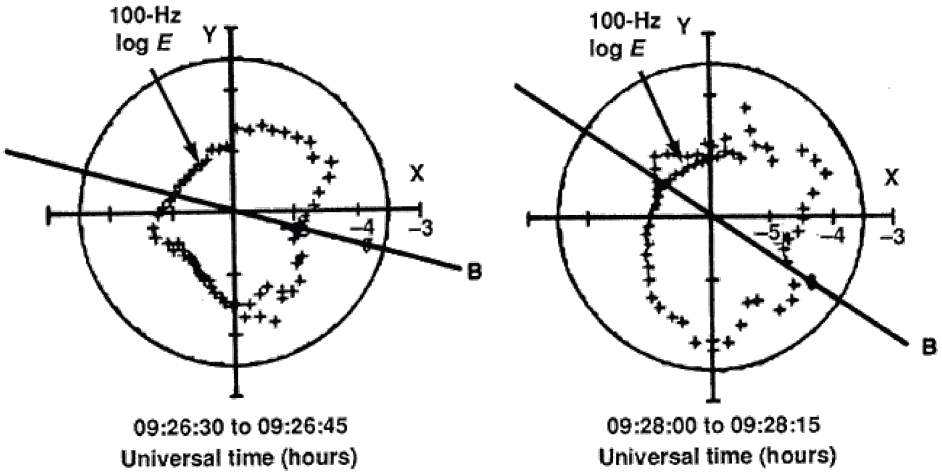

Figure 1.7: Polarization of 100 Hz waves observed by PVO. The electric field wave amplitudes are greatest in the direction perpendicular to the magnetic field as expected for electromagnetic waves. From *Scarf and Russell* (1988, Fig. 2).

Jr. et al. (1985) calculated a wavelength of 3000 km, the wavelength of 100 Hz light waves in a vacuum. The actual wavelength of the measured waves is less than 1 km. *Scarf and Russell* (1988) refuted the claim of electrostatic waves by performing two tests. First, they showed that the waves did not exhibit the Doppler shifts one would expect from electrostatic waves. The second test was to calculate the direction of maximum electric field perturbation. The electric field wave amplitudes are larger in the direction perpendicular to the magnetic field as demonstrated in Figure 1.7. Thus, the waves are indeed electromagnetic as originally hypothesized, but the debate over the geographic association was not addressed any further. *Russell* (1991) conceded that the geolocation argument was justifiably questioned. *Singh and Russell* (1986) decided to expand criteria for lightning impulses as originally defined by *Scarf et al.* (1980a) because they deemed it too conservative. They showed that as periapsis rose to higher altitudes, the occurrence rates of signals in the higher frequency bands diminished. While the occurrence rates of the 100 Hz signals showed little variation with altitude, the higher frequencies attenuated so quickly that they could be used to estimate proximity to the source. After comparing planetary longitudinal maps of observations with local time

maps, *Russell et al.* (1989a) concluded that the correlation was most likely associated with local time and not geography.

Under the assumption that the 100 Hz waves are electromagnetic whistler-mode waves propagating along the magnetic field, *Russell et al.* (1989b) calculated estimates of the Poynting flux (S). Since PVO lacked wave magnetic field measurements, they use the following form

$$S = 0.0796 N E^2 \; W m^{-2} \tag{1.1}$$

where N is the index of refraction, E^2 is the measured wave power in $V^2 m^{-2} H z^{-1}$, and the coefficient is said to account for the 30 Hz bandwidth of the instrument. The authors plot their results for three quantiles of field strength in *Russell et al.* (1989b, Fig. 3). The quantiles are for field strengths below 7 nT, between 7 nT and 15 nT, and above 15 nT. Their plot is combined with results from the research presented in this study and shown in section 4.3 (Figure 4.10). Their results show little variation with increasing altitude, but perhaps a slight decrease, which would imply a source from below the ionosphere. The central Poynting flux value from *Russell et al.* (1989b, Fig. 3) is $\sim 6 \times 10^{-8}$ W m^{-2}. It should be noted that this value is likely higher than the actual Poynting flux of the signals because a burst may consist of multiple signals due to the instrument response, as discussed earlier. The occurrence rates show little variation for the data analyzed (*Russell et al.*, 1988a), so they conclude that the altitude and local time variations would not be affected.

The neutral and ion mass spectrometers onboard PVO provided additional support for the existence of lightning on Venus with their measurements of nitric oxide (NO) in the atmosphere (*Niemann et al.*, 1980; *Taylor Jr. et al.*, 1980). NO production occurs in the high temperature and pressure environment of lightning channels in planetary atmospheres. *Krasnopolsky* (1983a) estimated a concentration of 5 – 40 ppb in the cloud layer from the PVO measurements. More recently, *Krasnopolsky* (2006) derived a mixing ratio of 5.5 ± 1.5 ppb in the lower atmosphere with observations from the NASA Infrared Telescope Facility on Mauna Kea. Lightning is the only known source of NO in the lower atmosphere, so

assuming a typical terrestrial flash energy of of $\sim 10^9$ J, the observed concentration of NO would be produced by a global flash rate of 87 s^{-1} (*Krasnopolsky*, 2006).

In PVO's twilight years, the Galileo mission was sent to explore Jupiter, aided by a gravity assist from Venus. During the flyby of Venus, the onboard plasma wave instrument detected radio signals at frequencies well above the local electron plasma frequency, which were interpreted to be generated by lightning (*Gurnett et al.*, 1991). Nine impulses were detected in a 53 minute span at 4 R_V. These results were called into question 10 years later, but that will be discussed in subsection 1.4.4.

In April of 2006, Venus Express (VEX) entered orbit around Venus and began sampling the local magnetic field. It regularly detected lightning-generated whistler-mode waves in the ionosphere with its dual fluxgate magnetometer (MAG) (*Zhang et al.*, 2006, 2007; *Russell et al.*, 2013) with the first signals being observed during the first orbit that utilized the high resolution 128 Hz sampling. Because the waves were observed with a magnetometer instead of an electric antenna, they were unequivocally electromagnetic waves, something repeatedly called into question with the PVO observations. The MAG instrument was susceptible to noise from currents generated by the spacecraft, so the solution was to design a gradiometer configuration with one fluxgate magnetometer mounted on the body of the spacecraft and one mounted on a 1 meter boom. The difference in the two signals would be due to the spacecraft noise and the agreement in the signals would be from a natural source. Unfortunately, no cleaning procedure existed prior to launch, so one was developed at UCLA (*Leinweber et al.*, 2008; *Russell et al.*, 2013). It would be $\sim$7 years before the full bandwidth of the instrument could be used for scientific analysis. The cleaning procedure is discussed in more detail in section 2.2.

Like PVO, VEX was placed into a polar orbit, but with its periapsis near the North pole instead of the equator. Both spacecraft passed through all local times at periapsis in a Venus year, $\sim$225 Earth days. The VEX periapsis was always within 18° of the North pole (Figure 1.8). Therefore, any low altitude measurements were necessarily at high latitudes and solar

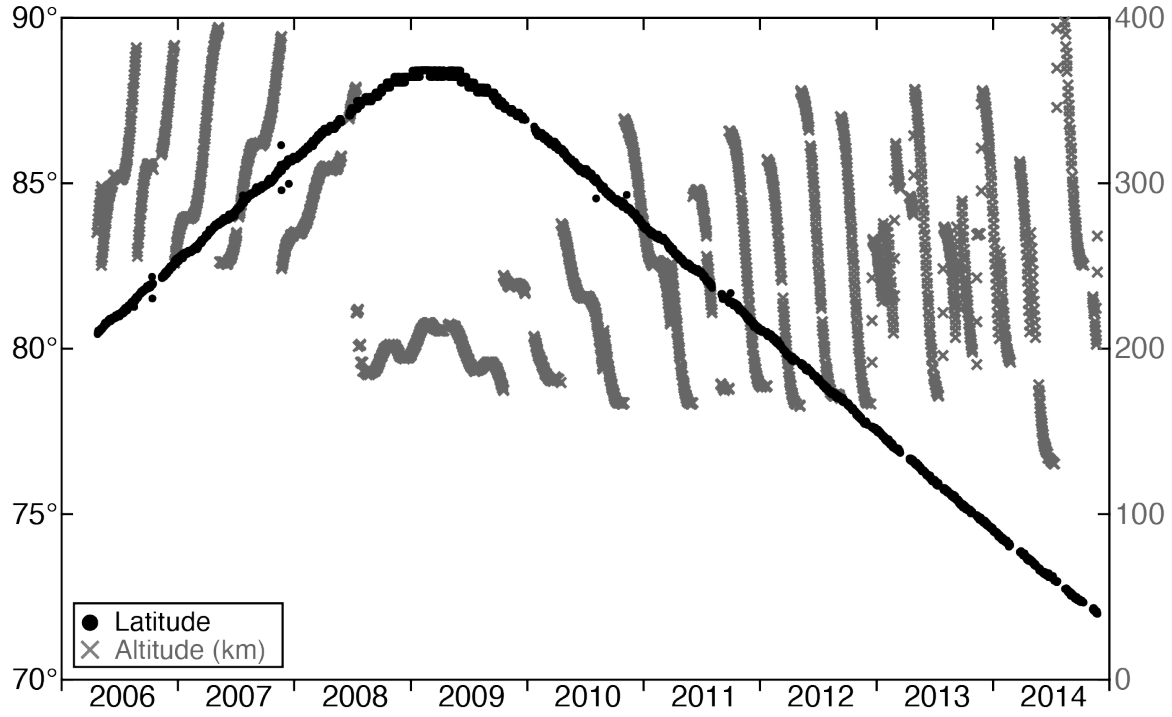

Figure 1.8: Latitude (black) and altitude (gray) variations of the VEX periapsis. The periapsis latitude increase ∼3° per year until 2009 when it began to decrease at the same rate. The altitude of periapsis was raised periodically due to the gravitationally decaying orbit. VEX did not descend well below 250 km until 2008-07-15. From then until 2009-10-19, the periapsis altitude remained below 225 km. In July 2014, the spacecraft descended to 130 km altitude while performing an atmospheric braking maneuver to reduce its orbital period.

zenith angles (SZA) near 90°. VEX was unable to sample the ionosphere near the subsolar point or in the deep night, but measurements in the ionosphere were rarely below 60° SZA. Thus, the field always maintained at least some radial component and was not completely horizontal as it is at the subsolar point. The periapsis of VEX varied in altitude from 165 km to 400 km, allowing for low altitude measurements, but not nearly as low as PVO. Initially, the latitude of the periapsis increased by 3° per year and then began decreasing at the same rate in 2009, ending the mission at 72°. The lightning rate near the poles relative to the rest of the planet is unknown. However, due to the IMF draping around Venus and because of

the planet's slow rotation, there is some azimuthal symmetry with respect to the Venus-Sun line. The main conclusions to be drawn from VEX whistler-mode wave observations are that waves were observed 8% of the time when the spacecraft was at 250 km altitude. This result leads to a global flash rate of 320 flashes s^{-1}. The details of the of the VEX observations will be discussed in this dissertation.

1.4.3 Optical observations

Remote visible observations of lightning on Venus are difficult because the cloud layer is optically thick to flashes occurring near the bottom or below the clouds, however, there has been some success. In 1975, Venera 9 orbiter arrived at Venus and began making observations with its visible spectrometer. *Krasnopolsky* (1980) reported lightning flashes observed within a 70 s interval, ∼2 per second and lasting ∼250 ms each. The luminous energy of each flash was calculated to be 3×10^7 J. The duration is longer than a typical lightning flash on Earth, which causes the optical energy released to be much less than a terrestrial flash (*Levin et al.*, 1983).

In addition to orbital observations, *Hansell et al.* (1995) observed flashes on the nightside of Venus with a 153 cm Earth-based telescope. Six flashes were observed at 777.4 nm and one at 656.3 nm. The calculated optical energies ranged from 7×10^7 to 2×10^9 J suggesting a global flash rate of 1.2×10^{-3} s^{-1}, but only for lightning with enough energy to penetrate the cloud tops. If lightning on Venus occurs as frequently as it does on Earth, then *Hansell et al.* (1995) only observed 0.02% of potential flashes. We cannot know what the true flash rate is from these observations without knowing the strength of a typical flash on Venus.

The most recent attempt at visible observations was with the Lightning and Airglow Camera (LAC) onboard the Japanese Venus Climate Orbiter, Akatsuki (*Takahashi et al.*, 2008). The spacecraft entered orbit around Venus at the end of 2015 after a missed attempt in 2010. The unplanned 5 year orbit around the Sun meant that the mission would not be able to operate at Venus as originally intended. The orbital period is 10.8 days, 8 times

longer than originally intended and with a much higher periapsis. The longer orbit means that the spacecraft will spend less time in eclipse, thus limiting the viewing opportunities. To date, the camera has observed one lightning flash with an optical energy of 1.1×10^7 J, comparable to the Venera 9 observation and 1 order of magnitude below that reported by *Hansell et al.* (1995) (*Takahashi et al.*, 2021). The flash duration was 220 – 230 ms, which is in complete agreement with the Venera 9 flash as well. Prior to Akatsuki's detection of a flash, *Lorenz et al.* (2019) estimated that the flash rate at Venus must be ∼1000 times less than on Earth. However, as with the previous visible observations, no consideration is given to the possibility of weaker optical intensities for Venus lightning. The paucity of visible observations emphasizes the difficulty with which light can escape the thick Venus cloud layer, also suggesting that lightning likely occurs well below the cloud tops with only the brightest flashes able to escape.

1.4.4 Non-detections

PVO was equipped with a star sensor which was designed to aid with navigation. It was utilized by *Borucki et al.* (1981) to search for lightning, but no signals above the noise level were recorded. Based on the observation time and assuming Earth-like properties for lightning, they calculated an upper limit for the average lightning occurrence to be 30 flashes km^{-2} yr^{-1}. Under the assumption that lightning is ubiquitous on Venus, their result is equivalent to a global flash rate of 438 s^{-1}, which is about 10 times the terrestrial rate. *Levin et al.* (1983) used the energy of the dimmer stroke observed by Venera 9 to recalculate the upper limit to be 85 flashes km^{-2} yr^{-1}, or 1240 flashes s^{-1} globally. The null result from the PVO star sensor provides an upper limit for lighting occurrence on Venus that is far above what anyone had previously considered.

In June 1985, the VEGA 1 and 2 balloons entered the atmosphere of Venus near the equator (*Sagdeev et al.*, 1986). They were each equipped with photometers, but they did not detect any unambiguous signals from lightning. Each balloon also had an acoustic sensor to

listen for thunder, but they were saturated by the wind.

In 1998 and 1999, the Cassini spacecraft performed two gravity assist flybys of Venus. The Radio and Plasma Wave Science instrument (RPWS) was used to search for lightning signals of 100 kHz to 5.6 MHz in the vicinity of Venus in much the same way as the Galileo probe (*Gurnett et al.*, 2001, 2004). Some signals were detected, but no impulses above the gaussian background noise. During its flyby of Earth, it detected 1101 events greater than 3 standard deviations above the noise. For these measurements, the detector used 75 channels, compared to the 20 used at Venus, in order to eliminate signals from terrestrial radio stations. While the inconsistency between the Earth and Venus observations seems striking, we don't know the likelihood of detecting these signals on any given flyby. A statistical study making use of currently orbiting terrestrial spacecraft would close the debate regarding the flybys of Venus.

Cardesín Moinelo et al. (2016) reports the most recent non-detection of Venus lightning. Using the Visible and Infrared Thermal Imaging Spectrometer (VIRTIS) onboard Venus Express (*Piccioni et al.*, 2007), they examined ∼14 hours of nighttime data in search of lightning. Thousands of transient signals were detected, but they could all be explained by cosmic rays. This is further evidence that visible observations of lightning on Venus are very difficult.

1.4.5 Lightning on other planets

While there has been an ongoing debate about the existence of lightning on Venus, there have been discoveries of lightning on other planets in our solar system. Lightning-generated whistlers were detected by Voyager I during its flyby of Jupiter and more recently with the Juno spacecraft (*Cook II et al.*, 1979; *Kolmašová et al.*, 2018). Voyager 2 detected high-frequency radio waves from electrostatic discharges at Uranus and whistler-mode waves at Neptune (*Zarka and Pedersen*, 1986; *Gurnett et al.*, 1990). It was not until the Cassini spacecraft arrived at Saturn that visible images of lightning were captured anywhere other

than on Earth (*Dyudina et al.*, 2010). High-frequency radio waves from electrostatic discharges were also observed at Saturn (*Burns et al.*, 1983). At Mars, there has only been one detection of an electrical discharge. Using NASA's Deep Space Network (DSN), *Ruf et al.* (2009) observed non-thermal microwave radiation that was postulated to be from a discharge in a Martian dust storm.

CHAPTER 2

Venus Express Mission

2.1 Primary objectives

Prior to Venus Express (VEX) entering orbit in 2006, there had not been a dedicated mission at Venus since the Magellan spacecraft deorbited in 1994, and no in situ space plasma science since PVO deorbited in 1992. With the success of the Mars Express mission, which launched in 2003, the European Space Agency (ESA) decided to repurpose the spacecraft and instrumentation designs for Venus Express. They were also able to largely maintain the same science teams, allowing them to develop and launch the mission within 4 years. VEX arrived at Venus in May 2006 and transmitted its last scientific observation in November 2014. The nominal mission was to last until October 2007, but its continued success earned it four mission extensions. The purpose of the mission was "aimed at a global investigation of the Venusian atmosphere, circumplanetary plasma, and some properties of the surface from the orbit" (*Titov et al.*, 2006). The mission was divided into seven scientific themes: atmospheric dynamics, atmospheric structure, atmospheric composition and chemistry, cloud layer and hazes, radiative balance, surface properties and geology, and plasma environment and escape processes. There were also seven instruments onboard, but they were not necessarily correlated one-to-one with the themes. The instruments and their main objectives

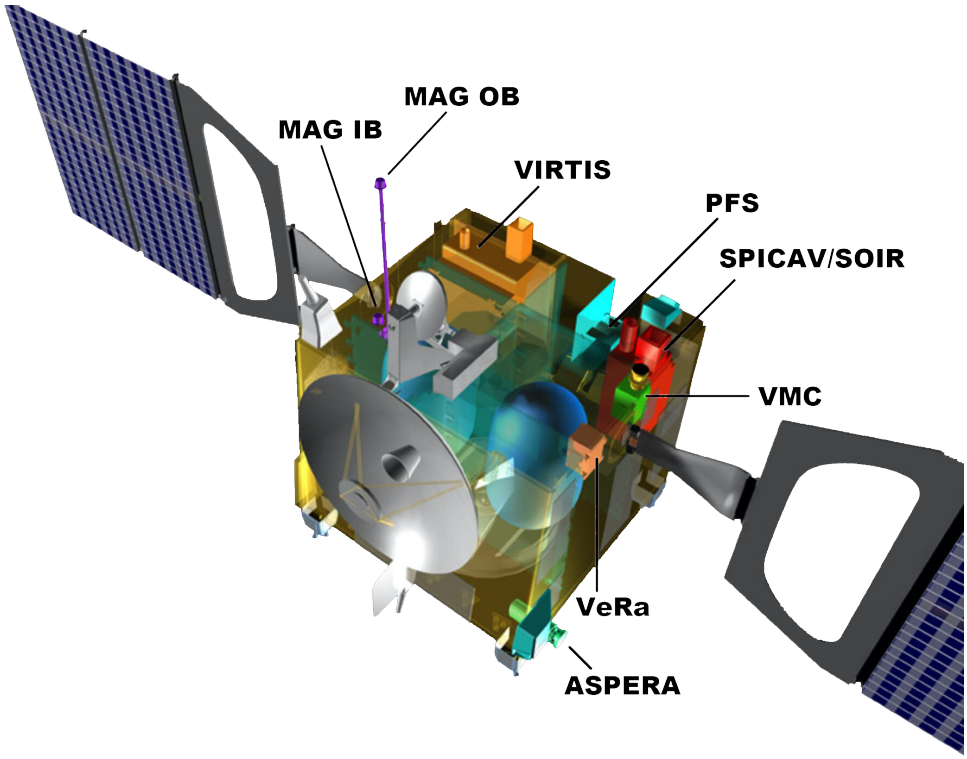

Figure 2.1: Diagram of the Venus Express spacecraft showing the location of each instrument in the suite.

are listed below (Figure 2.1).

Analyser of Space Plasmas and Energetic Atoms (ASPERA-4) (*Barabash et al.*, 2007)

- Investigate the interaction between the solar wind and the atmosphere of Venus.
- Characterize the impact of plasma processes on the atmosphere.
- Determine the global distribution of plasma and neutral gas.
- Identify the mass composition and characterize the atmospheric outflow.
- Investigate the plasma domains of the near Venus environment.
- Provide undisturbed solar wind parameters.

Fluxgate magnetometer (MAG) (*Zhang et al.*, 2007)

- Provide the magnetic field data for any combined field, particle, and wave studies such as lightning and planetary ion pickup processes.

- Map the magnetic properties in the magnetosheath, magnetic barrier, ionosphere, and magnetotail.
- Identify the boundaries between the various plasma regions.
- Study the solar wind interaction with the Venus atmosphere.

Planetary Fourier Spectrometer (PFS) (*Formisano et al.*, 2007)

- Perform long-term monitoring of the temperature field in the lower atmosphere.
- Measure the distribution of known minor atmospheric constituents.
- Search for unknown atmospheric constituents.
- Determine the size, distribution and chemical composition of atmospheric aerosols.
- Investigate the radiation balance of the atmosphere and the influence of aerosols on atmospheric energetics.
- Study global circulation, mesoscale dynamics and wave phenomena.
- Analyze surface to atmosphere exchange processes.

Spectroscopy for Investigation of Characteristics of the Atmosphere of Venus (SPICAV) (*Bertaux et al.*, 2007)

- Characterize the escape of deuterium from the upper atmosphere and give more insight about the evolution of water on Venus.
- Provide a sensitive search for new species in the upper atmosphere of Venus.
- Monitor SO_2 in various modes of observations.

Venus Radio Science (VERA)(*Häusler et al.*, 2006)

- Perform radio sounding of the Venus atmosphere and ionosphere.
- Determine dielectric characteristics, roughness, and composition of the surface.
- Study the solar corona, extended coronal structures, and solar wind turbulence.

Visible and Infrared Thermal Imaging Spectrometer (VIRTIS) (*Piccioni et al.*, 2007)

- Study the lower atmospheric composition below the clouds.

- Study the cloud structure, composition and scattering properties.
- Track clouds in UV (dayside) and IR (nightside).
- Measure temperatures to determine the zonal winds.
- Lightning search on the nightside.
- Map temperatures of the surface and search for possible volcanic activity.
- Search for seismic waves from the propagation of acoustic waves to the mesosphere.

Venus Monitoring Camera (VMC) (*Markiewicz et al.*, 2007).

- Perform support imaging.
- Facilitate the study of dynamic processes in the atmosphere of Venus..
- Study the distribution of the unknown UV absorber at the cloud tops.
- Monitor the UV and visible airglow and its variability as a dynamic tracer.
- Map the surface brightness distribution and search for volcanic activity.

2.1.1 Applications to this study

Measurements by MAG are the only data collected by Venus Express that were used in this study. The other instruments could not reliably be used to do such a comprehensive statistical analysis. The ASPERA-4 instrument is comprised of four sensors: the Neutral Particle Imager (NPI), the Neutral Particle Detector (NPD), the Ion Mass Analyzer (IMA), and the Electron Spectrometer (ELS). The particle data collected by these sensors could, in theory, complement the magnetic field data used in this study, but it was not practical to do so. There are 2×10^6 s of 128 Hz magnetometer data available under 1000 km altitude. For much of that time there are no contemporaneous particle measurements to use in conjunction with MAG measurements. In the future, we would like to perform some case studies that incorporate the particle data, but for this statistical study it cannot be used. We would also like to use VIRTIS and VMC observations to search for any visible anomalies that might occur near the strongest whistlers observed in this study.

2.2 Magnetometer data

Venus Express was a near copy of the Mars Express spacecraft bus with the addition of a fluxgate magnetometer gradiometer, which consisted of one magnetometer on the body of the spacecraft (inboard) and another on a 1 meter boom (outboard) (*Zhang et al.*, 2006, 2007). There was no pre-existing cleaning method for such a configuration prior to the launch of the mission, thus one needed to be developed. With the assistance of the instrument Principal Investigator (PI), Tielong Zhang, Co-Investigator Christopher Russell and programmer Hannes Leinweber at UCLA developed code to clean the high resolution 128 Hz magnetometer data. Hannes Leinweber is no longer at UCLA and the knowledge of his procedure was not transferred to anyone before his departure. Subsection 2.2.1 is adapted from the description of his method, which is also available in *Russell et al.* (2013). The cleaned final data product is available through the NASA Planetary Data System (PDS) *Russell et al.* (2022). This section is an expanded description of the one prepared for the PDS data product.

Initially, the 128 Hz sampling by the magnetometer was only activated for 2 minutes about periapsis corresponding to an altitude of $\sim$10 km above periapsis. After 2006, the high resolution observations were extended to tens of minutes and occasionally full orbits during its last year. While there are only 2 minutes of observations per orbit in 2006, the available data per orbit in later years is sufficient for this study. Since our search was for low altitude whistler-mode waves, we only utilize data within the ionosphere. Data collected beyond 10 minutes from periapsis was typically outside of the ionosphere due to the elliptical orbit of VEX. The magnetometer sampled at 1 Hz resolution for full 24 hour orbits throughout the mission.

2.2.1 Data cleaning method

The basic principle of the data cleaning algorithm for the AC signals is that differences between the inboard and the outboard sensors are due to magnetic interference from the spacecraft (Figure 2.1) (*Leinweber et al.*, 2008; *Russell et al.*, 2013). The inboard sensor can measure interference that is below the noise level at the outboard sensor. The observed signals at both sites were Fourier analyzed. Since the source of any interference seen by the magnetometers can have a wide range in the relative proximity to the two sensors, the relationship between the signals that are seen at both sites must be examined and the ratio to be used for correcting each one must be determined. If an apparent interfering signal is seen only on the inboard sensor, even more interference can be introduced to the measurements of the outbound sensor by attempting to clean it. Running amplitude spectra of the outboard measurements are used to identify frequency bands in which there is interference. The windowed (Hanning) amplitude spectra are 20 seconds long (segment length) and are shifted by 5 seconds. The threshold for interference is five times the noise level. Inverse Fourier transforms of each of the identified frequency bands are computed for the outboard as well as the difference between the inboard and the outboard sensor. Only the central portion of a segment is used due to edge effects of the windowed inverse Fourier transform. This leads to pairs of inverse transforms for each identified frequency band. The pairs are then matched with running 12 parameter fits to correlate the noise between the two signals. The 12 parameters are equivalent to a matrix and an offset vector. The window length for the fits is 21 points and the shift step is one point. The fit is then subtracted from the outboard sensor. Portions of the overall data set were mirrored at the beginning and at the end of the data set to reduce edge effects of the whole algorithm. The algorithm also removes low frequency content of the outboard sensor. The lower frequencies were restored from a 21-point running average and the zero levels were adjusted according to the independently corrected low-resolution data. The detrended data before this final step are also included in this bundle. *Russell et al.* (2013) demonstrate the success of this procedure.

2.2.2 Coordinate systems

The data were processed in spacecraft coordinates (SC) and rotated into Venus Solar Orbital (VSO) coordinates afterwards. In VSO coordinates, the x-axis points toward the Sun, the y-axis points opposite the orbital direction of Venus, and the z-axis points out of the ecliptic plane, completing the right-handed set. The calibrated 1 Hz data available in the ESA Planetary Science Archive (PSA) are in VSO coordinates. The 1 Hz data were interpolated up to 128 Hz and used to calculate the rotation angles, which were then used to calculate the rotation matrices using Rodrigues' rotation formula (2.1) (*Rodrigues*, 1840).

$$\mathbf{R} = \mathbf{I} + (\sin\theta)\mathbf{K} + (1 - \cos\theta)\mathbf{K}^2 \tag{2.1}$$

where $\mathbf{R}$ is the rotation matrix, $\mathbf{I}$ is the identity matrix, θ is the angle of rotation, and $\mathbf{K}$ is the antisymmetric matrix such that

$$\mathbf{K}\mathbf{v} = \mathbf{k} \times \mathbf{v} \tag{2.2}$$

with $\mathbf{k}$ being the vector about which the rotation is applied and $\mathbf{v}$ is an arbitrary vector. Instead of performing three rotations about the coordinate axes, Rodrigues' rotation formula allows one to rotate a given vector about an arbitrary axis onto another vector. The cleaned 128 Hz data set also includes the data in Radial-East-North coordinates (REN), which are equivalent to spherical coordinates with East being the azimuthal component and North being the negative of the polar component, i.e. the angle increases from the South Pole to the North Pole.

An anonymous reviewer of *Hart et al.* (2022) suggested that the authors use the Venus Solar Electric (VSE) coordinate system. In VSE coordinates the x-axis remains the same as in VSO coordinates, the y-axis is along the component of the IMF that is perpendicular to x, and the z-axis points in the direction of the convective electric field $\mathbf{E} = -\mathbf{v_{sw}} \times \mathbf{B}$. In these coordinates, the draping pattern is normalized for the IMF clock angle, which is the angle of the IMF projected onto the y–z plane. The propagation direction of the waves is not

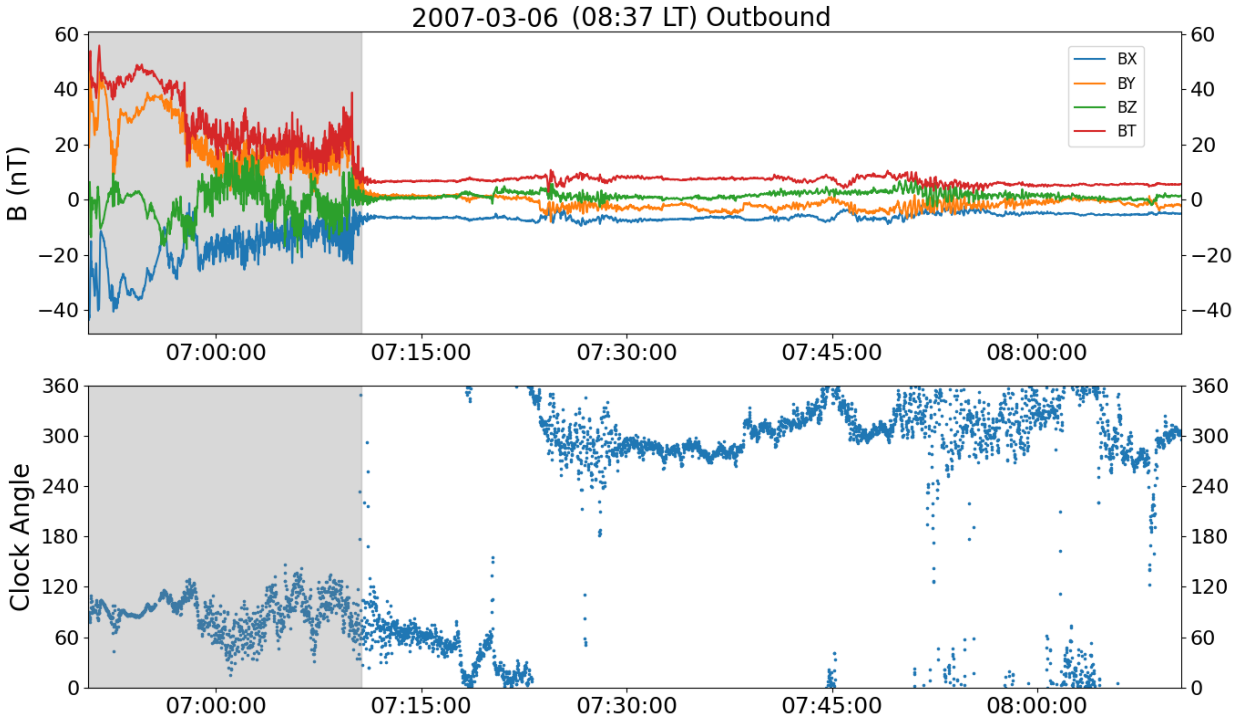

Figure 2.2: Magnetic field components (top) and IMF clock angle (bottom) plotted for the outbound portion of the orbit on 2007-03-06. The shaded regions highlight where our code estimated the spacecraft to be inside the bow shock. This shock crossing is well-defined and followed by a relatively quiet solar wind, yet the IMF experiences significant rotations.

necessarily dictated by the global field geometry, but by the local magnetic fields in the lower ionosphere. If we were to conduct a ray tracing analysis, then the global field orientation would be significant. We make no attempt to geolocate the sources in this study, so the coordinate system in which we do our analysis is irrelevant. The comprehensive statistical analysis performed in this study does not lend itself well to the VSE coordinate system. The proper rotation requires knowledge of the IMF simultaneously with in situ measurements of waves in the ionosphere. As Venus Express is the only spacecraft at Venus, there is no opportunity for truly simultaneous measurements. On many occasions, this is not a problem because the solar wind is relatively quiet and does not vary significantly between the IMF and ionospheric measurements. Two problems arise when attempting to obtain an accurate

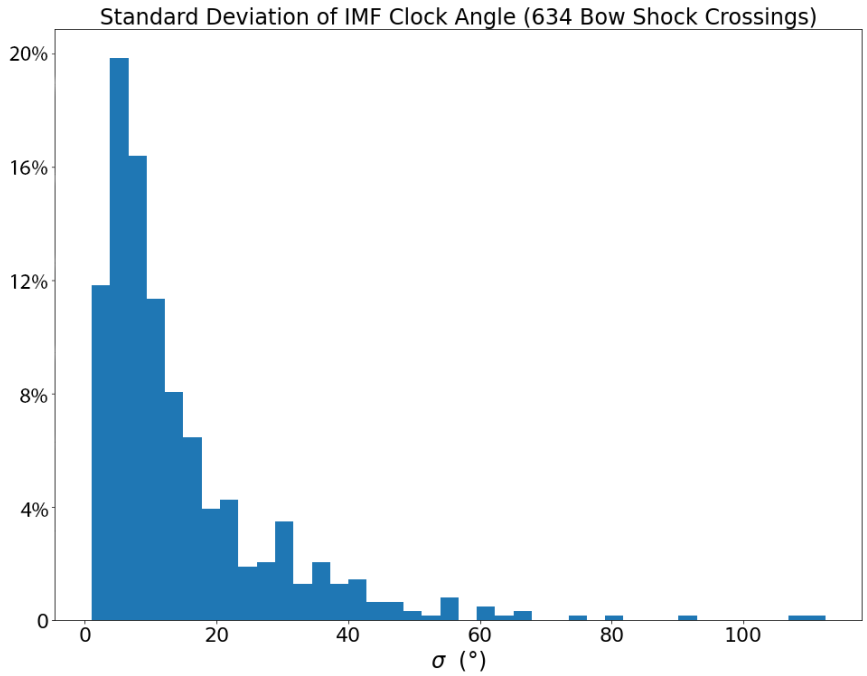

Figure 2.3: Standard deviations of clock angles for 634 well-defined bow shock crossings. The standard deviation for each crossing was determined for data acquired 5 – 15 minutes upstream of the shock.

rotation. The first is determining the closest point at which the spacecraft is in the solar wind. The plasma boundaries are usually apparent in the field data on the dayside, but near the terminators they become less clear. On the nightside, there is almost never a sharp boundary. Since the dayside crossings are not always clear either, this eliminates more than half of the 5,268 available crossings. The second problem is that even in a seemingly calm solar wind the IMF can experience significant rotations as shown in Figure 2.2. We randomly chose 634 well-defined bow shock crossings to determine the typical variations in the IMF clock angle. The histogram in Figure 2.3 shows the standard deviations of the clock angle for 5 – 15 minutes upstream of the selected bow shock crossings. About 75% of the crossings have a standard deviation less than 20°. Therefore at least 25% of the orbits could not be used to rotate into the VSE coordinate system, essentially eliminating one quarter of the statistics from this study. Because the ability to rotate into VSE coordinates is directly

correlated with solar activity, there would be a selection bias introduced into the results. While the VSE coordinate system may be beneficial for case studies or smaller sample sizes, it is not feasible to use it for comprehensive statistical analysis.

2.2.3 Data sets

The high resolution 128 Hz data were only recorded for 2 minutes about periapsis until the end of 2006, after which the sampling period was extended to tens of minutes and occasionally full orbits in the last year of the mission (Figure 2.4). The only set of 128 Hz data in PSA is the raw data. In addition to the cleaned 128 Hz data (*Russell et al.*, 2022), the calibrated 1 Hz data was also used in this study for purposes other than signal analysis. Because the cleaned 128 Hz data were not produced from the currently available raw data, the availability of the two sets does not always match. The original raw data that was used to produce the cleaned data are no longer available, but the official raw 128 Hz data is available in PSA.

Figure 2.4: Sampling intervals for each available orbit in the three data sets referenced herein. Each value is the difference between the first and the last times of that particular orbit.

2.2.4 Data caveats

The cleaning procedure of this data product was an overall success, however, there are some caveats that should be noted. It is no longer possible to run the code for the cleaning algorithm to regenerate any of the data, so a discussion of any known issues to the data is included here. A data errata file was also produced to log some of the issues discovered during wave analysis. The cleaned 128 Hz data have been utilized for this thesis work and they are compiled into a data product for submission to PDS. As part of this work, the dynamic spectra of all data that were sampled below 1000 km altitude were scanned, ∼30% of the set. The dynamic spectra include the coherence between the two axes perpendicular to the DC field, ellipticity, propagation angle, transverse power and compressional powers. The errata contain periods of unusual behavior that were happened upon while searching for whistler-mode waves. The list contains 52 days, however, it is not intended to be exhaustive; it is intended to provide the data user with a significant sample of any known peculiarities within the data. It should be noted that the caveats discussed in this section are a very small portion of the data.

2.2.4.1 Post-processing correction

In 2019, it was discovered that certain periods of the cleaned data were not in agreement with the lower resolution 1 Hz data set in the ESA PSA. After some time examining the problem, it was determined that the incongruity was due to a difference in offsets occurring sporadically throughout the mission, but most frequently in the first two years. As data became available in the early mission, offsets were received directly from the instrument PI, which were later updated before being submitted to PSA. Because the programmer was no longer available, along with the knowledge of his procedure, the data were unable to be reprocessed from the raw 128 Hz data in PSA. Instead, a 1 second running average was subtracted from the original cleaned data and the 1 Hz data from PSA were added

in to restore the low frequency content, thus ensuring that the cleaned data set has offsets consistent with the publicly available data from the Venus Express mission. In order to make sure the whole data set was in agreement, the correction was applied to all orbits even if no offset correction was needed. If a data gap existed in only one of the data sets, it resulted in a gap in the final reprocessed data set since both were required for the correction. We compared the pre-correction spectra with the post-correction spectra for orbits that did not need correcting to confirm that no signal was lost and that no new artifacts were introduced. The correction proved to be a success and no further reprocessing was necessary (Figure 2.5).

2.2.4.2 Bursts at 4.5 Hz

On occasion, from 2008 through 2010, the data exhibit short ($\sim$4 seconds), periodic bursts (Figure 2.6). When these anomalies are present, they occur every 40 seconds. There are 34 days logged in the errata in which this behavior was exhibited. The bursts in the errata all occur above 450 km, beyond solar zenith angles of 115°, and within 2 hours of local midnight. Noise due to the reaction wheels on the spacecraft has been ruled out because they operate at approximately 40 Hz, as evidenced in Figure 2.6e. Thrust maneuvers are also an unlikely culprit as the orbital adjustments were not made on days corresponding to the data anomalies. While the signals appear to be artifacts from either the spacecraft or the data cleaning procedure, the source is unknown, so they have been left untouched.

2.2.4.3 Full bandwidth circular waves

There are certain periods in which the data exhibit strange harmonic behavior exemplified in Figure 2.7. This anomalous behavior tends to show significant power at all frequencies in the bandwidth of the instrument ($<$ 64 hz). The signals are circularly polarized, either in the right- or left-handed sense, and often both simultaneously at different frequencies.

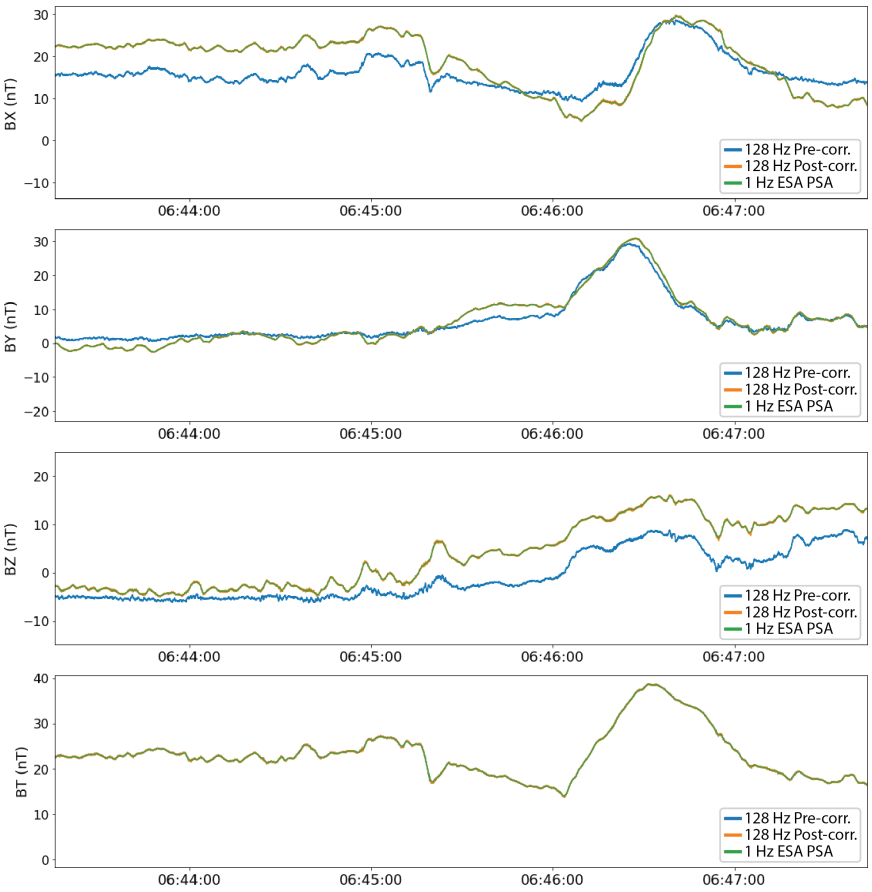

Figure 2.5: Time series of magnetic field components on 2007-06-16 demonstrated the original error in the data and the correction. The orange curve is the high resolution equivalent of the green curve, so only portions of it are visible in this plot.

They are often propagating at an angle perpendicular to the background field with some exceptions in narrow frequency bands. Again, while these signals appear to be artifacts, the source is unknown, so they are left intact in the data. There are 18 days of such behavior in the errata.

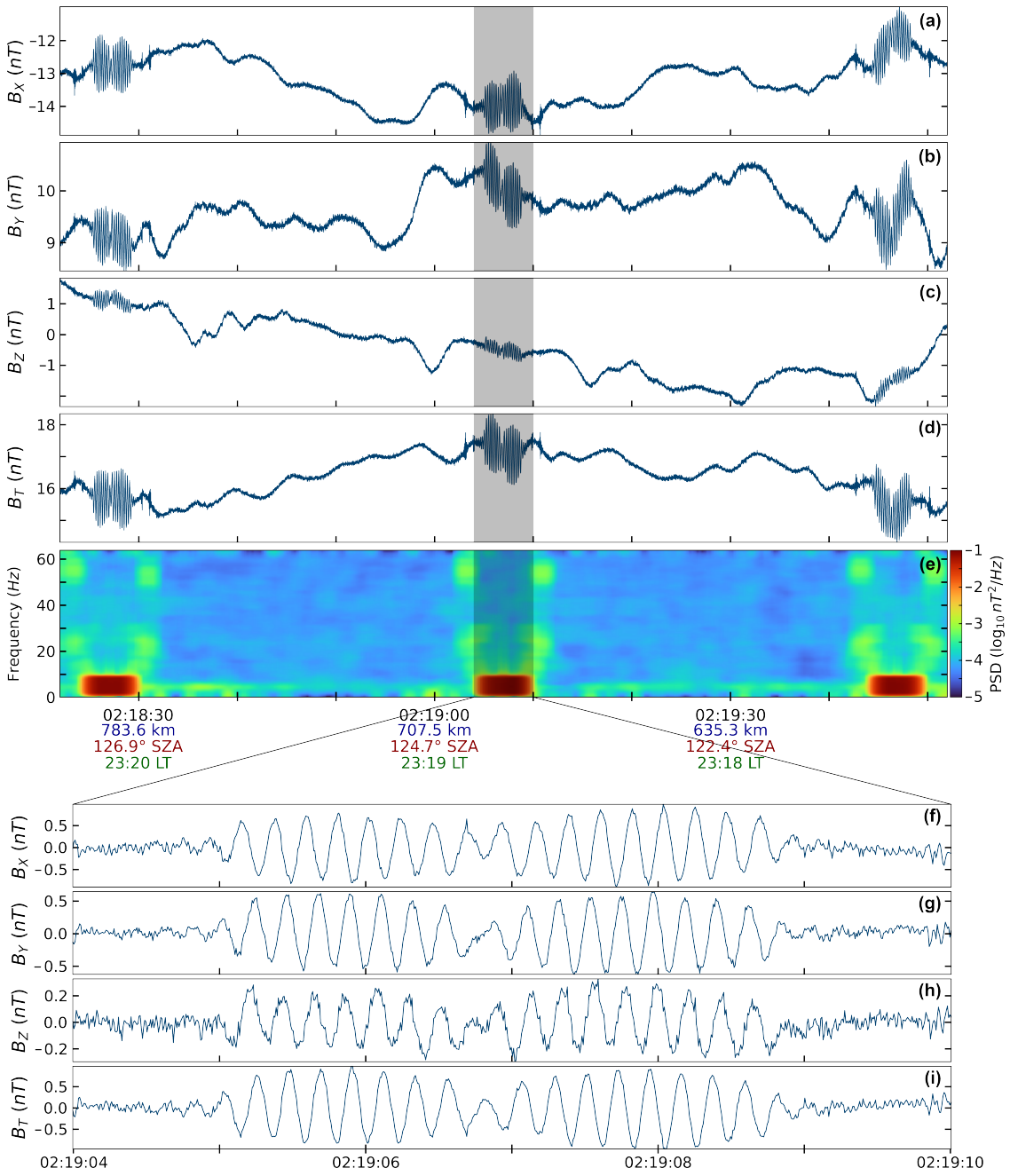

Figure 2.6: Example of 4.5 Hz bursts in the data on 2009-09-15. When the anomalies are present, they occur every 40 seconds. (*a–d*) The magnetic field components in VSO coordinates and the field strength. (*e*) The power spectral density of the field strength from 0 to 64 Hz. (*f–i*) The respective waveforms of the shaded interval in *a–d*. Frequencies below 0.5 Hz have been removed.

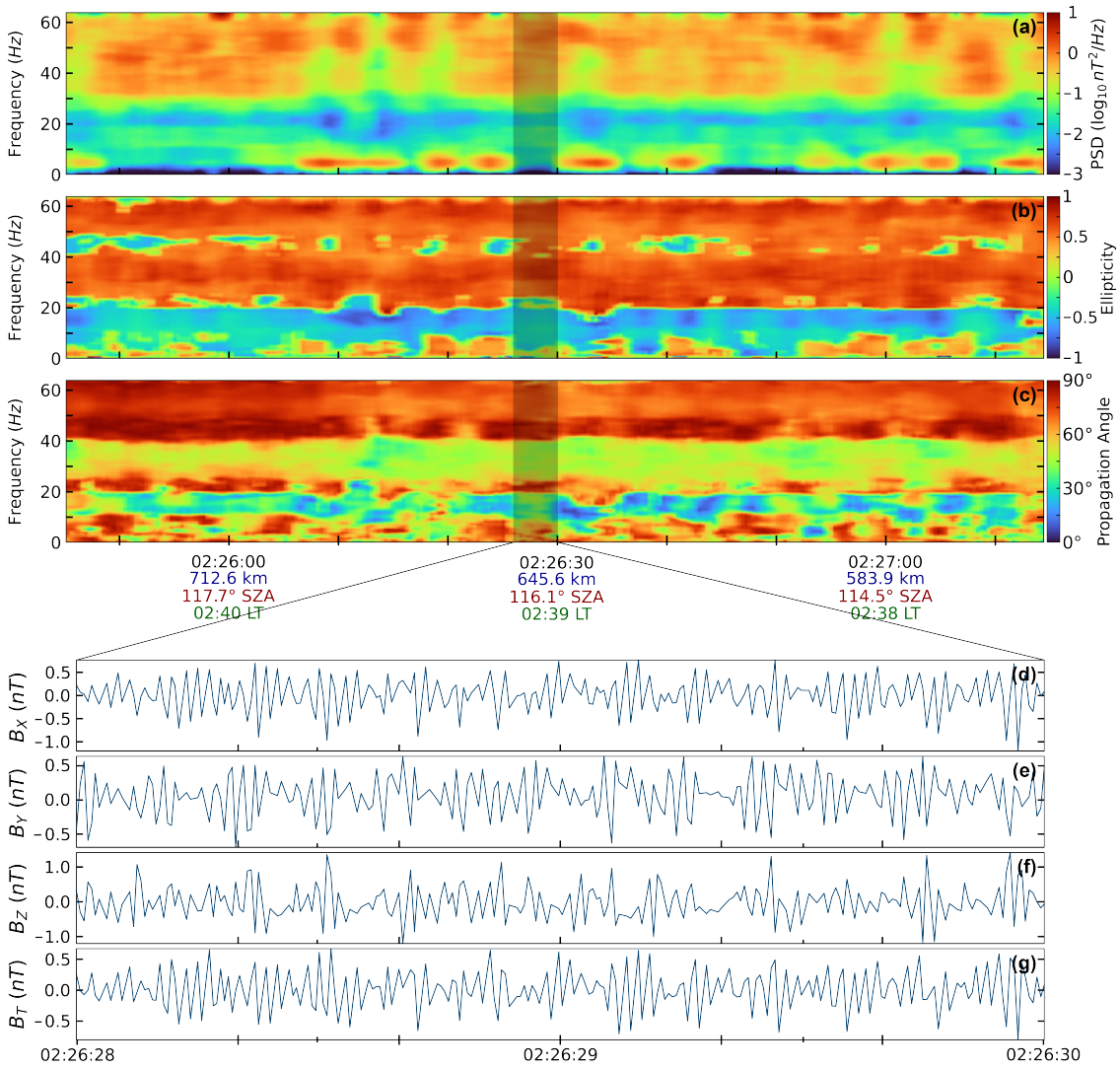

Figure 2.7: Example of a full bandwidth wave exhibiting circular polarity and perpendicular propagation on 2011-01-08. (a) The power spectral density of the field strength from 0 to 64 Hz. (b) The ellipticity from left-hand (-1) to right-hand ($+1$) circular polarization. (c) The propagation angle relative to the background magnetic field. (d–g) The waveforms of B_X, B_Y, B_Z, and B_T from the shaded interval in a–c. Frequencies below 0.5 Hz have been removed.

CHAPTER 3

Wave Analysis

In this chapter we discuss the work undertaken in this study. This chapter will cover the details of our wave analysis and setup the framework for the statistical analysis to follow. We begin with the theoretical background necessary to understand to physics of whistler-mode waves. We then describe the Fourier analysis used to analyze and characterize these waves. The methods have evolved over time, from amateurish techniques to more sophisticated analyses as skills and knowledge were developed over the years. This chapter includes a description of the evolution of the four major iterations of the wave analysis, culminating in an automated process written in Python.

3.1 Theoretical background

3.1.1 Whistler-mode wave theory

We primarily follow the formulation of the of the wave dispersion relation in terms of the refractive index as described in *Russell et al.* (2016, Ch. 13). Using Maxwell's equations and the harmonic perturbation assumption, we derive a general description of plasma wave propagation and apply it to the conditions necessary for whistler-mode propagation. Under the harmonic perturbation assumption, we search for plane wave solutions of the form

$\mathbf{E}_0 e^{i(\mathbf{k}\cdot\mathbf{r}-\omega t)}$ that are first-order perturbations. We can then adopt new definitions for the spatial and time derivative operators (3.1, 3.2).

$$\nabla \equiv i\mathbf{k} \tag{3.1}$$

and

$$\frac{\partial}{\partial t} \equiv -i\omega \tag{3.2}$$

We begin with the continuity (3.3), momentum (3.4), and energy (3.5) equations

$$\frac{\partial \rho}{\partial t} + \nabla \cdot (\rho \mathbf{u}) = 0 \tag{3.3}$$

$$\rho \frac{D\mathbf{u}}{Dt} = \nabla \cdot \mathbf{P} - \mathbf{j} \times \mathbf{B} = 0 \tag{3.4}$$

$$\frac{D}{Dt}(P\rho^{-\gamma}) = 0 \tag{3.5}$$

where ρ is the density, $\mathbf{u}$ is the particle velocity, $\mathbf{P}$ is the pressure, $\mathbf{j}$ is the current density, $\mathbf{B}$ is the magnetic field, γ is the heat capacity ratio, and (3.6) is the total derivative.

$$\frac{D}{Dt} \equiv \frac{\partial}{\partial t} + \mathbf{u} \cdot \nabla \tag{3.6}$$

The heat capacity ratio (γ) for an ideal gas with three degrees of freedom is $5/3$. Linearizing (3.3) – (3.5) results in

$$-i\omega\delta n_s + i n_s \mathbf{k} \cdot \mathbf{u}_s = 0 \tag{3.7}$$

$$-i\omega n_s m_s \mathbf{u}_s + i\mathbf{k}\delta P_s = n_s q_s (\mathbf{E} + \mathbf{u}_s \times \mathbf{B}_0) \tag{3.8}$$

$$\delta P_s = \frac{\gamma_s P_s}{m_s n_s} m_s \delta n_s = \gamma_s K T_s \delta n_s \tag{3.9}$$

where the subscript refers to species s, n is the particle number density, q is the particle charge. Combining Eqs. 3.7 – 3.9 produces

$$\omega^2 \mathbf{u}_s - \frac{\gamma_s K T_s}{m_s}\mathbf{k}(\mathbf{k} \cdot \mathbf{u}_s) = i\omega \frac{q_s}{m_s}(\mathbf{E} + \mathbf{u}_s \times \mathbf{B}_0), \tag{3.10}$$

the general form describing the interaction of the perturbation flow velocity of species s with the electric field $\mathbf{E}$.

In a cold plasma the wave phase velocity is much greater than the species sound speed. We can then ignore the effects of the plasma pressure and (3.10) becomes

$$\mathbf{j}_s = i\frac{\omega_{ps}^2}{\omega}\epsilon_0\mathbf{E} + i\frac{\Omega_s}{\omega}\mathbf{j}_s \times \hat{\mathbf{b}} = i\frac{\epsilon_0\omega_{ps}^2}{\omega^2-\Omega_s^2}\begin{pmatrix} \omega & i\Omega_s & 0 \\ -i\Omega_s & \omega & 0 \\ 0 & 0 & \omega^2-\Omega^2 \end{pmatrix}\begin{pmatrix} E_x \\ E_y \\ E_z \end{pmatrix} \tag{3.11}$$

where ω_{ps}^2 is the species plasma frequency and Ω_s is the species gyrofrequency. Without loss of generality, we have assumed a cartesian coordinate system with the z-axis along the ambient field direction. Although whistler propagation tends to be along the ambient field direction, it is not strictly true so we must consider oblique propagation. We will assume that the wave vector $\mathbf{k}$ lies in the x – z plane at some angle θ to the magnetic field. We now adopt the notation of *Stix* (1992), where $S = \frac{1}{2}(R+L)$ and $D = \frac{1}{2}(R-L)$ with

$$R \equiv 1 - \sum_s \frac{\omega_{ps}^2}{\omega(\omega+\Omega_s)}, \qquad L \equiv 1 - \sum_s \frac{\omega_{ps}^2}{\omega(\omega-\Omega_s)}, \qquad P \equiv 1 - \sum_s \frac{\omega_{ps}^2}{\omega^2} \tag{3.12}$$

Incorporating the refractive index $\mu = kc/\omega$, (3.11) becomes

$$\begin{pmatrix} S-\mu^2\sin^2\theta & -iD & \mu^2\sin\theta\cos\theta \\ iD & S-\mu^2 & 0 \\ \mu^2\sin\theta\cos\theta & 0 & P-\mu^2\sin^2\theta \end{pmatrix}\begin{pmatrix} E_x \\ E_y \\ E_z \end{pmatrix} = 0 \tag{3.13}$$

Taking the determinant of (3.13) provides the biquadratic general dispersion relation for cold plasma waves

$$A\mu^4 - B\mu^2 + C = 0 \tag{3.14}$$

where

$$\begin{aligned} A &= S\sin^2\theta + P\cos^2\theta \\ B &= RL\sin^2\theta + PS(1+\cos^2\theta) \\ C &= PRL. \end{aligned} \tag{3.15}$$

Using the quadratic equation to solve for μ^2 yields what is known as the Appleton-Hartree dispersion relation

$$\mu^2 = 1 - \frac{\dfrac{\omega_{pe}^2}{\omega^2}}{1 - \dfrac{\Omega_e^2 \sin^2\theta}{2\left(\omega^2 - \omega_{pe}^2\right)} \pm \left[\left(\dfrac{\Omega_e^2 \sin^2\theta}{2\left(\omega^2 - \omega_{pe}^2\right)}\right)^2 + \dfrac{\Omega_e^2}{\omega^2}\cos^2\theta\right]^{1/2}}\,. \tag{3.16}$$

We have invoked the high frequency approximation wherein ions are stationary, so only electron motion is considered. On choosing the minus sign in the denominator in (3.16) the waves are right-handed due to the gyroresonance with electrons. When $\theta = 0$, the wave vector is completely aligned with the background field and the wave is circularly polarized (+1 ellipticity). With increasing obliquity, the polarization becomes more eccentric. As will be discussed in a section 3.3, we require that observed signals be nearly circularly polarized.

There is a simplified version of (3.16) that is useful for discussing the behavior of the wave. When the second term in brackets in the denominator is much larger than the first term in the brackets, we have what is called the quasi-longitudinal approximation and (3.16) takes the form

$$\mu^2 \approx 1 - \frac{\omega_{pe}^2}{\omega\left(\omega - |\Omega_e|\cos\theta\right)}\,. \tag{3.17}$$

It is clear that there is a resonance condition when $\cos\theta = \omega/|\Omega_e|$. This is known as the resonance cone angle and beyond it the wave phase velocity tends to zero. With the VEX magnetometer we can only resolve frequencies up to 64 Hz. As is apparent in Figure 3.1, the gyrofrequencies at the times of whistler observations are generally $\sim$200 Hz on the nightside and several hundred Hertz on the dayside. Even when the gyrofrequency is as low as 100 Hz the resonance cone is 50°, but most often above 70°. To maintain a conservative approach to this study, we searched for quasi-longitudinal waves, so the resonance cone almost never needs to be considered. In future work we would like to carry out a broader search for waves that does not require quasi-parallel propagation.

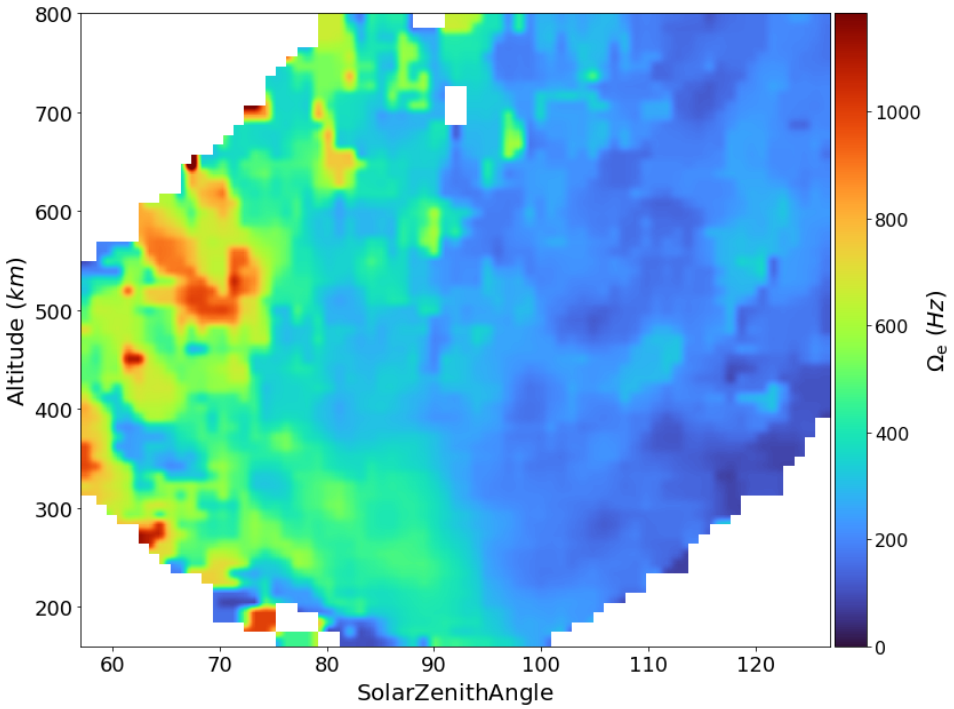

Figure 3.1: Electron gyrofrequencies observed at times of whistler observations in the Venus ionosphere as a function of altitude and solar zenith angle.

3.1.2 Wave energy flux

If one has measurements of both the electric and magnetic fields, the energy flux of the waves is simply the calculation of the Poynting vector

$$\mathbf{S} = \frac{1}{\mu_0}\mathbf{E} \times \mathbf{B} \tag{3.18}$$

where $\mathbf{E}$ and $\mathbf{B}$ are the electric and magnetic fields of the wave and μ_0 is the vacuum permeability. Since we only have magnetic field measurements, 3 of the 6 necessary components, we must find another way. The magnetic and electric fields of a purely electromagnetic wave are related by the index of refraction

$$\mathbf{E} = \frac{c}{n_r}\mathbf{B} \tag{3.19}$$

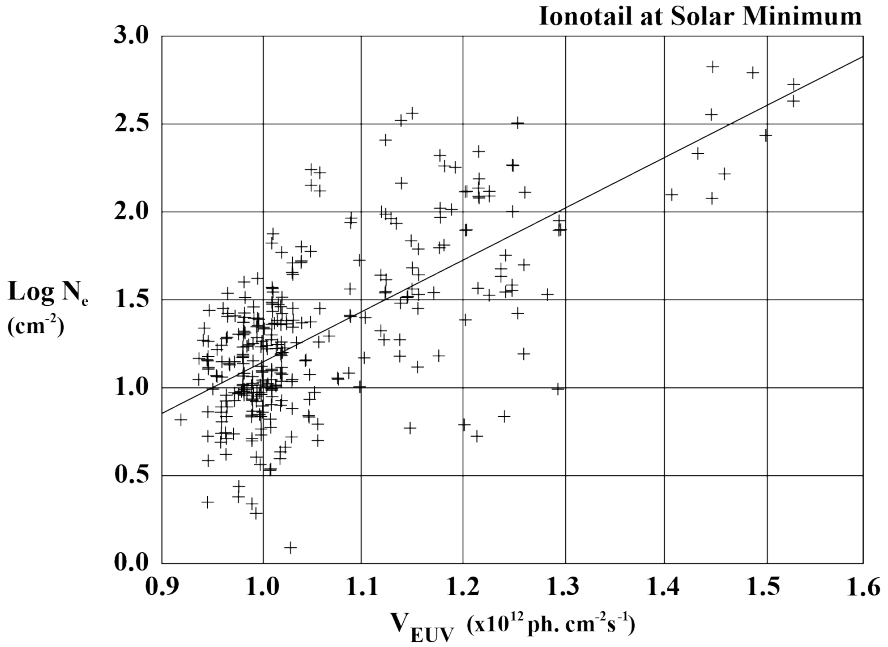

Figure 3.2: Power law scaling of the electron density and solar EUV flux observed by PVO (*Brace et al.*, 1997, Fig. 9). Venus Express was in operation during an unusually weak solar cycle, so the VIRA electron density model would need to be scaled accordingly.

where c is the speed of light and n_r is the index of refraction of the medium. We change from using μ to n_r for the refractive index to avoid confusion with the magnetic permeability. We are now dependent on the quantities contained in the whistler dispersion relation, more specifically, within the electron plasma frequency (3.20) and gyrofrequency (3.21),

$$\omega_{pe} = \sqrt{\frac{n_e e^2}{m_e \epsilon_0}} \tag{3.20}$$

$$|\Omega_e| = \frac{eB_0}{m_e} \tag{3.21}$$

where n_e is the electron number density, e is the electron charge, and m_e is the electron mass. The only unknown quantity is the electron density. The ASPERA-4 instrument could be very useful if there were collocated measurements with the waves in this study. Instead, we employ the electron density model from the Venus International Reference Atmosphere (VIRA) (*Bauer et al.*, 1985; *Brace et al.*, 1997). The model was developed from 14 years of

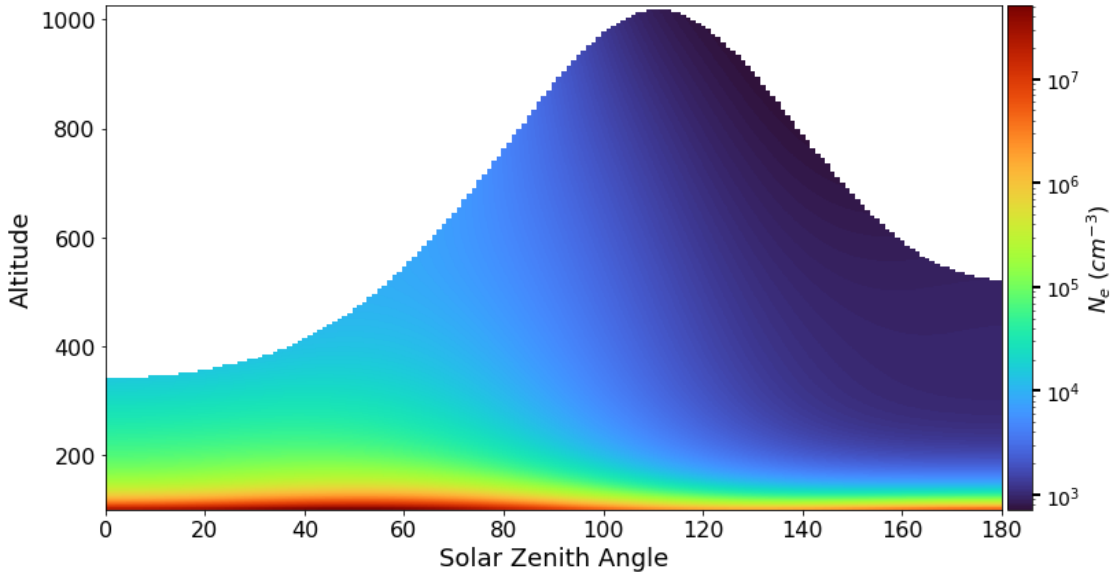

Figure 3.3: Electron density from the VIRA ionospheric model (*Bauer et al.*, 1985; *Brace et al.*, 1997). The values in this figure are calculated for the median solar EUV flux during the Venus Express mission.

PVO observations in which there were considerably higher solar extreme ultraviolet (EUV) fluxes than during the VEX campaign. Figure 3.2 shows that there exists a power law that can scale the electron densities from the VIRA model to match the solar conditions at times of VEX observations. The model was coded into a function with inputs of altitude, solar zenith angle, and solar EUV. We used the solar EUV measurements obtained by the Solar Extreme Ultraviolet Monitor (SEM) instrument onboard the Solar and Heliospheric Observatory (SOHO), which were rotated and scaled to the orbit of Venus. We were then able to calculate the Poynting flux of every signal using the number density values determined from the function. The model for the whole ionosphere is shown in Figure 3.3.

3.2 Initial analysis methods

In order to identify signals as whistler-mode waves we consider the expected properties of lightning-generated whistler-mode waves. They are field-aligned, transverse electromagnetic waves that are circularly polarized in a right-hand sense. Therefore, we calculated the ellipticity, propagation angle relative to the ambient field, transverse power, and compressional power. We also calculated the coherence of the signals.

This thesis work began with the aid of analysis software that was developed in the Russell group decades prior, which were adapted to an X-Windows environment for Solaris workstations. They were originally called Banal and Manal, short for B analysis and magnetic analysis, and then BX and MX in their graphical user interface evolutions. BX was useful for plotting time series and 2-D spectra and MX was useful for plotting 3-D spectra to see how the properties of the wave evolved with time. The spectral analysis utilized the *Means* (1972) method. The programs were very useful for analyzing specific cases, but because they required manual user input, they were not well suited for analysis of large data sets. Nonetheless, these programs were the tools utilized to search for whistler-mode waves at Venus. What follows is a description of the manual analysis process and how it ultimately became an automated procedure.

There are 2,634 orbits of available data for the 128 Hz magnetometer. As mentioned previously, the first 8 months in orbit only offered 2 minutes of observations about periapsis, but that was then increased to tens of minutes or more. First, BX was used to plot the time series of each orbit in 2 minute intervals. After filtering out frequencies below 1 Hz, intervals with significant transverse wave activity were identified, i.e. two axes with a strong signal that was not apparent in the total field (Figure 3.4). The data were plotted in Radial-East-North coordinates under the assumption that a radial component is necessary for the waves to access the spacecraft. Within BX, the identified signal intervals are use to plot the power spectra for the transverse and compressional directions. It is clear from Figure

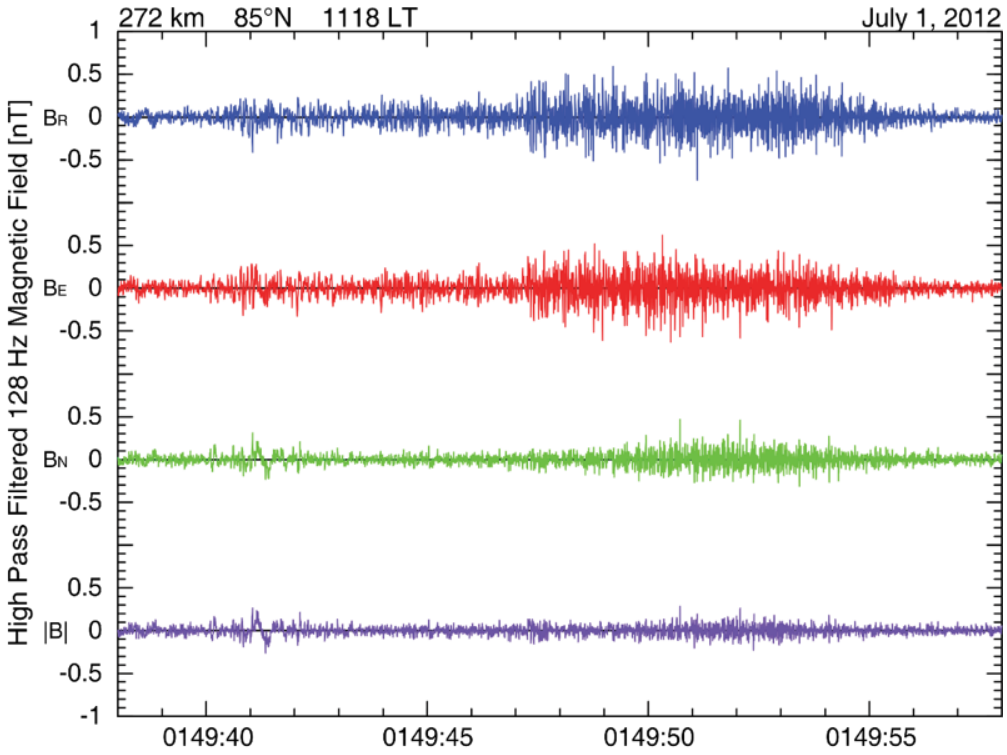

Figure 3.4: Waveform of a whistler signal on 2012-07-01. The wave is propagating nearly along the the North direction (BN) with the wave signal mostly in the radial (BR) and East (BE) components. Signals were initially identified by looking for two components with significant wave activity that was not strong in the total field, signifying a transverse wave.

3.5 that the power is predominantly in the transverse direction. The criteria for selecting a wave was that the transverse power had to exceed the compressional power by an order of magnitude and span at least 20 Hz. If the criteria were met, the waveform plot and the power spectra were captured with screenshots, the start and stop times of the signal interval were logged, and then the next portion of the time series was examined. These criteria were not strict since this was done manually. Over selecting waves was not a problem because this was not the last step in identifying them. In fact, over selection helped ensure the signals were not accidentally overlooked. After parsing through all the orbits in this manner, the dynamic spectra were produced in MX (Figure 3.6). A useful feature of MX was that a

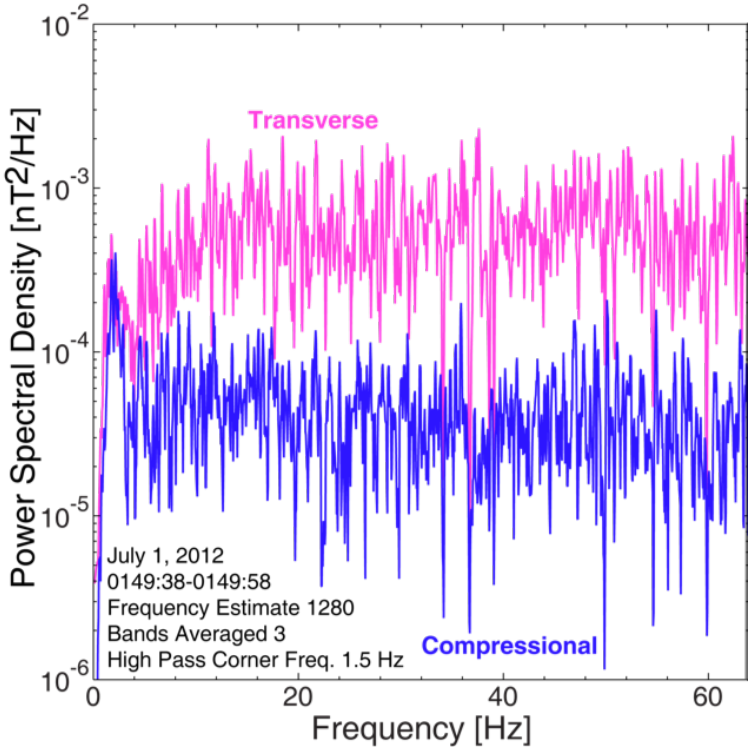

Figure 3.5: Transverse and compressional power spectra of the wave shown in Figure 3.4. The criteria for identifying a whistler-mode wave was that the transverse power had to exceed the compressional power by at least an order of magnitude for at least 20 Hz.

coherence mask could be created to filter out any signal that did not meet a certain value. For this analysis, the black portions of Figure 3.6 fell below a coherence of 0.5. As coherence is a calculation made between two axial components, all three combinations were produced and the one that agreed best with the other spectral calculations was chosen. The criteria for identifying the wave interval were that the transverse power had to be greater than the compressional power, the ellipticity greater than 0.5, and the propagation angle below 30°. Since this selection was made by eye and the smoothing on the figures was not ideal, best judgement was used to determine the start and stop times of each signal to the nearest half second. Once the list of signal intervals was complete, it was expanded by filling in between the start and stop times in 1 second steps. A signal spanning 10 seconds would contribute 10

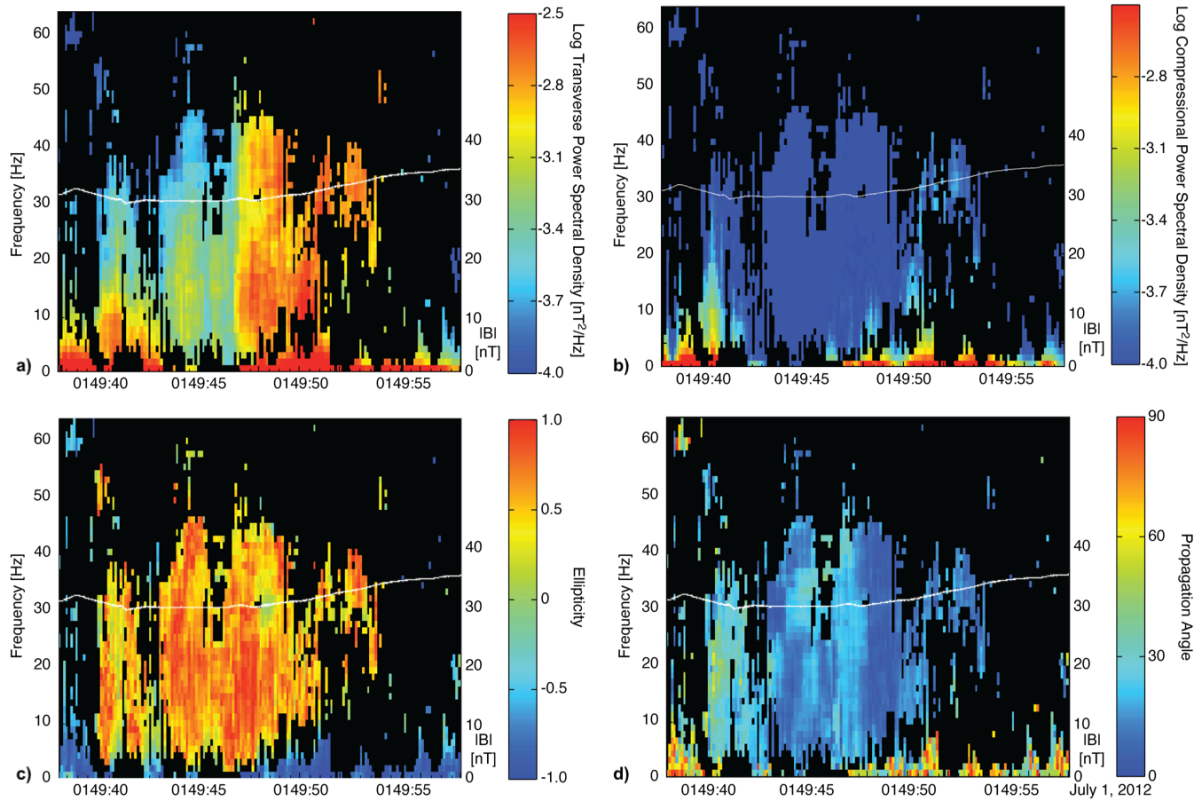

Figure 3.6: Dynamic spectra of the signal identified in Figure 3.5. The four panels are (a) transverse power spectral density, (b) compressional power spectral density, (c) ellipticity, and (d) propagation angle relative to the ambient field. The white line is the field strength in nT scaled to match the frequency axis.

records to the table along with corresponding field measurements and position information, such as altitude, latitude, solar zenith angle and local time. This completed the spectral analysis of the data and the statistical analysis could begin.

3.3 Automated signal analysis

It was later determined that an automated procedure would be necessary to develop a robust and objectively identified set of whistler-mode waves. Modules were extracted from BX and MX to be used in an automated process that produced the figures used in identifying

whistlers. This saved time since there was no need to manually use the graphical interface, but ultimately the signals were still being selected manually. Other potential options, such as SPEDAS (*Angelopoulos et al.*, 2019), would require significant reworking to be able to apply to the VEX MAG data. In the end, the prudent option was to invest time developing code from scratch to analyze the data. The first iteration of the process was written in MATLAB. It was able to successfully and efficiently produce all the spectral plots needed to identify the waves, but still lacked a routine to automatically and objectively identify whistlers. The MATLAB code was migrated to Python and some newly available methods were incorporated. Below is a description of the Python procedure.

For each periapsis, the analysis was restricted to data under 1000 km altitude, which are collected and passed into the spectral analysis routine. However, 97% of whistler observations occurred below 800 km and 76% below 400 km. As mentioned in subsubsection 2.2.4.1, the VEX 128 Hz magnetic field data contains numerous gaps; the first step of the procedure interpolates over any gaps to make the data continuous. Next, the data are rotated into field-aligned coordinates, such that the z-axis is aligned with the ambient field. A moving average of the data is used to calculate the background field, but some care must be taken when choosing the averaging window. If too many points are used for the moving average, then the field direction will not be accurate as too many points from distant measurements are included. In the extreme case where all points are used, the field becomes a horizontal line. If too few points are used, then fluctuations in the data or other wave activity will result in a wildly varying average. After examining the results from numerous smoothing intervals, it was determined that a 1 minute (7680 points) average would provide the best results for the vector rotation. Rodrigues' rotation formula, as described in subsection 2.2.2, was used to align the z-axis with the averaged field. Since whistler-mode waves are transverse, using a field-aligned coordinate system has the effect of aligning the plane of the wave along two axial components with the third component being aligned with the background field. Without this rotation, the wave power is spread across all three axes and the precision with

which any one value can be known diminishes. The analysis was performed with and without field-aligned coordinates, and the identification of whistlers increased by a factor of 3 when the rotation was included. Signals that may have fallen just short of meeting the criteria before the rotation were much more well-defined after the rotation.

Next, begins the Fourier analysis. The analysis interval was 2 seconds (256 points) and shifted by 0.25 seconds (32 points) for each step. A fast Fourier transform (FFT) is taken and the powers are calculated. The total power being the sum of the squares of the three field components. The compressional power is the square of the field strength and the transverse power is the difference of the total and compressional powers. Each power is smoothed across all frequencies with an 8-point convolution. Following the *Means* (1972) method, the cospectral and the quadrature spectral matrices are calculated:

$$\mathbf{C}_i = Re\left[\mathbf{B}_{\omega i}\mathbf{B}^*_{\omega i}\right] \qquad and \qquad \mathbf{Q}_i = Im\left[\mathbf{B}_{\omega i}\mathbf{B}^*_{\omega i}\right] \tag{3.22}$$

where $\mathbf{B}_{\omega i}$ is the i$^{\text{th}}$ frequency component of the FFT. Each set of matrices is smoothed across frequencies with an 8-point convolution. The coherence and signal-to-noise ratio (SNR) are calculated for each frequency. Note that the x- and y-components are the transverse coordinates.

$$Coh_i = \frac{C^2_{ixy} + Q^2_{ixy}}{C_{ixx}C_{iyy}} \tag{3.23}$$

$$SNR_i = \frac{C^2_{ixx} + C^2_{iyy}}{C_{izz}} \tag{3.24}$$

The wave vector $\mathbf{k}$ can be calculated from the out of phase cross powers.

$$\mathbf{k}_i = \frac{(Q_{iyz},\ Q_{izx},\ Q_{ixy})}{\left(Q^2_{iyz} + Q^2_{izx} + Q^2_{ixy}\right)^{1/2}} \tag{3.25}$$

then

$$\theta_{\mathbf{k}} = \arccos\left(\mathbf{k}\cdot\hat{\mathbf{b}}\right) \tag{3.26}$$

where $\theta_{\mathbf{k}}$ is the propagation, or obliquity, angle and $\hat{\mathbf{b}}$ is the normalized median magnetic field vector for the analysis interval. It must be stated that when using only magnetic field

data the wave vector can only be determined on a hemispheric surface. Therefore, we cannot know if the direction of propagation is $\theta_{\mathbf{k}}$ or $\theta_{\mathbf{k}} - 180°$.

Lastly, we calculate the ellipticity of the signal from the eigenvalues of the cospectral matrix. The ratio of the intermediate and maximum eigenvalues determine the magnitude of the ellipticity and the sign of Q_{ixy} determines whether the wave is polarized in a right-hand (+) or left-hand (−) sense with respect to the ambient magnetic field. Once the process has run through all time steps, we have a frequency-time grid of values for each quantity calculated. The last step is to perform a 2D smoothing by convolution over each grid. The spectra and the corresponding data are stored in a package for use in the next step of the procedure.

The next routine runs through each spectral package in search of whistler-mode waves. Four criteria for identifying the waves are defined:

$$\begin{aligned} Coherence &> 0.3 \\ Ellipticity &> 0.5 \\ Obliquity &< 45° \\ Power_{\perp} &> Power_{\parallel} \end{aligned} \tag{3.27}$$

Ideally, the coherence would be at least 0.5, but that tends to cut off the edges of the signal, so it is difficult to determine proper start and stop times. The value of 0.3 was chosen as a compromise. We chose 45° for the propagation angle in order to limit the number of false positives identified by the code, but the large resonance cone angle allows for whistler-mode propagation at even greater angles above our criterion, as discussed in subsection 3.1.1. Thus, the results in this study are a lower bound for whistler occurrence rates. These criteria must be met for at least 1 second in time and 6 Hz in frequency (∼10% of the bandwidth) in order to be considered a valid signal. A binary matrix is constructed from these criteria and contours are drawn around all identified waves. The contours are overlaid on the plots of the spectra that are produced at the end of the routine (Figure 3.7). The signal in the 30 – 40 Hz band of Figure 3.7 is due to noise from the reaction wheels on the spacecraft.

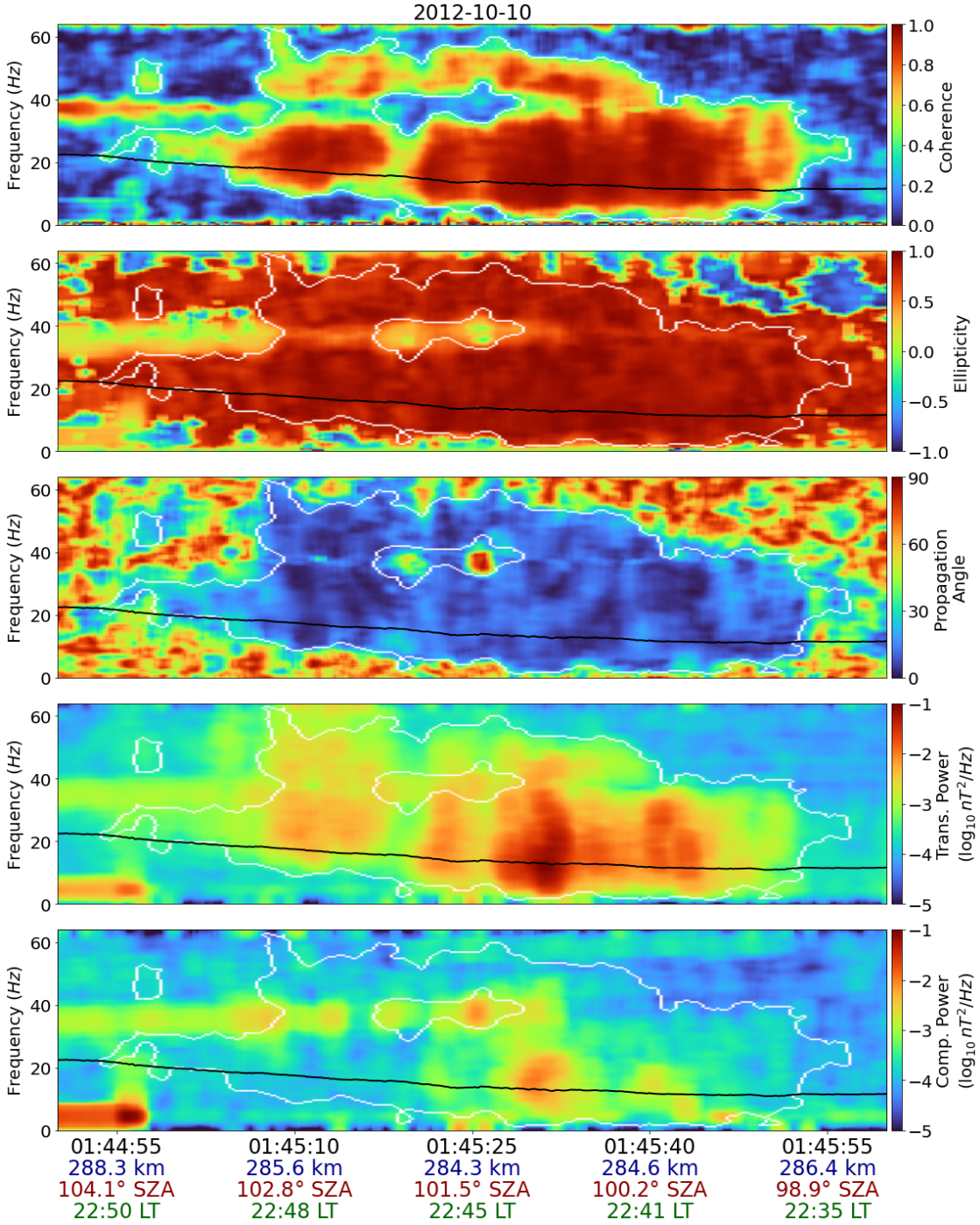

Figure 3.7: Dynamic spectra of coherence, ellipticity, propagation angle, transverse and compressional powers highlighting the criteria used to identify whistler-mode waves in this study. The white contour is the outline of the signal. The black line is the magnetic field strength with nT on the same scale as Hz.

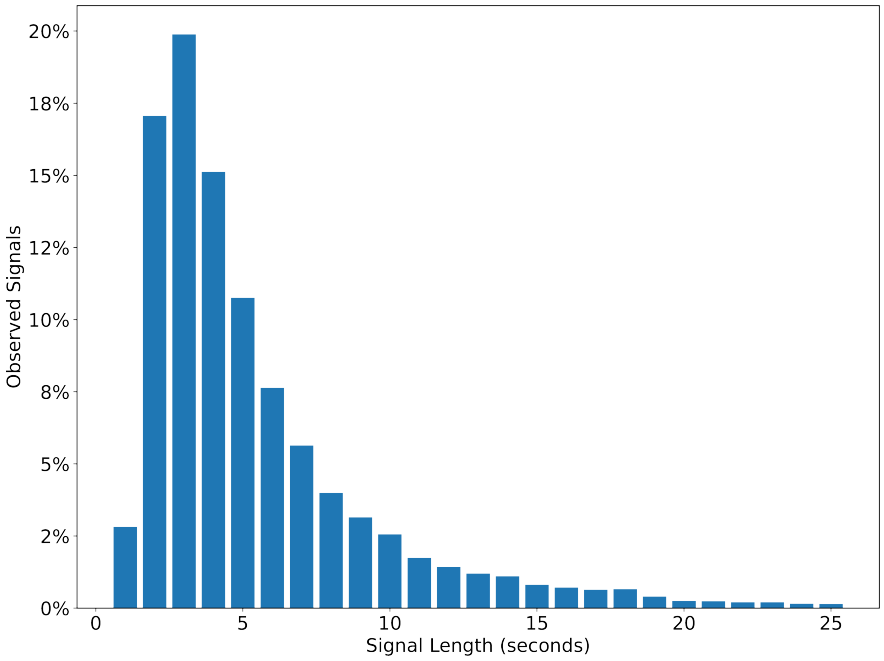

Figure 3.8: Occurrence rate of whistler-mode waves as a function of signal length. A signal is defined as a whistler-mode wave if it spans at least one second and is separated from other signals by at least one second. Signals observed for more than 25 seconds account for only 1.5% of all signals. The longest continuous signal is 140 seconds.

The cleaning procedure was unable to identify and remove those artifacts. Each second of the signal interval between the start and stop times is logged in a table. The table contains 23 measured and derived quantities for every second of whistler activity identified in the data. The dynamic spectra for each orbit are manually scanned and compared with the start and stop times of the signals to rule out any false positives. The false positive rate is low ($\sim$1%), but it is still necessary to remove them for a robust statistical analysis.

A unique signal is defined as being at least one second long and separated from any other signal by at least one second. The signal lengths range from one second up to 140 seconds (Figure 3.8). However, signals longer than 25 seconds account for only 1.5% of all signals. Whistler-mode waves are short bursts, typically under one second, so we interpret the longer signals as periods when the spacecraft was magnetically connected to a region

above an electrical storm. A continuous signal is actually a wave train lacking the resolution to distinguish between any particular burst. Ducted whistlers span the frequency range of $\sim$10 – 50% of the local electron gyrofrequency, but since the VEX magnetometer only resolves signals up to 64 Hz, much of the signal cannot be observed.

CHAPTER 4

Statistical Analysis

4.1 Occurrence rates

The automated spectral analysis procedure cataloged 61,690 seconds (∼17 hours) of lightning-generated whistler-mode wave activity in the ∼8.5 years that Venus Express was in orbit. About 13 cumulative hours of signal detections were below 400 km altitude. The number of signal detections means nothing without some sort of normalization, so we define the percent occurrence rate of signals as the number of seconds of detections in a given bin divided by the total amount of time the instrument observed in that bin. There are a total of 614 hours of high resolution magnetometer measurements over the whole mission. To avoid any effects from statistics of low numbers, we assert that there must be a minimum of 5 minutes of measurements in a bin for it to be considered in the statistics. About half of the signals were observed when the spacecraft was between 200 to 300 km altitude with an occurrence rate of 7% averaged over all local times (Figure 4.1). All detections are within the ionosphere, so the higher altitude observations occurred beyond the terminators toward the nightside. The dayside ionopause of Venus rarely exceeds a few hundred kilometers in altitude. At solar zenith angles of 90°, the ionopause is 700 – 1000 km. At the lowest solar zenith angle observations in this study (51°), the ionopause is at approximately 550 km altitude. In order to

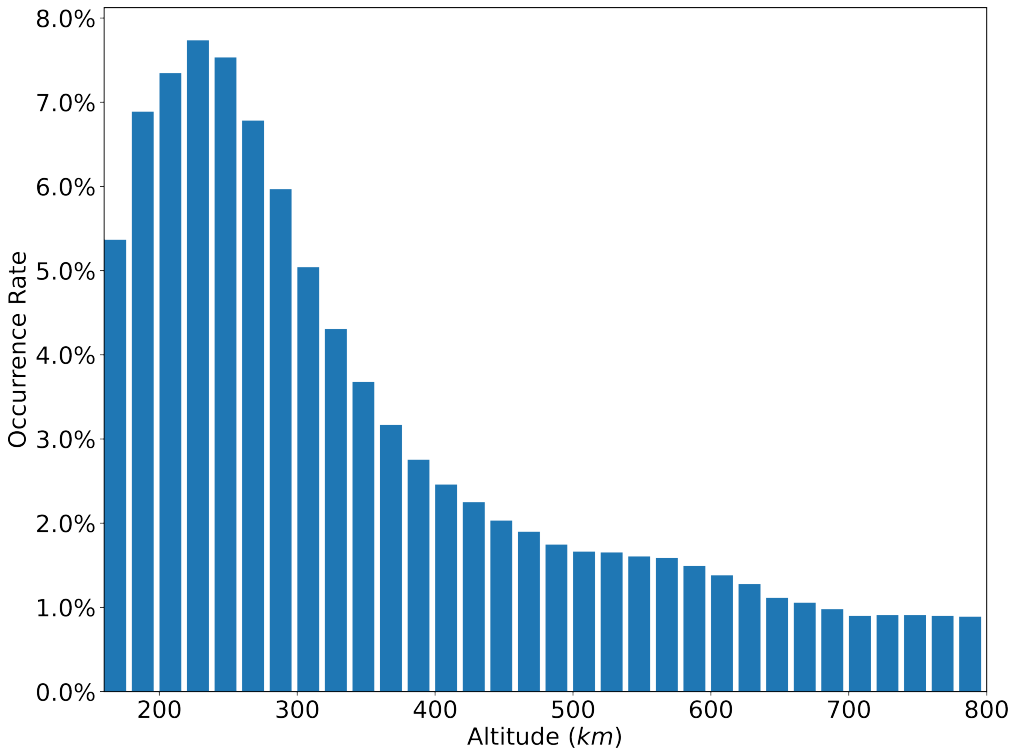

Figure 4.1: Occurrence rate of whistler-mode waves as a function of altitude. Because we are searching for low altitude waves, we restrict our analysis to observations below 400 km.

compare all local times fairly, including orbits with an unusually low ionopause, we restrict our statistical analysis to observations below 400 km. Figure 4.1 and Figure 4.2 illustrate that this is a reasonable altitude for an upper limit. The figures highlight that the whistlers are predominantly observed at low altitudes in the ionosphere by a significant margin. For the first two years of the mission, the spacecraft periapsis (white dots in Figure 4.2) remained above 245 km altitude. Therefore, VEX did not sample from a significant portion of the most active altitude range. In contrast, from mid-2008 through most of 2009, the periapsis never exceeded 215 km altitude. These consistently low altitude periapses facilitated the most abundant whistler observations of the mission. It should be noted that the statistical plots in this study are created with overlapping bins, which has the effect of smoothing the histograms without changing the overall result. There are some edge effects which can be ignored, such as data appearing to be sampled below periapsis.

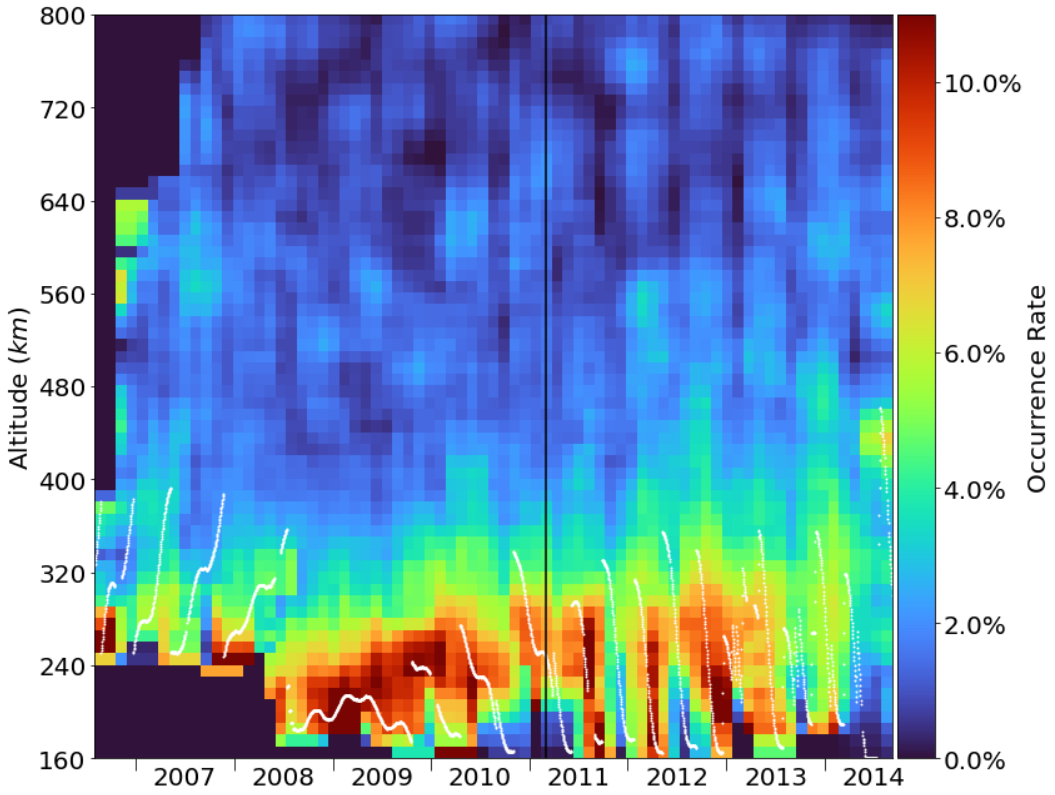

Figure 4.2: Occurrence rate of whistler-mode wave observations as a function of altitude and time throughout the mission. The white dots are the periapsis altitudes for each orbit. The vertical black line separates the solar minimum and solar maximum periods. During the first two years of operation, VEX did not descend below 245 km in altitude. From mid-2008 through most of 2009 the periapsis altitude remained below 215 km. The bins are overlapped for smoothing purposes, so edge effects make it appear as though measurements were made below periapsis.

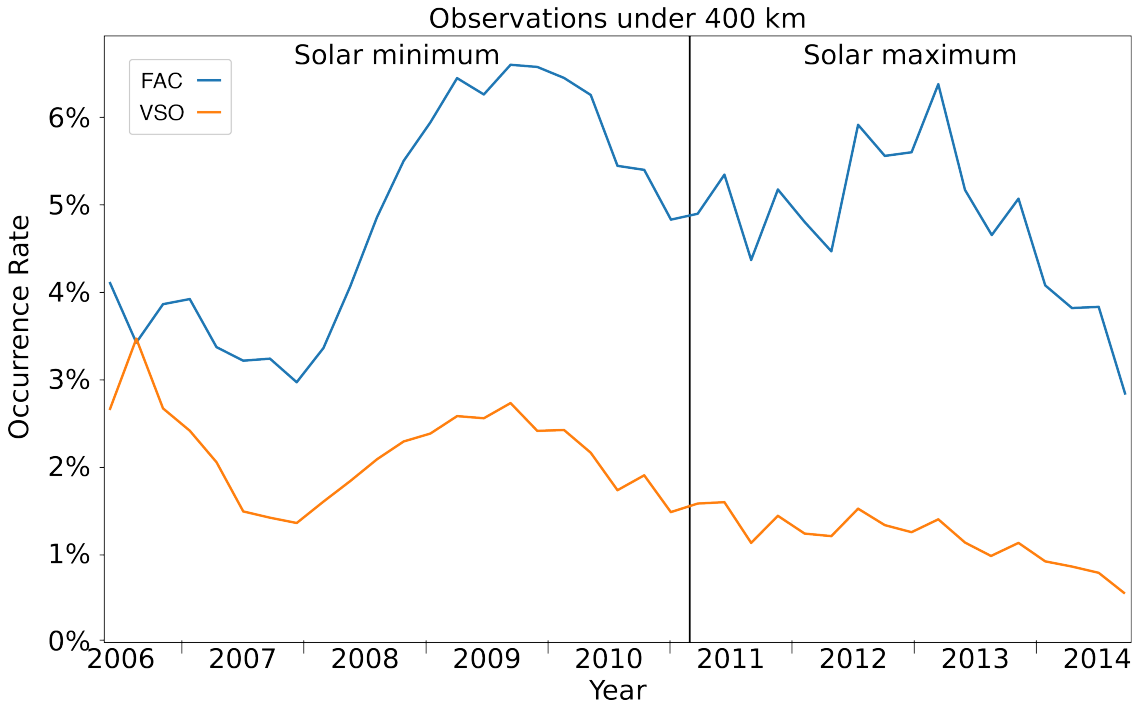

Figure 4.3: Histograms of occurrence rates of whistler-mode waves throughout the VEX mission. The blue curve are the rates when the data were rotated into field-aligned coordinates (FAC) before the wave analysis. The orange curve are the rates when the data were analyzed in VSO coordinates. The vertical black line separates the solar minimum and solar maximum periods. The lower rates in the early mission are due to lack of low altitude observations, below 245 km (see Figure 4.2).

4.2 Solar cycle influence

Venus Express was in orbit for ∼80% of a solar cycle, so we were able to see the effects that solar activity had on whistler-mode wave observations. When we first performed the wave analysis without rotating into field-aligned coordinates, we thought the occurrence rates showed an anticorrelation with solar activity as shown in the orange curve of Figure 4.3. The black line separates the two solar periods. It denotes the time of the median of the solar EUV during the VEX mission. The orange curve does not appear as pronounced as when we

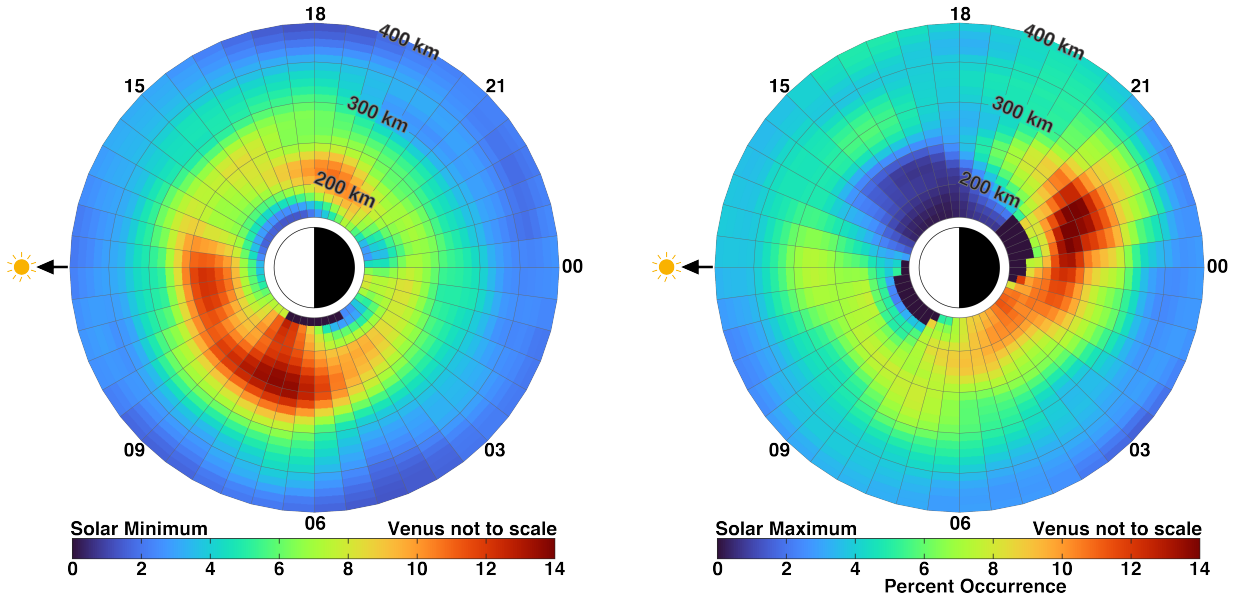

(a) (b)

Figure 4.4: Percent occurrence of whistler-mode wave observations as a function of altitude and local time (a) during the solar minimum period and (b) during solar maximum.

analyzed the data because we had to expand the scale to include the the blue curve. Again, the low rates in the beginning of the mission are due to fewer low altitude measurements. Once we reprocessed the wave analysis in field-aligned coordinates, it became clear that the solar cycle had little to no influence on the overall occurrence rates. The solar minimum and solar maximum periods produced occurrence rates of 5.4% and 5.0%, respectively. However, the spatial distribution of the waves was quite different for the two periods. Figure 4.4 shows the occurrence rates of whistler detections as a function of altitude and local time, split into the solar minimum and solar maximum periods. During high solar activity, the solar EUV intensity is high and produces a relatively dense ionosphere. The resulting strong induced currents limit the IMF that penetrates the ionosphere. During low solar activity, the ionospheric currents are weaker and the IMF is more likely to penetrate the ionosphere and connect to the atmospheric entry point of the whistler-mode waves.

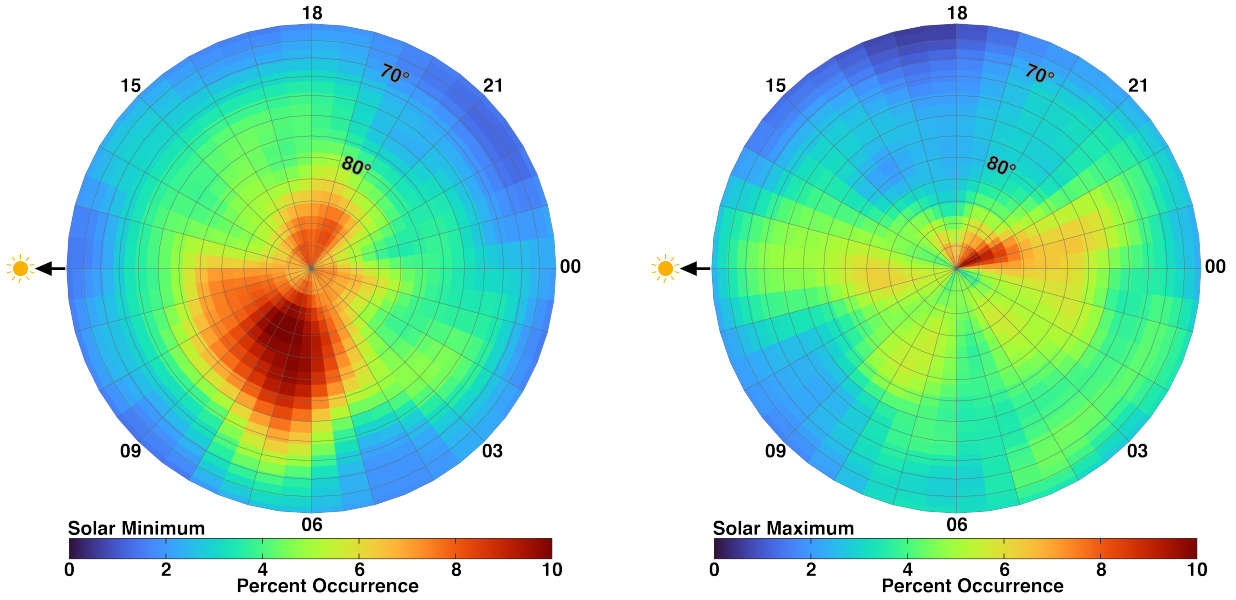

(a) (b)

Figure 4.5: Percent occurrence of whistler-mode wave observations as a function of latitude and local time (a) during the solar minimum period and (b) during solar maximum.

During solar minimum, the maximum occurrence rates are between 0600 LT and 1200 LT. This strong peak is due to the field configuration and not necessarily because more lightning occurs near dawn. The dawn peak is a result of a strong B_Y component in the magnetic field. *Dubinin et al.* (2014) demonstrated that whether there is a positive or negative y–component in the IMF, it will result in positive B_Y for low altitudes in the ionosphere. The negative B_Y IMF rotates toward the positive B_Y direction while a positive B_Y IMF will adjust its geometry over the pole such that the draping effect is reduced and B_Y becomes even stronger. In both cases, the rotation results in more waves being ducted toward dawn. Additionally, *Villarreal et al.* (2015) showed that a buildup of the field occurs at high northern latitudes near dawn when the ionosphere is magnetized and there is a significant positive y–component to the field. This build up is due to an asymmetry in the plasma flow from the subsolar point to the poles caused by the mass difference between ion species. During solar maximum,

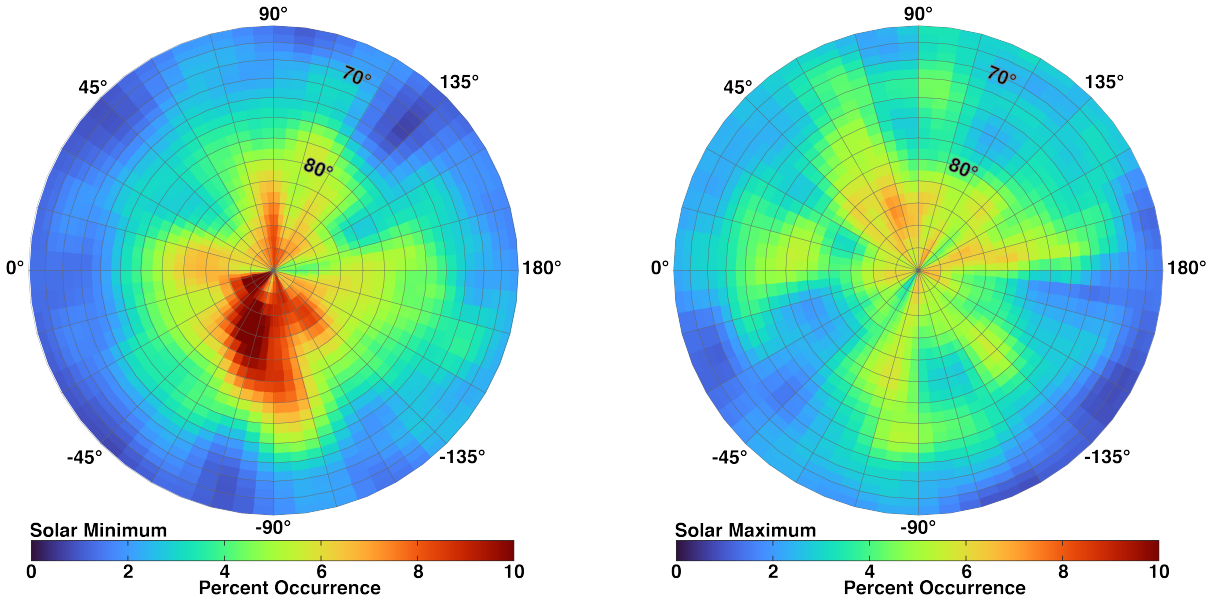

(a) (b)

Figure 4.6: Percent occurrence of whistler-mode wave observations as a function of latitude and longitude (a) during the solar minimum period and (b) during solar maximum. The longitude and local time plots are similar because the length of a Venus year and a Venus day are comparable (225 and 243 Earth days, respectively).

the peak occurrence rates are observed between 200 and 300 km altitude, just before local midnight. When the ionosphere is not strongly magnetized the wave ducting is dictated by the draped IMF geometry and the majority of whistler-mode waves are detected near local midnight, guided by the increased radial component in the tail.

Figure 4.5 shows the occurrence rates with respect to latitude and local time. During solar minimum we see that the dawn peak spans 20° of latitude. The tail peak during solar maximum is also apparent, but it is concentrated near the pole. Because a Venus day and a Venus year are of comparable length (225 and 243 Earth days, respectively), local time and longitude are closely related. The two quantities drift apart by only 8% for any given period of time. Figure 4.6 shows the occurrence rates with respect to latitude and

longitude. It is clear that Figure 4.5 and Figure 4.6 are similar, but it is not immediately obvious whether local time or longitude is more responsible for the patterns in occurrence rates. *Fukuhara et al.* (2017) reported a large stationary gravity wave observed at the cloud tops of Venus that was associated with elevated regions on the surface of the planet. If longitude is controlling the wave observation rates, then the lightning rates would necessarily be associated with surface topography, possibly linked by gravity waves. The Ishtar Terra highlands are at longitudes that could be associated with the peaks in occurrence rates seen in the solar minimum longitude plot, but not at such high latitudes. A local time dependence would necessarily be influenced by the ionosphere and a longitudinal dependence would be influenced by geography. The fact that both the local time and longitude plots show significant differences from solar minimum to solar maximum suggest that local time is the more dominant variable. As discussed previously, the varying intensity of solar EUV between solar cycle periods changes the structure of the ionospheric fields. The waves are being transported toward dawn during solar minimum and down tail during solar maximum.

4.3 Poynting Flux

In order to infer the energy or the flash rate of the lightning that produces these waves we need to calculate the Poynting flux, which requires the six components of the wave electric field and magnetic field. The plasma wave instrument onboard PVO was able to measure one electric field component in an arbitrary direction. With additional plasma data and some assumptions made about the wave properties, *Russell et al.* (1989b) were able to estimate the Poynting flux of waves detected in the 100 Hz band. Assuming the waves propagated in the whistler-mode, along the magnetic field, and the measured wave electric field was perpendicular to the wave magnetic field, the Poynting flux can be calculated with

$$\mathbf{S} = \frac{1}{\mu_0}\mathbf{E} \times \mathbf{B} = \frac{1}{\mu_0 v_{ph}}\mathbf{E}^2 = \frac{n_r}{\mu_0 c}\mathbf{E}^2 \tag{4.1}$$

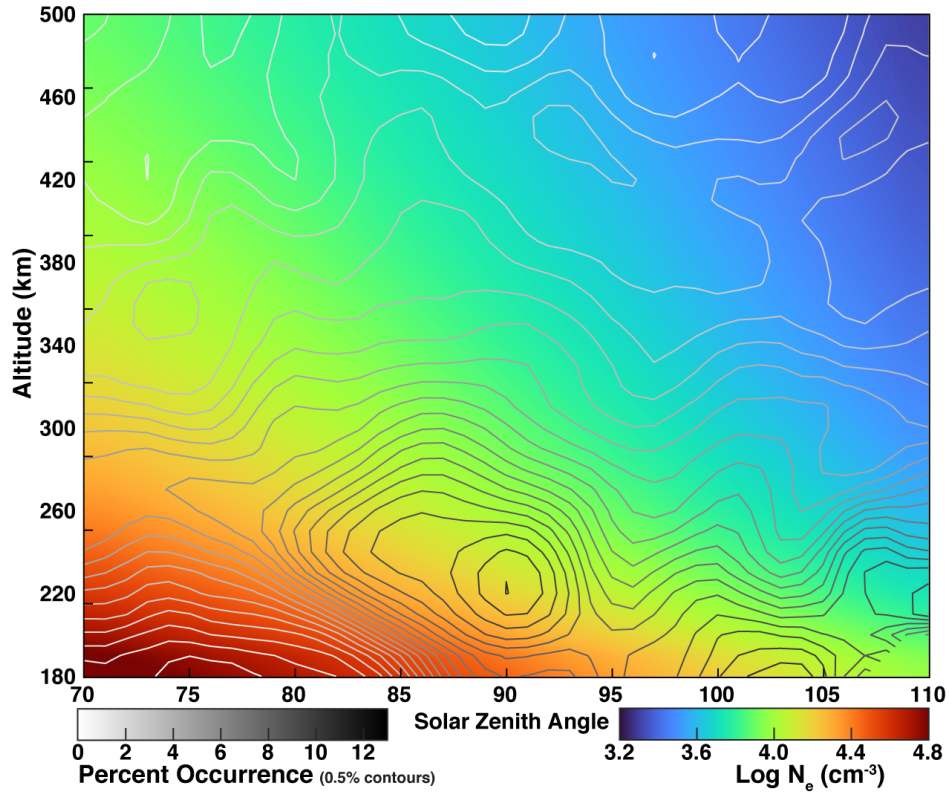

Figure 4.7: VIRA electron density model (color) and whistler-mode wave occurrence rates (contours) as a function of altitude and solar zenith angle. The electron density is calculated from the *Brace et al.* (1997) model and scaled to the median solar EUV during the VEX mission (2.318×10^{10} ph cm^{-2} s^{-1} for 0.1 – 50 nm photons).

where $\mathbf{E}$ and $\mathbf{B}$ are the electric and magnetic fields of the wave, μ_0 is the vacuum permeability, v_{ph} is the phase velocity, n_r is the index of refraction, and c is the speed of light. Their results are plotted as a function of altitude in *Russell et al.* (1989b, Fig. 3), but we have combined it with an equivalent plot from the results of this study (Figure 4.10). Since the figure includes results from this study that have yet to be discussed, the reader is cautioned about skipping ahead. Their results show little variation with increasing altitude, but if there is any change, then it's a slight damping at higher altitudes, which would suggest a source from below. As discussed in subsection 3.1.2, we lack the electric field components to calculate the Poynting flux, so we rely on the VIRA electron density model (*Brace et al.*, 1997). We

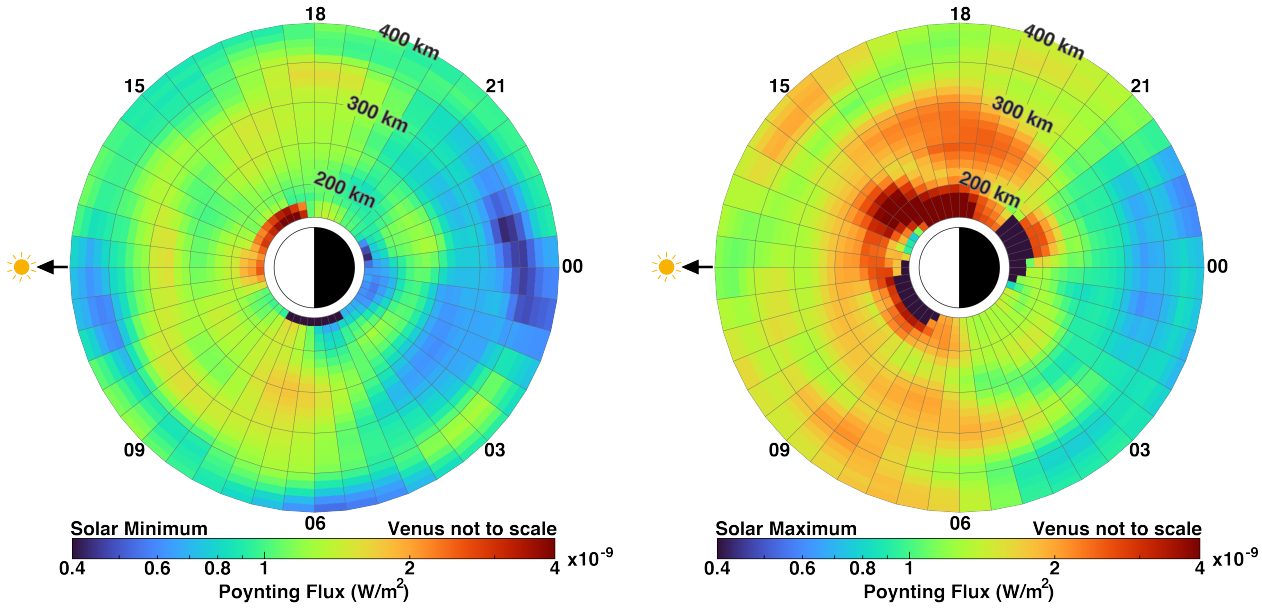

(a) (b)

Figure 4.8: Median Poynting flux of whistler-mode wave observations as a function of altitude and local time (a) during the solar minimum period and (b) during solar maximum.

don't need to assume exactly parallel propagation as *Russell et al.* (1989b) did because we know the direction of the wave vector **k**. Figure 4.7 shows the electron density model calculated for the median solar EUV of the mission overlaid with contours of whistler-mode wave occurrence rates. It is clear from the figure that whistler-mode waves in the ionosphere of Venus propagate most effectively when the electron density is $\sim 10^4$ cm^{-3}. The Poynting flux of each signal is calculated with consideration of the contemporaneous solar EUV.

Figure 4.8 shows the median Poynting flux for the solar minimum and solar maximum periods with respect to altitude and local time. Local time is represented as a clock with noon to the left and altitude is radially outward. Figure 4.9 is the same except as a function of latitude and local time. Because the wave ducting is better on the nightside during solar maximum, a greater abundance of low energy waves are able to propagate to the spacecraft, which is why the energy flux is relatively low despite a peak in occurrence rates. The waves

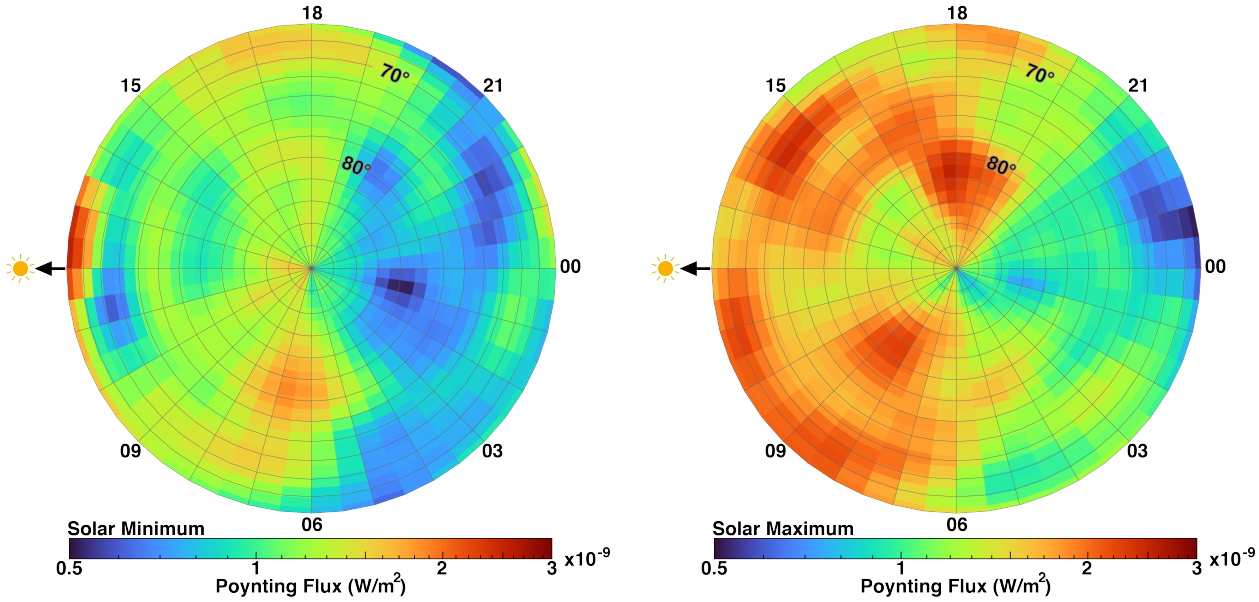

(a) (b)

Figure 4.9: Median Poynting flux of whistler-mode wave observations as a function of latitude and local time (a) during the solar minimum period and (b) during solar maximum.

are strong at low altitudes as expected for a source from below the ionosphere, consistent with these whistlers being produced by lightning. This agrees with *Russell et al.* (1989b) as discussed earlier. This conclusion is less clear for solar minimum. The improved wave ducting in the ionosphere during solar minimum allows the waves to travel further than they would otherwise. Therefore, we observe fairly well-distributed energy flux across the dayside, although the strongest waves were all observed below 350 km. The low altitude peaks just before dusk demonstrate very strong waves at the lowest altitude, however, it must be noted that these regions suffer from low statistics as is apparent in Figure 4.2.

In the *Russell et al.* (1989b) PVO study, the central Poynting flux is $\sim 6 \times 10^{-8}$ W m^{-2} (Figure 4.10), about 1.5 orders of magnitude greater than the median value from this study, 1.4×10^{-9} W m^{-2}. The median value for the peak Poynting fluxes observed by VEX is 2.7×10^{-9} W m^{-2}. While this seems to be a significant discrepancy, *Russell et al.* (1989b)

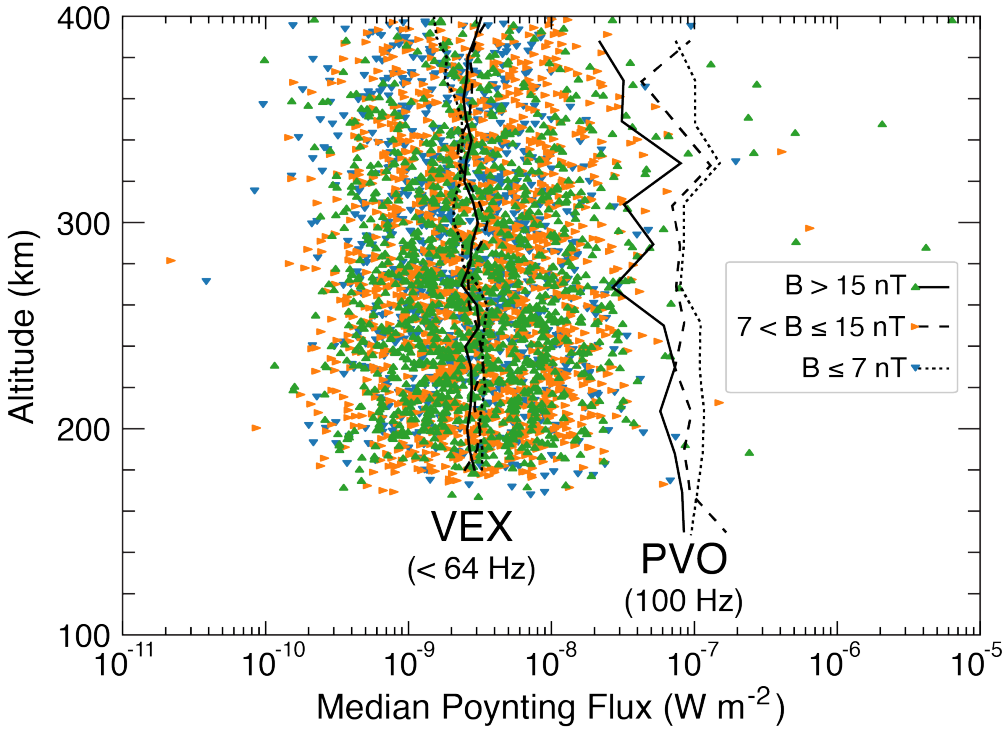

Figure 4.10: The Poynting flux values plotted in three quantiles of field strength. The peak Poynting flux for each unique signal in this study is plotted as a colored triangle: blue for low field strengths, orange for medium field strengths, and green for high field strength. The PVO data are adapted from *Russell et al.* (1989b, Fig. 3).

note that their calculations are almost certainly too high because they incorporate multiple signals due to the low instrument response time. Instrumentation has also greatly improved in the decades since PVO, so a less sensitive instrument would necessarily observe only the strongest signals. It is clear from Figure 4.11 that the energy fluxes for these whistler-mode waves span more than 4 orders of magnitude. The VEX data plotted in Figure 4.10 could easily incorporate the signals observed by PVO without significantly changing the results. The VEX observations were collected entirely over the North polar region while PVO sampled near the equator. It is possible that lightning is simply more intense near the equator where solar insolation is greatest. The more likely explanation is due to the improvements in instrumentation since the PVO era. While PVO relied on intense whistler-

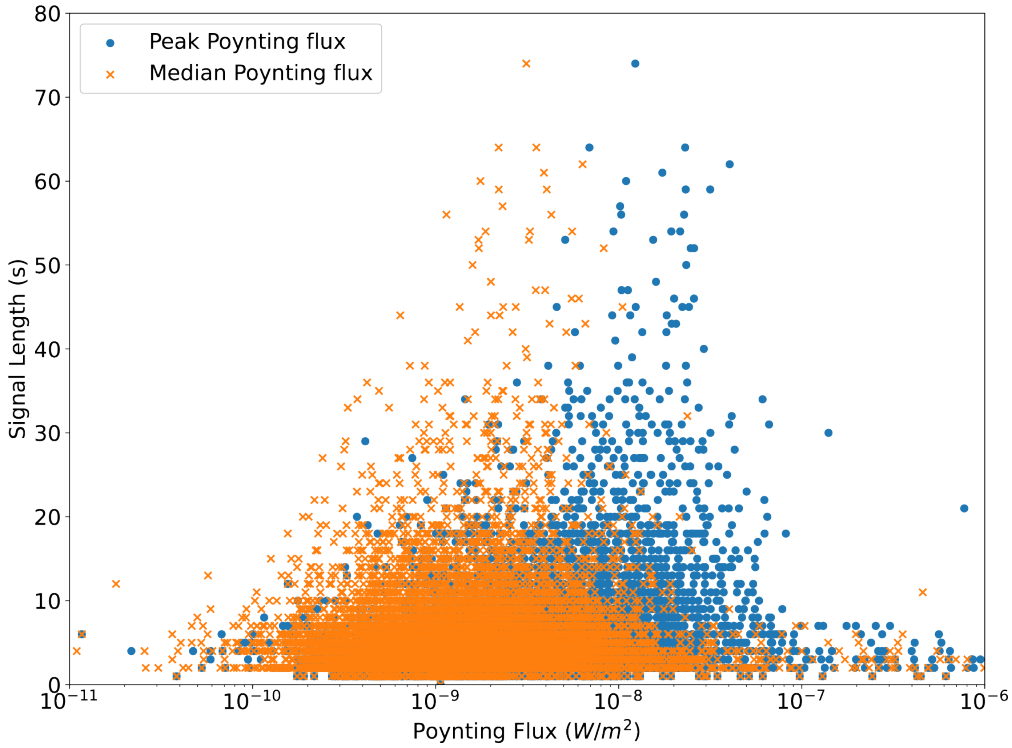

Figure 4.11: Signal length with respect to Poynting flux. The peak and median Poynting fluxes are determined within the interval of each signal observed. Signal lengths are rounded to the nearest second.

mode waves, VEX provided a more robust set of observations which includes more low energy waves. These weaker waves reduce the median Poynting flux significantly. Figure 4.11 shows the length of observed signals with respect to Poynting flux. For each signal, the median and the peak values are both plotted. For signals 30 seconds or longer, 76% of the median values are above the central value while 96% of the peak values are greater than the corresponding central value. The PVO Poynting flux values would fit well within the range of peak values from this study, but not much else can be said about the comparison without an equivalent set of statistics from PVO.

CHAPTER 5

Conclusions

5.1 Discussion

In May 2008, VEX observed whistler-mode wave activity near periapsis on 4 out of 6 consecutive orbits, which suggests that it was in the vicinity of a persistent storm. Figure 5.1 shows the power spectral density for the observations on those 4 orbits. The observations occurred just above 300 km altitude. The strongest activity was encountered on the second day (18 May) when the spacecraft was in a position that magnetically connected it to a very active region of the storm. As we are familiar with on Earth, storms have a tendency to migrate, and the location of periapsis changes slightly with each orbit, so it's no surprise that the intense wave activity was only observed on one day. While the orbit of Venus Express is predictable, thunderstorms are stochastic by nature. Thus, it is also not surprising that no whistler detections were made on the two days in the middle of the interval. The storm likely shifted to a position that was no longer magnetically connected to the path of VEX. Given the persistence of this storm, it would be interesting to see if there are any observations with VIRTIS or VMC on Venus Express that show unusual cloud structures within the region. Since whistlers don't necessarily travel radially outward, the region of interest could be vast. A search for a visual correlation with the whistler observations would not be a trivial task,

so it has not been included as a part of this study.

One of the aims of this study is to determine the global occurrence rate of lightning on Venus. We have shown that lightning-generated whistler-mode waves were regularly observed at low altitudes throughout the Venus Express campaign. Even with observations as high as 1000 km altitude, it is clear from Figure 4.2 that these waves are certainly low-altitude phenomena. During those observations, the spacecraft was magnetically connected to an electrical storm somewhere in the cloud layer of Venus. Since we cannot resolve individual whistlers in the spectra, we cannot know how many lightning flashes produce any given observation. A problem similar to the one encountered with the PVO observations. Thus, we must infer a local flash rate by other means. The magnitude of the power spectral density in Figure 3.7 is typical for signals observed in this study. Using a signal observed on 9 Jun 2006, which is discussed thoroughly in *Russell et al.* (2013), *Pérez-Invernón et al.* (2017) demonstrated that waves with peak powers of $\sim 10^{-2}$ $\mathrm{nT^2\ Hz^{-1}}$ must be produced by $\sim$100 flashes $\mathrm{s^{-1}}$. The calculation was made assuming that the total energy released by each lightning stroke is 2×10^{10} J. However, terrestrial lightning is commonly an order of magnitude lower in energy per flash. Venus lightning is likely another order of magnitude below that because the breakdown voltage is reduced in a CO_2 environment (*Robledo-Martinez et al.*, 2011). *Levin et al.* (1983) estimated 3×10^7 J from the Venera 9 observation, so it is reasonable to assume that lightning on Venus is less intense than on Earth. We take a conservative adaptation of the results from *Pérez-Invernón et al.* (2017) and suggest that at least 1000 flashes are necessary to produce the spectra in this study. Therefore, when whistler-mode waves were detected by Venus Express, the spacecraft was magnetically connected to a region producing $\sim$1000 lightning flashes per second.

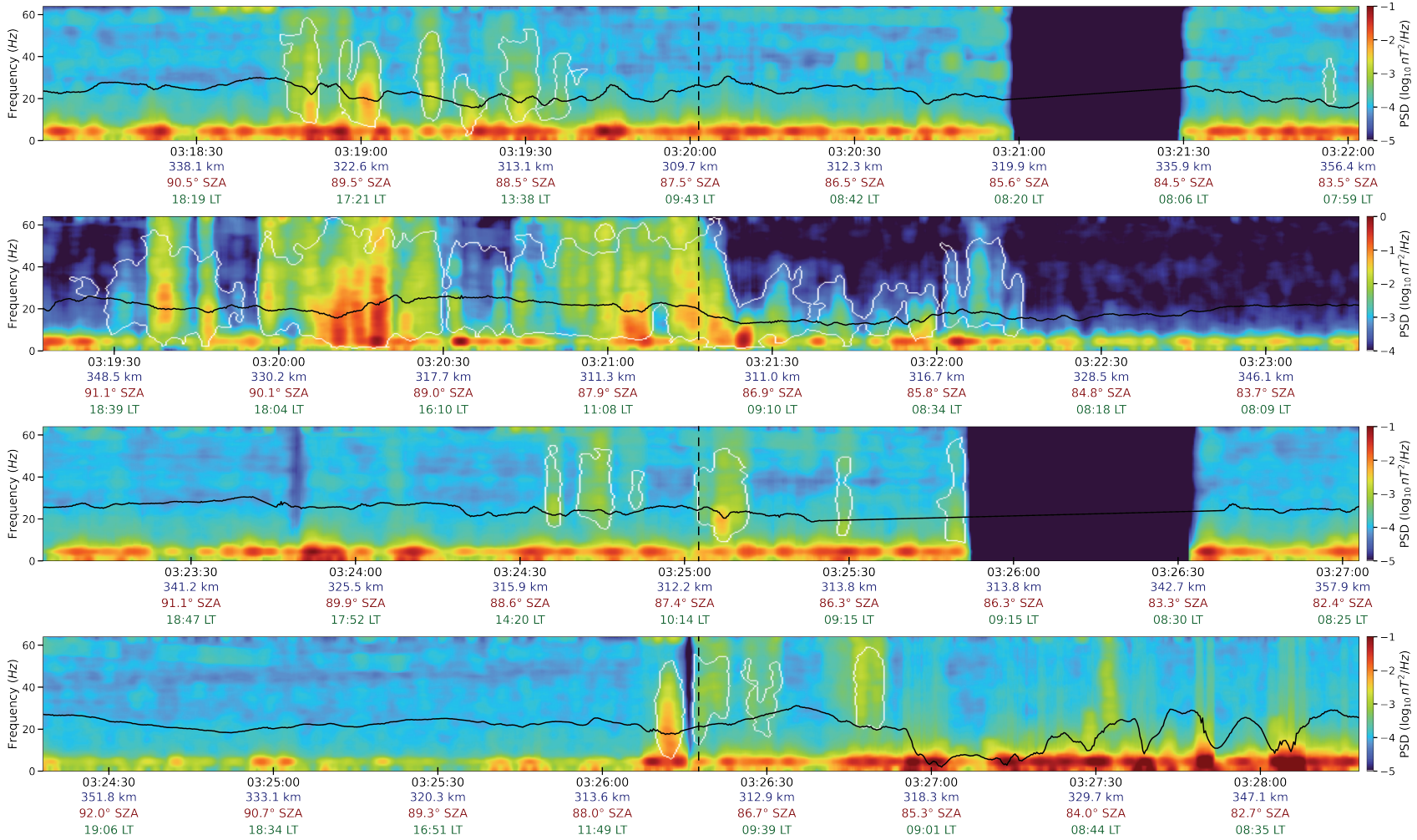

Figure 5.1: Power spectral density of apparent storm activity on Venus. The four panels span 6 days in May 2008. From top to bottom the days are May 17, 18, 21, and 22. No whistler-mode waves were detected on days 19 and 20. The white contours outlines of identified whistler-mode waves, as described in section 3.3. The vertical dashed line is where periapsis occurred. The black curve is the total field strength with nT on the same scale as Hz.

Because of the slow rotation of Venus, its global cloud coverage, and its lack of oceans, there is no reason to assume that lightning occurrence should be significantly different around any particular part of the planet. We can therefore conclude that a spacecraft in a circular orbit at 250 km altitude, such as the upcoming VERITAS mission, would likely observe lightning-generated whistler-mode waves 8% of the time on average, as Venus Express has done when at that altitude. This implies that 8% of the time the spacecraft would be connected to a source producing 1000 flashes s^{-1}, or one could say 80 flashes s^{-1} within the spacecraft's spatial observation window. The observation window scales with the distance a typical whistler-mode wave travels before being observed, which is not well-characterized at Venus. We resort to a very conservative estimate in order to obtain a lower limit of global lightning occurrence on Venus. If we estimate that the average whistler-mode wave travels no more than 60° around the planet from its source before being detected, then the observation window would be 25% of the planet's surface. Again, invoking the assumption that lightning is ubiquitous on Venus, we can extrapolate a global lightning flash rate of ∼320 s^{-1}.

Since these are low altitude observations, it is more likely for these signals to be observed closer to their sources, so the actual flash rate could be much greater. Using the lower limit for optical detections calculated by *Borucki et al.* (1981), *Levin et al.* (1983) determined that dimmer lightning strokes with energies similar to those observed by Venera 9 would need to produce 85 flashes km^{-2} $year^{-1}$ in order for the PVO star sensor to achieve a signal-to-noise ratio greater than unity. 85 flashes km^{-2} $year^{-1}$ is equivalent to a global flash rate of 1240 s^{-1}, which is comparable to the results of this study if we assume the waves are observed 30° from their sources on average instead of the more conservative 60°. Compared with the terrestrial global flash rate of 44 ± 5 s^{-1} (*Christian et al.*, 2003), the global occurrence of Venus lightning that we have estimated is an order of magnitude greater than lightning on Earth. Terrestrial lightning occurs predominantly over land with an average land/ocean ratio of ∼10:1 (*Christian et al.*, 2003). Having no oceans, Venus has more than 3 times the land area as Earth does in addition to global cloud coverage. It is not unexpected that

the global rate of lightning on Venus is higher than on Earth, although possibly an order of magnitude less intense on average.

5.2 Future Work

There are no publications that report studies of VEX whistler-mode wave observations in the ionosphere of Venus outside of the Chris Russell research group. This is likely due to the unavailability of cleaned 128 Hz MAG data, which we have recently submitted to PDS for public accessibility (*Russell et al.*, 2022). Being the only group to pursue this research meant that this study could go in any direction it needed to without infringing upon other researchers. As such, there were numerous diversions into side projects, which were not carried out to completion. They either became too large or it didn't seem like they would amount to something worth the time invested. One example of the latter is the audification of signals. This process has been demonstrated to be useful and has often been used for terrestrial and Jovian whistlers (*Alexander et al.*, 2014). The frequency range of whistler-mode waves at Earth ($\sim$1 – 10 kHz) happens to overlap with the hearing range of humans (20 Hz – 20 kHz), so the descending tone "whistling" is very apparent. The highest frequency that VEX MAG could detect was 64 Hz, essentially at the lower limit for detection by the human ear. Since this is also the lower end of the whistler frequency range in the Venus ionosphere, we don't see much structure in the waves. Therefore, once converted to audio, the waves simply sound like noise. Perhaps with a future mission we can obtain higher frequency data and revisit this topic. The rest of this section summarizes the topics that were envisioned in this study, but not undertaken.

5.2.1 Schumann resonances

This research project began with the intention of searching for Schumann resonances at Venus (subsection 1.3.2). It quickly evolved into the whistler-mode wave study presented

herein before any Schumann resonance investigation took place. Given that the Schumann resonance probes the surface to depths of ∼40 km (*Simões et al.*, 2008), it can serve as a divining rod for subsurface water content (hundreds of ppm H_2O) and help in determining the lithospheric composition (*Grimm et al.*, 2012). The resonances should be detectable by VEX in the MAG frequency range that we have used for our whistler investigation. We have not performed a dedicated search, but we do have a catalog of spectral plots near the periapsis of each orbit. A brief scan of the existing spectra did not reveal any obvious signs of Schumann resonance, but this is likely due to insufficient resolution. The spectra were produced based on the criteria we defined for the whistlers. The plots have 0.5 Hz frequency resolution and 0.25 second temporal resolution. The Schumann resonance at Earth tends to occupy very narrow frequency bands that would be engulfed by noise without the proper resolution. By analyzing longer intervals of data, we can increase the frequency resolution and determine if the Schumann resonances actually exist in the data. The code already exists, but the improved resolution would increase the processing time from weeks to months without the aid of a supercomputer. The study is worthwhile, but not feasible as a side project.

5.2.2 Earth and Mars

Thorough studies of whistler-mode waves in the near-space environment of Earth have been conducted, including numerous statistical studies. A global statistical study at Earth that incorporates the wealth of field and particle data from the many spacecraft in orbit would be interesting and beneficial to the terrestrial community, but perhaps not immediately impactful on Venus studies. However, replicating our study at Earth with the same limitations would allow us to compare the lightning-generated whistler propagation between the two planets. The greatest hurdle would be accounting for the considerable differences in magnetospheres. The field structure at Earth is more conducive to entry into the ionosphere, but if we can develop a means of normalizing that, then we could directly compare the Earth and Venus results. The rate of whistler observations at Earth compared with the lightning rate

would provide great insight into the accuracy of our flash rate calculation at Venus, more specifically, the accuracy of our assumptions in the calculation.

In addition to replicating the whistler study, it would be of great benefit to do a statistical study on the types of VLF observations that Cassini saw during its flyby of Earth. *Gurnett et al.* (2001) came to the conclusion that the Venus lightning rate must be orders of magnitude below the terrestrial rate because Cassini successfully detected lightning emissions at Earth, but not at Venus. However, we don't know how often that a spacecraft would observe the same rate as Cassini on any given flyby. If the rate is relatively constant, then the argument of *Gurnett et al.* (2001) holds water, otherwise it may be that lack of detections at Venus was just unfortunate timing.

There are no reports of ELF or VLF emissions from lightning on Mars, but that does not necessarily mean they don't exist. Mars experiences global dust storms that can create an environment with sufficient charging to produce lightning. Mars lacks an intrinsic dynamo, just as Venus does, but in some locations it does have a significant crustal field (*Connerney et al.*, 1999). The magnetometer (MAG) (*Connerney et al.*, 2015) onboard the MAVEN spacecraft(*Jakosky et al.*, 2015) provides sampling up to 32 Hz, 25% of the VEX MAG range. Typical field strengths in the Martian ionosphere are 5 – 10 nT, not too dissimilar from Venus. A future study at Mars would come in two parts: one that replicates the Venus Express study by only using magnetic field data and the other one using all available plasma and field data from MAVEN. We have had numerous long-term orbiters and landers at Mars, so it is not shrouded in quite as much mystery as Venus. Nonetheless, lightning on Mars cannot be ruled out, especially without a comprehensive statistical study.

5.2.3 Ray Tracing

Perhaps the most useful study to pursue regarding this research is ray tracing signals to the location that they entered the ionosphere. One requirement of robust ray tracing is knowledge of the global field structure. The structure of Earth's dipole field is well understood, so

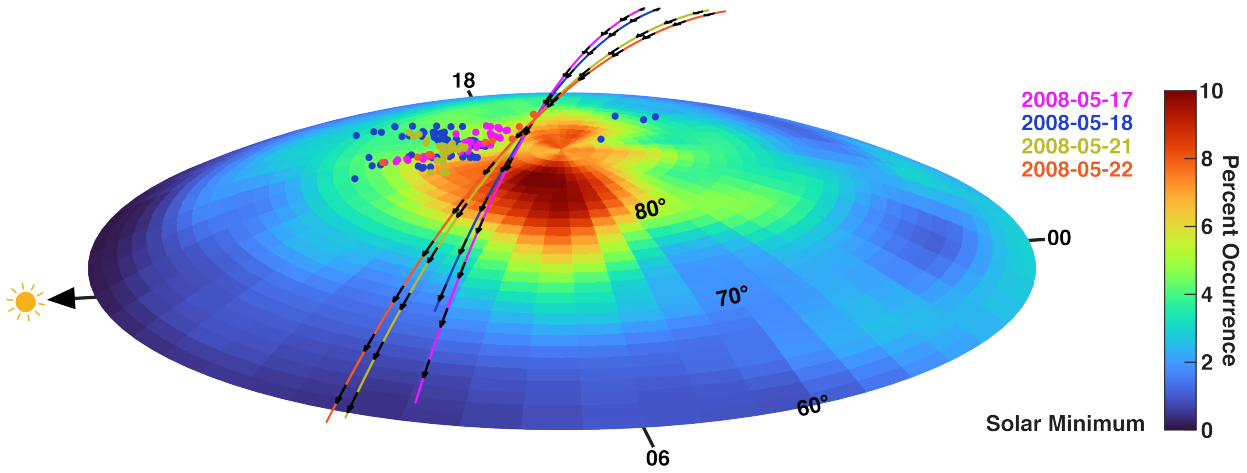

Figure 5.2: Tracks of the 4 orbits plotted in Figure 5.1. Dots are where straight-line tracings of the field from a whistler observation would intersect the base of the ionosphere. The surface color is the occurrence rate of signals as a function of local time and latitude from Figure 4.5a.

it is possible to trace terrestrial whistlers to the region in which they enter the ionosphere (*Bortnik et al.*, 2003; *Chum et al.*, 2006). In some cases, low latitude observations from the surface can be traced to storms at the conjugate foot points (*Gokani et al.*, 2015). Since Venus does not have an intrinsic dipole field, the temporal variations in its structure are much less predictable. Any changes in the ionospheric field of Venus is a direct result of a change in the solar wind. One advantage of the VEX whistler observations is that they are all at low altitudes. While terrestrial observations can be well into the magnetosphere, those in this study are close to periapsis and below 400 km. This allows us to do straight-line traces to the base of the ionosphere without too much deviation in the field direction. Figure 5.2 shows where the field line traces from observations on the four orbits from Figure 5.1 would intersect with a surface at 130 km altitude, the approximate base of the ionosphere. For many whistler observations, a straight-line tracing of the field does not intersect with the base of the ionosphere. This occurs either when the field is mostly horizontal or when the spacecraft is at higher altitudes. In the former case, the field is either highly variable

in time or the wave entered the ionosphere far from its source. The dayside field is mostly horizontal to the surface, so a wave is less likely to enter the ionosphere at the zenith of its source. It is more likely to enter at angles toward the horizon, where the field lines and wave path are more aligned. The same argument can also be made for the higher altitude cases, but there is also the possibility of more variations in the field with increasing altitude.

To trace these signals accurately requires more assumptions to be made about the structure of the field and a technique that does not require a dipolar field, such as that provided by *Kimura et al.* (1985) and *Bortnik et al.* (2003). The code from the latter study can be adapted for use at Venus with a model of the magnetic field, such as that developed by *Ma et al.* (2013) (J. Bortnik, personal communication, 2017). This model includes solar wind effects, but omits transient events, such as CME's. Instead of a straight-line tracing, as in Figure 5.2, we will ray trace the full whistler paths to the base of the ionosphere. We assume that in the brief time it takes for the waves to reach the spacecraft the storm will have remained stationary and similarly active. With a complete set of ionospheric observations and a corresponding set of whistler source locations, we can determine if there is a correlation with geography, time, or other atmospheric and external contributors, such as solar EUV.

5.3 Summary

Prior to Venus Express, there had not been a plasma wave investigation at Venus for 14 years since PVO. Since then, instrumentation has improved greatly as well as data cleaning and analysis techniques. With the completion of the cleaning process of the 128 Hz magnetometer data, we were able to complete the search for whistler-mode waves in the VEX data set. We have demonstrated that these waves exhibit all the properties of lightning-generated whistler-mode waves. These waves were most frequently detected near 250 km altitude, about 8% of the time throughout the mission, which suggests a global flash rate of 320 s^{-1}. Detection of the waves was more common post dawn and above 70° latitude during solar minimum

and near midnight during solar maximum. High estimates of 10^{-9} W m^{-2} are less than previous studies with Pioneer Venus, but still within statistical agreement. They also agree with calculations performed by *Pérez-Invernón et al.* (2017). On average, the waves were strongest during solar maximum, but this is likely due to the attenuation of low energy waves without an efficient ducted path to the spacecraft. The Poynting flux is strong at low altitudes, consistent with a lightning source from below, but this conclusion is less clear during solar minimum because the waves are provided more opportunities to traverse the ionosphere. However, because the statistical analysis was restricted to below 400 km, all of the included signals were detected at low altitudes. While the radiation belts at Earth may provide the energization for whistler-mode waves, there is no known mechanism at these altitude in the Venus ionosphere that can generate them. Since the signals are observed at low altitudes, they must be produced by a source from below the ionosphere and not from one much further above, such as at the bow shock. Given the breadth of previous observations, it is clear that the most reliable method to observe lightning on Venus is through the detection of whistler-mode waves. The low number of visible observations could be due to a number of different factors, such as weaker lightning, longer pulse duration, or occurring in the lowest cloud layer, yet whistler-mode waves can propagate in great numbers to an orbiting spacecraft.

APPENDIX A

NASA Solar System Workings Grant

I began my thesis work while employed as the IT system administrator for my PhD advisor, Prof. Christopher T. Russell. As an employee, I received a discount on tuition at UCLA, which would be paid for by the Earth and Space Sciences department (ESS)[1]. My own support came from my 50% employment with the other 50% of my time being dedicated to my thesis work. I was spending nearly 75% of my time on IT work, so there was an impetus to search for funding that would allow me to commit all my time toward school. In 2015, we began submitting proposals to the NASA Earth and Space Science Fellowship (NESSF) and the NASA Solar System Workings (SSW) program. The NESSF grant would provide 1 year of support, renewable up to 3 years. The SSW grant would provide up to 3 years of support, but it could not be submitted with a graduate student as the principle investigator (PI). This created an unforeseen problem because we needed to convince the reviewers that the funding was for the student investigator and that the PI does not need any funding. After three submissions, our SSW proposal was selected in 2018, which provided the support necessary to finish my PhD. The project has evolved as new discoveries have been made, so the submitted proposal may not completely align with the current work. This appendix presents the proposal as submitted to NASA in 2017.

[1]ESS has since incorporated the word "planetary" to become EPSS.

A.0 Proposal Summary

Statement of Relevance: The Solar System Working program solicits proposals to understand the atmospheric, climatologic, dynamic, geologic, physical and chemical processes in the solar system. The proposal examines the planet-wide strength of Venus lightning as measured from 1979 through 1992 by the Pioneer Venus Orbiter Electric Field Experiment and the Venus Express Magnetometer from 2006 to 2014. While these measurements were made in the Venus ionosphere, the signals originate near 55 km altitude in Venus's upper atmosphere. This study pertains to the dynamics of the Venus atmosphere and its particulate content as well as to the chemistry of the upper atmosphere. The measurements by the two missions using different techniques will be compared to determine if the two observations provide consistent energy flux estimates and local time variations. The program also values research in comparative planetology. The proposed research takes the estimated electromagnetic energy flux calculated from the magnetic and electric fields observed by PVO and VEX and compares it with the energy flux in the analogous waves in the terrestrial ionosphere. The energy flux is important because if it is significantly greater than the terrestrial values, which is likely because of the greater heating of the atmosphere at 0.72 AU than 1 AU, the concentration of constituents that are created in the non-LTE conditions in a lightning stroke, such as NO_2, will be much greater than they are in the Earth's atmosphere. This study could then be influential in the designs of future Venus atmospheric measurements as well as giving a quantitative value for the energetics of lightning on Venus.

Science Goals and Objectives: This study aims to end the debate of whether or not there is lightning in the atmosphere of Venus. Previous studies have provided convincing evidence, but a statistical database of lightning-generated whistler-mode waves detected by Venus Express over 9 years will allow us to map the location of the electrical storms and determine the energies of the lightning discharges. Using field-line tracing techniques, we can determine the location of each burst and ultimately find any geographic correlations that may

exist. Calculating the energies of the bursts and comparing them with energies measured for terrestrial lightning will give us an estimate of the magnitude and frequency of the storms that occur on Venus and, in turn, the production rates for specific atmospheric constituents that are dependent on lightning, such as NO_2.

Methodology: We use the measurements of the dual fluxgate magnetometers on the Venus Express mission in orbit around Venus from 2006 – 2014 that are available from the European Planetary Science Archive (PSA). We identify with UCLA wave analysis routines the occurrence and amplitude of the magnetic signals from 3 to 64 Hz propagating as whistler-mode signals (right-handed relative to the magnetic field and propagating along the magnetic field). The occurrence rates, altitude profiles, and local time distribution are mapped. The propagation speed is calculated using the measured magnetic field and model electron densities. This allows a calculation of the vertical profile of the electron energy flux to determine whether the energy flux increases or decreases with altitudes. This was calculated in 1992 for the Pioneer Venus electric field data and the energy flux decreased with altitude. The comparison with these data will be threefold. Do the energy fluxes for the two missions agree quantitatively; does the wave energy decrease with altitude as expected for a source in the atmosphere; is the local time dependence the same for each data set? The comparison with the Earth will be with published terrestrial measurements. Is the Venus electromagnetic energy flux greater than or less than the energy flux in the terrestrial ionosphere for the corresponding signals?

A.2 Objectives and Expected Significance

A.2.1 A Brief History of the Investigation of Lightning in the Venus Atmosphere

Lightning on Venus has been a topic of interest since *Meinel and Hoxie* (1962) attributed the faint glow of the phenomenon known as Ashen Light to lightning. Multiple investigations

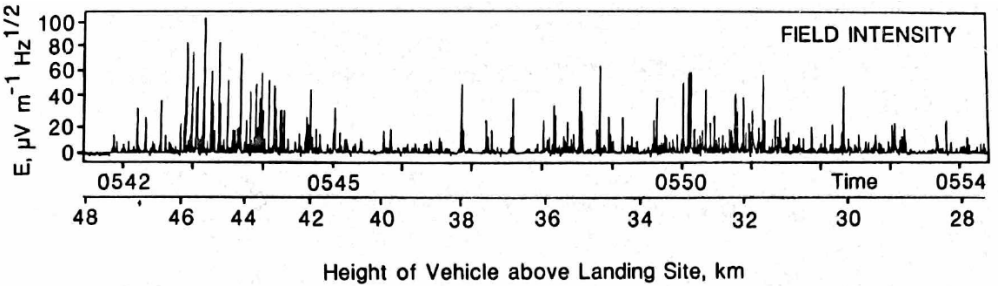

(a) High-resolution measurements of the wide band field intensity made with the Venera 12 magnetic coil antenna (*Ksanfomaliti et al.*, 1983).

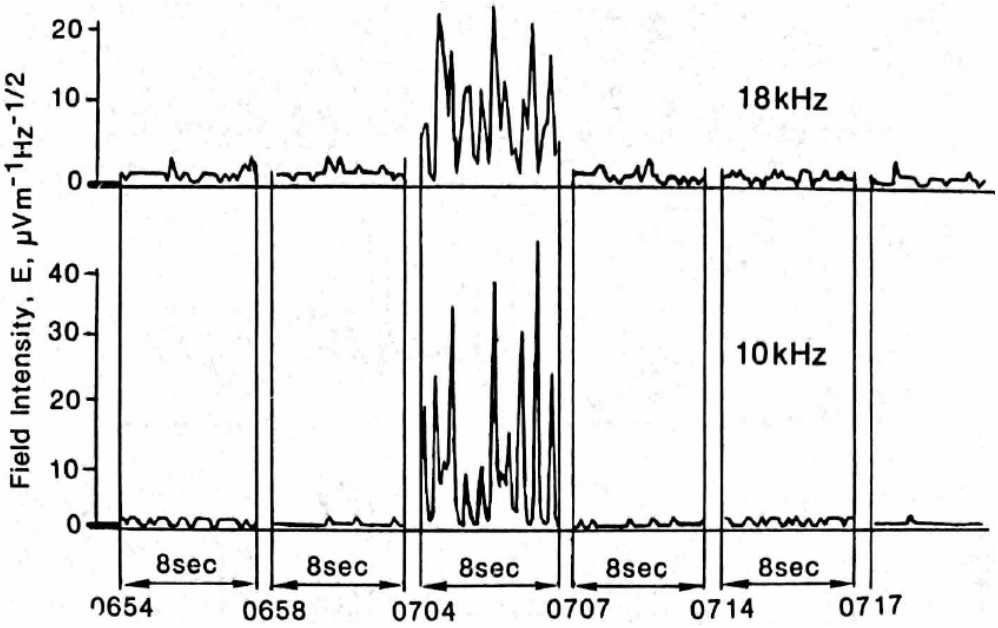

(b) Measurements of the wide-band field intensity with the Venera lander on the surface of Venus.

Figure A.1: Observations from the Venera 12 lander.

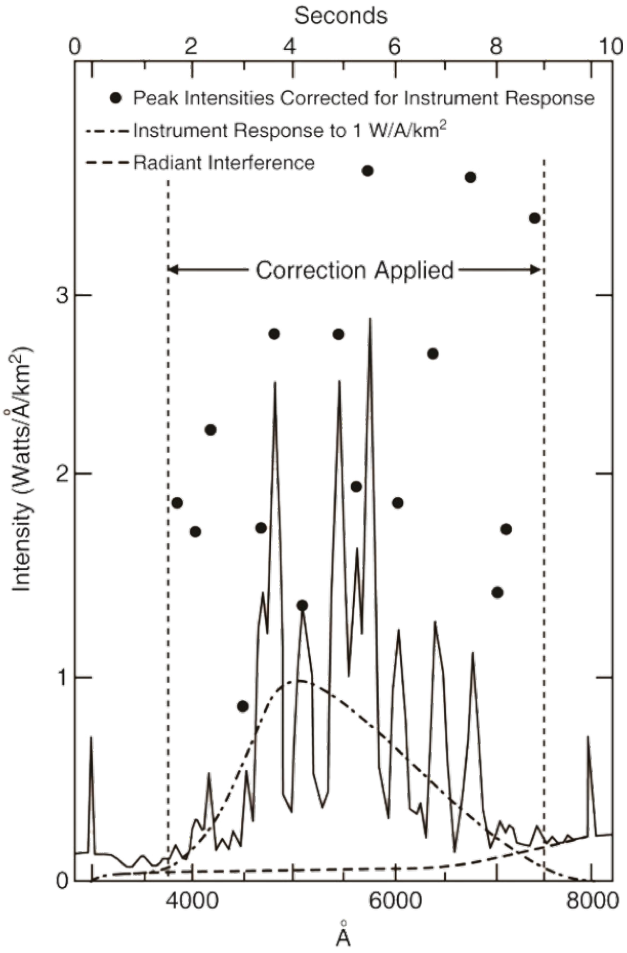

Figure A.2: Flashes observed while Venera 9 flew over the nightside of Venus. The signals are interpreted to be from a broadband source varying in time.

and observations have been made since that time. The Venera 11 to 14 landers included wire coil antennas capable of detecting the electromagnetic waves associated with lightning (*Ksanfomaliti*, 1979), and lightning was one of the objectives of the Pioneer Venus plasma wave investigation (*Colin and Hunten*, 1977). A photometer that might detect lightning was included in the Vega balloons released in the Venus atmosphere (*Sagdeev et al.*, 1986). The Venera landers did detect the expected signals, both in passage through the atmosphere and while on the ground, as illustrated in Figure A.1a and Figure A.1b.

Flashes were not observed by the Vega balloons (*Sagdeev et al.*, 1986), nor by the Pi-

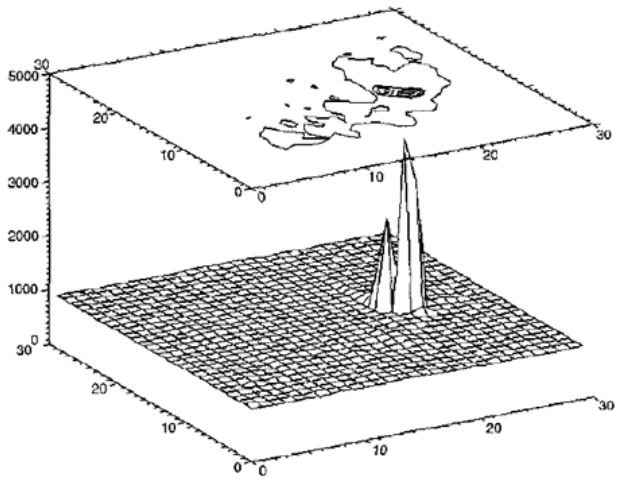

Figure A.3: A sample lightning flash seen at 777.4 nm wavelength. The multi-peak feature of the flash may be a result of pixelization (*Hansell et al.*, 1995).

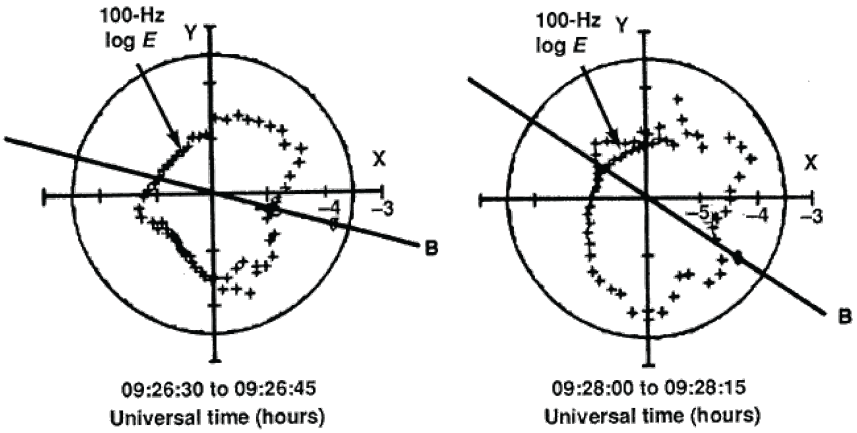

Figure A.4: The amplitude of the signals detected by the PVO electric field antenna at 100 Hz as a function of spin phase relative to the background magnetic field projected into the spin plane. This is as expected for an electromagnetic whistler-mode wave at these frequencies. (*Russell et al.*, 1988b).

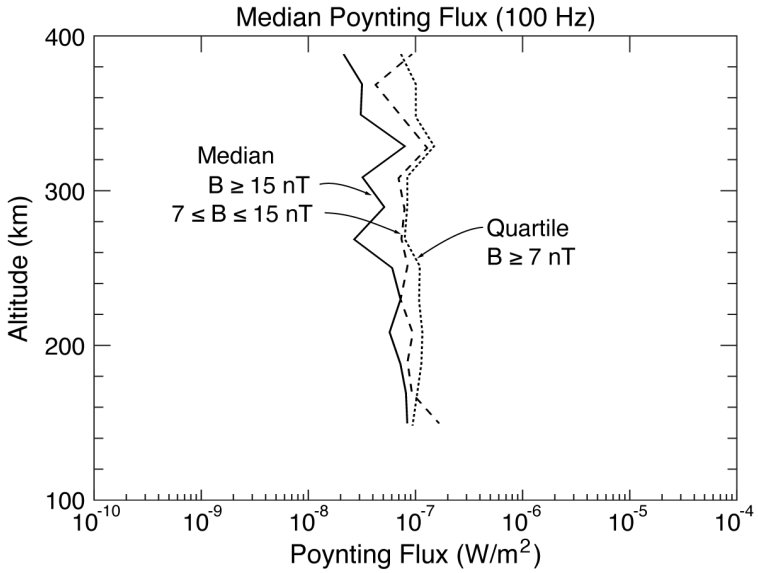

Figure A.5: Estimate of the electromagnetic energy flux in the PVO lightning signals as a function of altitude (*Russell et al.*, 1989b)

oneer Venus star sensor (*Borucki et al.*, 1991), but the observing conditions of the former (within the cloud) and the short observing times, ∼100 sec of the latter, were not favorable for these measurements. *Cardesín Moinelo et al.* (2016) were unable to find any flashes of lightning with the Visible and infrared spectrometer onboard Venus Express. This could be due to lightning occurring much lower than the cloud tops or because of the narrow observing window of the instrument. While in orbit, the visible spectrometer on Venera 9 collected optical data (Figure A.2) from an electrical storm (*Krasnopolsky*, 1983b). A terrestrial search with an Earth-based telescope (*Hansell et al.*, 1995) also reported the positive detection of lightning flashes (Figure A.3). The Pioneer Venus Orbiter (PVO) and the Venus Express mission (VEX) both reported positive detections of the electromagnetic waves produced by lightning. PVO used an antenna that was noisy in sunlight, so observations were available only in shadow on the nightside of Venus *Russell* (1993, and references therein). The waves detected by the narrow band receiver at 100 Hz were electromagnetic in nature, as evidenced by their polarization relative to the magnetic field and the control of the magnetic

field direction on the access of the signals to PVO (Figure A.4). A crude estimate of the electromagnetic energy flux showed that the energy flux decreased slowly with increasing altitude (*Russell et al.*, 1989b) (Figure A.5).

In 2006, 14 years after PVO atmospheric entry and fiery demise, Venus Express was inserted into an elliptical 24-hour orbit similar to that of PVO, providing access to electromagnetic lightning signals for a few minutes around periapsis, but with some critical differences. Most importantly, the signals were detected magnetically with fluxgate magnetometers sampling at 128 Hz providing a signal bandwidth of 64 Hz (*Zhang et al.*, 2006). While the spacecraft was not electromagnetically clean, a gradiometer configuration using two magnetometers separated by a meter allowed the detection of the whistler-mode waveforms over the full frequency band of the instrument. The spacecraft saw the whistler-mode waves at all local times, from lowest altitudes ($\sim$150 km) to over 500 km. Access to the spacecraft was again controlled by the magnetic field orientation (*Russell et al.*, 2008). The Venus Express Participating Scientist Program supported UCLA to analyze the lightning-associated measurements from the mission while the mission was still active. While it was possible to identify a small noise-free frequency band and analyze this part of the signals easily, it was very difficult to clean the entire bandwidth. It was not until 2013 that the algorithms were developed to correct the data over the entire bandwidth. We are now at the point where we have access to the entire set of low altitude data to determine where these signals were seen and how strong they were. **The first task of the proposed work will be to complete the cleaning of the 128 Hz magnetometer data.**

A.2.2 The Role of Lightning in the Chemistry of Planetary Atmospheres

A lightning discharge in a planetary atmosphere produces a rapid heating along the discharge channel that in turn produces an over-pressure of the gas. This leads not just to the thunder that we hear from terrestrial lightning discharges, but also chemical reactions that do not occur at standard conditions of temperature and pressure. An important product at Earth

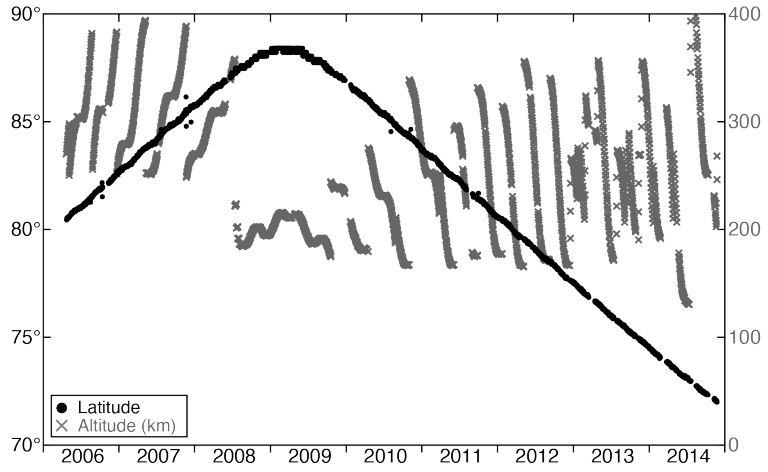

Figure A.6: Latitude and altitude variations of Venus Express periapsis. Periapsis gradually lowered from gravitational forcing, so thrusters were used periodically to raise it to higher altitudes again.

and Venus is the production of nitric oxide (*Krasnopolsky*, 1983b). An Earth-like lightning rate may be responsible for the observation that the terrestrial and Venus atmospheres have similar amounts of nitric oxide. Thus, lightning is an important process in the Venus atmosphere and its rate needs to be quantified.

A.2.3 The Contribution of Venus Express to the Study of Lightning

Venus Express provided lightning data in the form of electromagnetic wave power for the first time at all solar longitudes and over a band of frequencies extending up to 64 Hz. The measurements included three components of the magnetic field, which showed that the waves were right-handed about the magnetic field as expected for lightning-generated whistler-mode waves. They were also propagating along the magnetic field, as they should be at the observed frequencies. Because new processing software was needed to produce magnetically clean data at these higher frequencies (e.g. for the removal of reaction wheel noise), this process took several years under the Venus Express participating scientist program. However, we are now ready to produce an archive of the cleaned dataset and provide it to the community. While

all the data from the Venus Express magnetometer have been archived in the European Data Archive, we know of no other group that has developed data cleaning software for the 128-Hz data, including the group at the home of the PI, T.L. Zhang in Graz. **The main objective of this proposal is to use this new data set to further understand lightning on Venus.** While doing this, we realize our responsibility to deliver the data to either or both of the American archive (the PDS) or the European archive (PSA). This delivery will enable others to check our conclusions, a key factor in the scientific process.

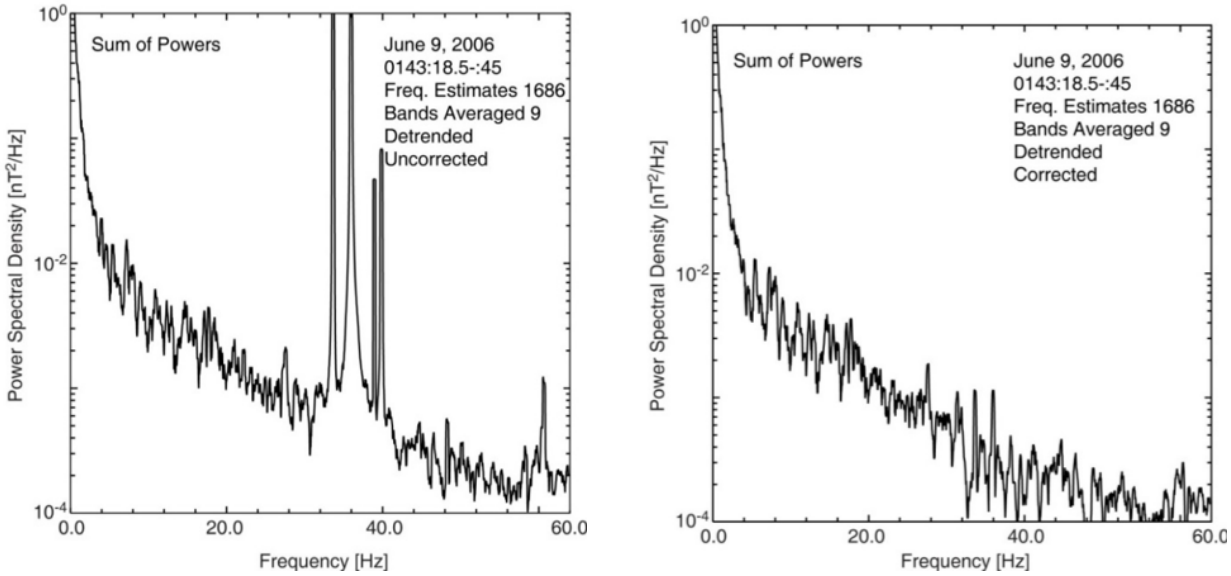

(a) Power spectrum before cleaning using the gradiometer sensor (*Russell et al.*, 2013).

(b) Power spectrum of data shown in Figure A.7a after cleaning.

Figure A.7: Power spectral density of observations of the whistler-mode band at low altitude in the Venus ionosphere.

Venus Express was in a 24-hour elliptical polar orbit for nearly 9 years, or about 14 Venusian years. The periapsis latitude ranged from 72° N to 88° N while the altitude fluctuated between 165 km and 400 km, with the exception of an aerobraking maneuver in 2014 that reached as low as 130 km (Figure A.6). The magnetometer collected data near periapsis, while Venus Express was in the ionosphere. This high-latitude, low-altitude data sampling

was complementary to the polar orbit of PVO, which had periapsis near the equator. The VEX orbit was fixed in inertial space, so the spacecraft passed through all local times over the course of one solar orbit. This enables us to tease out influences that may be due to geography versus solar activity.

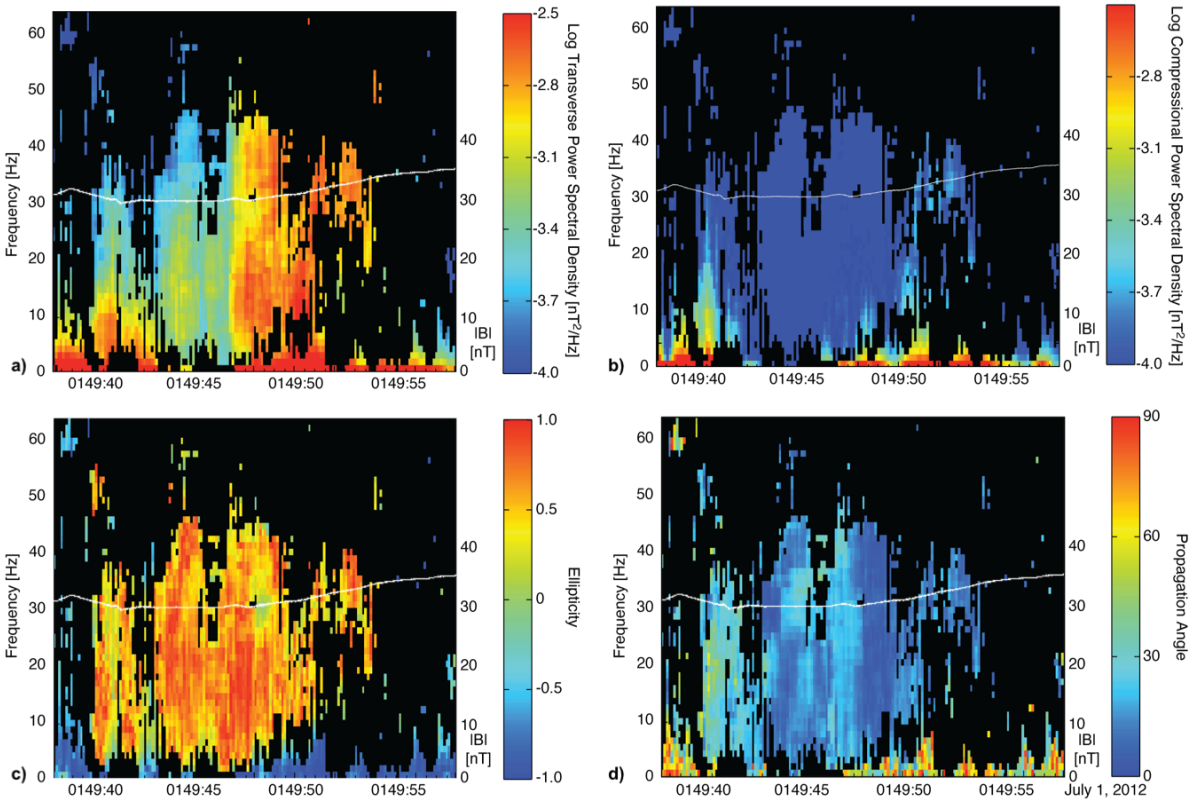

Figure A.8: (a) Transverse and (b) compressional power, (c) ellipticity, and (d) propagation angle of a wave demonstrating the criteria used to classify whistlers. White line is the total magnetic field.

Figure A.7a and Figure A.7b show a before and after pair of spectra illustrating the cleaning of the signals. The noise was likely due to the reaction wheels on the spacecraft, which spin at similar frequencies. Figure A.8a and Figure A.8b show an example of wave dynamic spectra of the transverse and compressional powers with respect to the background field, demonstrating that the wave is indeed transverse. The dynamic spectrum in Figure A.8c presents the ellipticity of the waves, where red is right-handed as expected for electromag-

netic (whistler-mode) waves at this frequency. Figure A.8d shows the angle of propagation of the waves to the magnetic field. Blue shading indicates the waves are propagating along the magnetic field as would be expected for whistler-mode waves at these frequencies. Linear waves produce the mottled regions of the spectra because their direction of propagation cannot be determined from the available data. We note the good signal-to-noise in the whistler-mode waves that have been detected. The *a*-panel shows that the waves are weaker during the first half of the signal, but the *c*- and *d*-panels show no difference in the wave properties as the amplitude drops. There is noise present at times, but the whistler waves, when present, dominate over the noise.

A.2.4 The Contribution of this Study

The data processing by the magnetometer PI, T.L. Zhang in Graz, is now complete, and the data are submitted to the archive. Some of these data would be more easily used if cleaned. We have perfected our data cleaning software so that we can now provide a complete cleaned data set for both the community and ourselves. We can now study the occurrence rates of the ELF signals as a function of solar longitude, latitude, and altitude. We need to convert the wave amplitude in nanoteslas to electromagnetic energy flux in W m^{-2} to compare with terrestrial power from lightning. We wish to develop a technique that locates lightning producing storms along the spacecraft track by determining the 'temporal' (actively spatial) change in the signal bandwidth and strength with time and use the laws of the propagation of electromagnetic signals in a magnetized plasma to establish the distance and direction to the storm. We also need to determine what measurements could be made on future Venus missions to advance the study of Venus's atmosphere. We note that the Japanese Akatsuki mission slipped into Venus orbit approximately one year after Venus Express ended, albeit not the orbit originally expected due to a failed orbit insertion in 2010, but one that should allow some of its original objectives to be pursued. One of these is the imaging of lightning flashes with the onboard Lightning and Airglow Camera (LAC). As yet, the LAC has not

seen any optical evidence of lightning, but there is still time in the mission and much data to pore through. This study would provide complementary evidence to any future observations made by Akatsuki, despite the lack of simultaneous coverage that was originally anticipated.

For the purposes of this proposal, we assume that we will, at a minimum, need to archive the data to be compliant with PDS4. If ESA is not yet PDS4-compatible themselves, we will supply PDS3-level metadata to them. The PPI node of PDS has agreed to ingest these data, and we have a letter of invitation from the head of the PPI node (R.J. Walker). We will generate a PDS archive bundle consisting of a data collection and a document collection. The data bundle consists of ASCII tables, and the document bundle contains the dataset description and the list of deliverables. The original creator of the dataset, H.K. Leinweber, is no longer with the research group, therefore the participating graduate student, Richard Hart, will handle the archive and any improvements to the data that may be required in the first year. We can ¬deliver the data and documents in the first two months of the effort, and we will resolve liens over the next several months as the data are reviewed.

A.3 Technical Approach and Methodology

A.3.1 Existing Database and Tools

The existing database is the Venus Express magnetic field archive available at the European Planetary Science Archive (PSA) together with the Venus Express Ephemeris, available from the same source. The submittal to the PSA included cleaned data for all but the 128-Hz data that contains reaction wheel noise and other strong sources of noise. UCLA already has a copy of this archive of noisy VEX fluxgate magnetometer data. We have developed software to use the gradiometer data to remove the spacecraft generated AC noise from the 128-Hz data. In this study, we work with cleaned data at the 128 Hz sample rate. To correct the data we remove the "DC" field, Fourier analyze the resulting data set, remove the coherent signal with much greater amplitude signals on the inboard sensor, and then

reconstruct the time series from the corrected Fourier coefficients and then add back in the "DC" background field. Figure A.7a and Figure A.7b demonstrate that this approach is successful. **We propose to make a complete set of "corrected" data and supply it to the European Planetary Science archive and/or for the NASA Planetary Data System within 12 months of the initiation of this study.** The examples shown throughout this proposal demonstrate this software is now working well.

When we have the complete data set, we will analyze it statistically to obtain the dependence of the occurrence rates of the whistler mode signals on altitude, local time, latitude, and solar activity. We will model wave propagation in the Venus ionosphere to determine if the time variation in the frequency-time dynamic spectra plots, such as Figure A.8, can be explained by frequency-dependent access to a single active site or storm. We will compare our results with those obtained by Pioneer Venus and with terrestrial ionospheric wave measurements on missions such as DEMETER, an Earth-borne spacecraft with a suite of instruments designed to detect magnetic and electric fields, plasma data, and particle densities. (*Parrot et al.*, 2006).

A.3.2 Proposed Tool Development

In Figure A.5, we showed an attempt to calculate the electromagnetic Poynting flux with an altitude based on the amplitude of a 100-Hz narrowband filtered electric field spectral density. To do this correctly, as we can do today with the full spectrum provided by Venus Express, we need to calculate the index of refraction, which depends on the electron density and the magnetic field strength. We have coded the wave dispersion relations for a cold plasma and made them available at the website, spacephysics.ucla.edu. On PVO, the electron density and the magnetic field strength were available, but the direction of propagation was assumed. Here we have a known direction of propagation, a known magnetic field strength, but we will have to use a model for the electron density since no measurements were taken with VEX at the altitudes observed in this study. Figure A.9 shows the Venus reference ionosphere (*Brace*

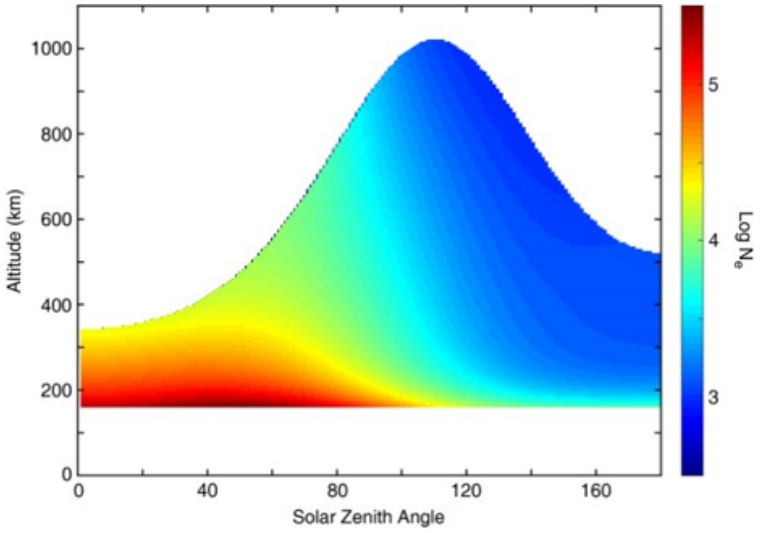

Figure A.9: The modeled number density of Venus ionosphere as a function of altitude and solar zenith angle (*Brace et al.*, 1997). We use the underlying equations from which this distribution was constructed.

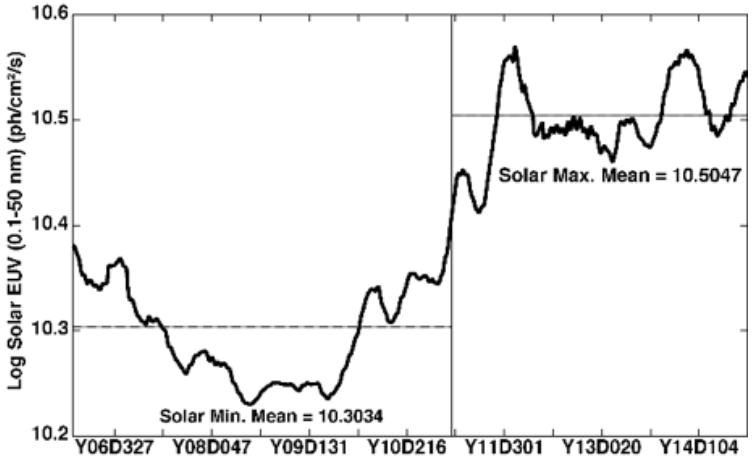

Figure A.10: The solar EUV flux while Venus Express was in orbit. The mission spanned almost a full solar cycle enabling observations during a range of ionospheric conditions. We note the log scale of this plot. The EUV flux varies by almost a factor of two at this wavelength.

et al., 1997) model of electron number density as a function of altitude and solar zenith angle. This model was produced during the PVO era, during stronger solar activity, so we will use the high altitude electron density measurements from both PVO and VEX to calibrate it for recent weak solar cycle. We expect that the resulting calculated electromagnetic energy flux will be accurate to at least a factor of two, affected mainly by the density uncertainty. This will allow us to compare directly with the Earth and its electromagnetic energy flux in the whistler-mode frequency range and to predict the difference in NO_2 production as well.

Venus Express was in orbit for nearly 9 years, the better part of one solar cycle. Figure A.10 shows the variation in solar extreme ultraviolet (EUV) flux throughout the mission. Solar EUV is one of the primary ionizing mechanisms in the Venusian ionosphere. When the solar EUV is high, as it is during solar maximum, the ionosphere is dense and thus able to stave off the interplanetary magnetic field (IMF). When the solar EUV is relatively weak, as it is during solar minimum, the ionosphere is weakly ionized. This enables the IMF to convect at low altitudes and produce a strongly magnetized ionosphere. Because whistler-mode waves are propagate parallel to the field, observations are dependent on the magnetization of the ionosphere. Thus, detection of lightning-generated whistlers will vary throughout the solar cycle. We will determine the strength of that variation and whether or not the changes in EUV have any effect on the location of observations.

A.3.3 Proposed Studies

A.3.3.1 Occurrence Rate Survey

We first geo-locate each observation in latitude, solar longitude, and altitude to determine the statistical behavior of the whistler mode signals as a function of frequency and solar cycle phase. The data includes the vector magnetic field during the interval and the model electron density. There are over 2,000 wave events in the data we have surveyed in the low-altitude ionosphere totaling over 3 hours of cumulative wave activity. Thus, there is much

to be done in this study.

A.3.3.2 Venus Electromagnetic Energy Flux

We use the Pioneer Venus-derived "International Venus Reference Ionosphere" (*Brace et al.*, 1997) with the VEX magnetic field to calculate the electromagnetic energy flux. With this electron density model, we calculate the index of refraction at each frequency at each time step, and we convert the observed magnetic signals to electromagnetic energy densities. We then study these as a function of solar longitude, latitude, and altitude and compare with terrestrial values, such as obtained on the DEMETER spacecraft. Are the energies of these signals comparable to those at Earth? Again, there are over 2,000 events in our catalog.

A.3.3.3 Venus Lightning Source Distributions

Because the structure of Earth's dipole field is well understood, it is possible to trace terrestrial whistlers to the region at which they entered the ionosphere (*Chum et al.*, 2006; *Bortnik et al.*, 2003). In some cases, low latitude observations from the surface can be traced to storms at the conjugate foot points (*Gokani et al.*, 2015). Since Venus does not have an intrinsic dipole field, the temporal variations in its structure are much less predictable. The IMF drapes around Venus like a comet, so any change in the ionospheric field is a direct result of a change in the solar activity.

One advantage of the VEX observations is that they are all at relatively low altitude. Where terrestrial observations can be well into the magnetosphere, those in this study are close to periapsis and below 600 km. In some cases, when the magnetic field is less variable, we are able to trace the field line straight to the base of the ionosphere where the waves would have connected with the magnetic field (Figure A.11). In other cases, where the field is either highly variable or the altitude at which the wave was detected was too great, more assumptions must be made about the structure of the field and we must use a technique

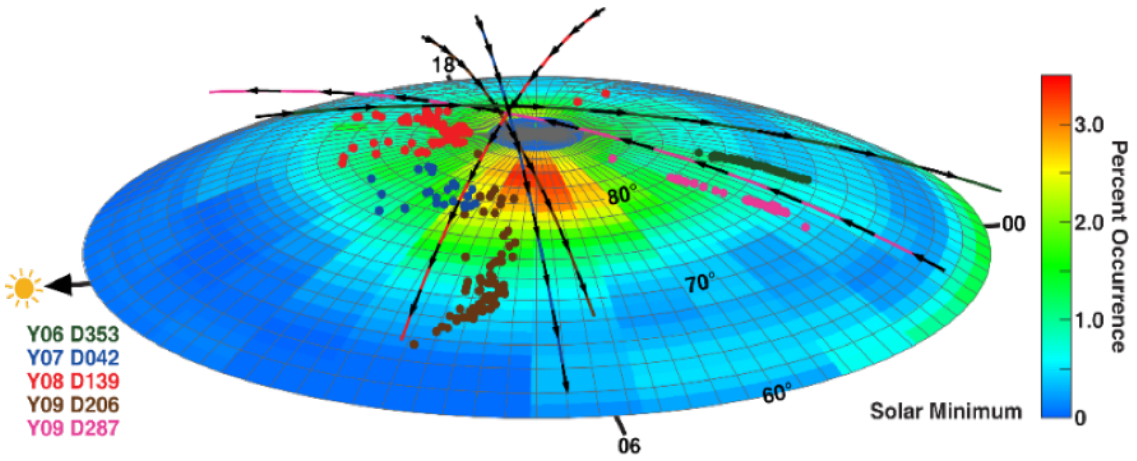

Figure A.11: Tracks of five orbits near periapsis. Dots mark the intersections of straight-line field tracings from a whistler observation to the base of the ionosphere. The surface color is the percent occurrence of signals as a function of local time and latitude.

that does not require a dipolar field, such as that provided by *Kimura et al.* (1985) and *Bortnik et al.* (2003). The code from the latter study can be adapted for use at Venus with a model of the magnetic field (J. Bortnik, personal communication, 2017), such as that developed by (*Ma et al.*, 2013). This model includes solar wind effects, but omits transient events, such as CME's, which would be averaged out in a statistical analysis. Developing the ray tracing code will be left to future work, but this study will still take advantage of the magnetic field model. Instead of a straight-line tracing, as in Figure A.11, we will trace the model field to the base of the ionosphere. We assume that over the tens of seconds for which the waves arrive, the storm has remained stationary and similarly active. The interval of changing spectrum and ultimate disappearance is interpreted as the propagation path to the spacecraft changing, preventing certain frequencies from reaching the spacecraft. We will use the whistler dispersion relation to constrain the source location that could create this pattern of wave amplitudes as a function of frequency and time. In two examples (Figure A.12 and Figure A.13), it is important to note that the narrowing of the spectrum is accompanied by changes in the propagation angle. This suggests that geolocation of the storm is possible,

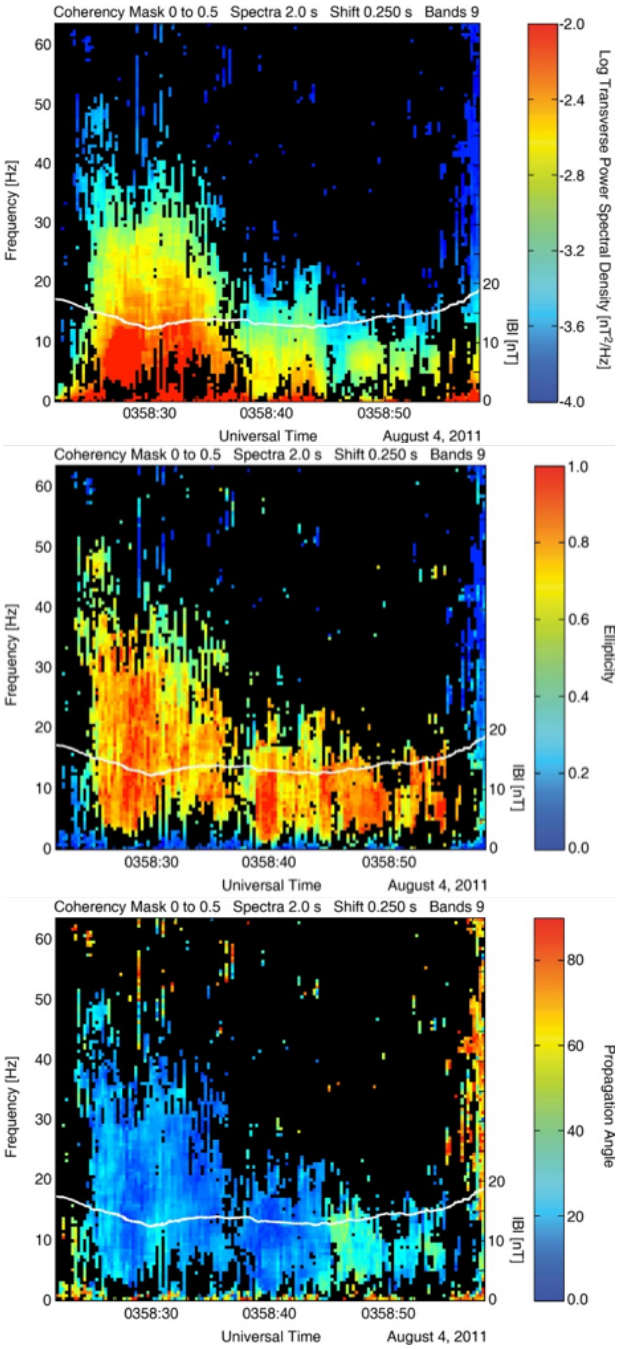

Figure A.12: Transverse power, ellipticity, and propagation angle of ELF waves on August 4, 2011.

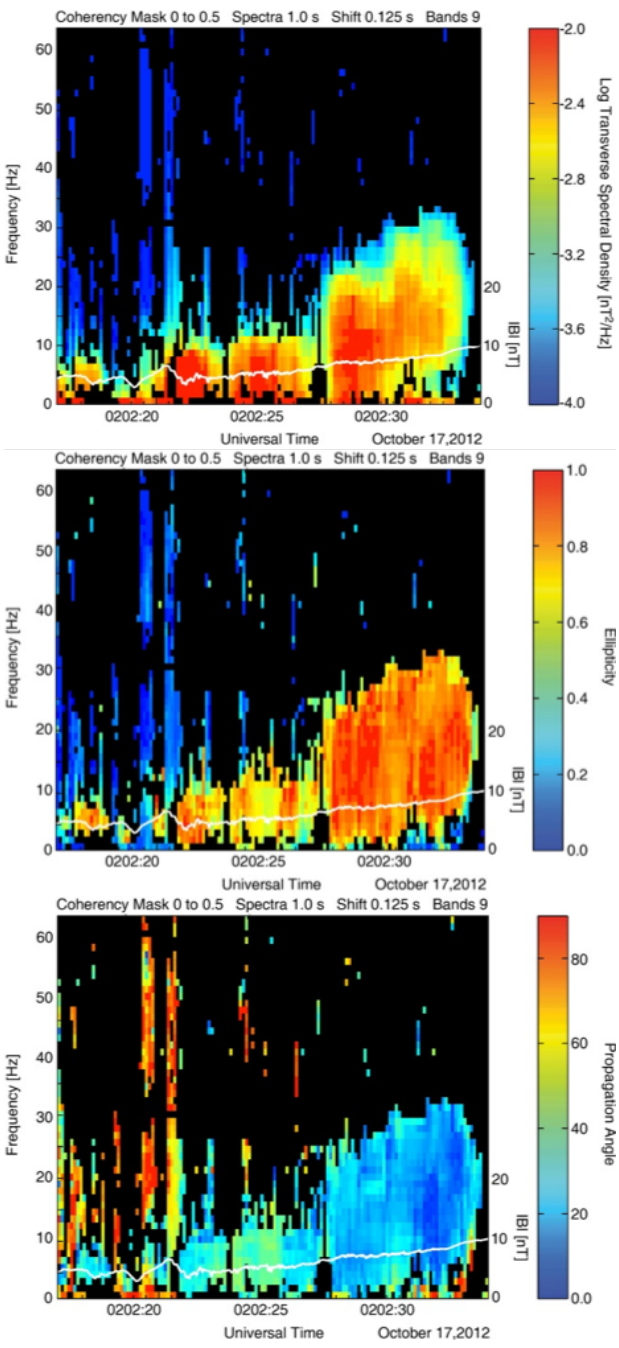

Figure A.13: Transverse power, ellipticity, and propagation angle of ELF waves on October 17, 2012

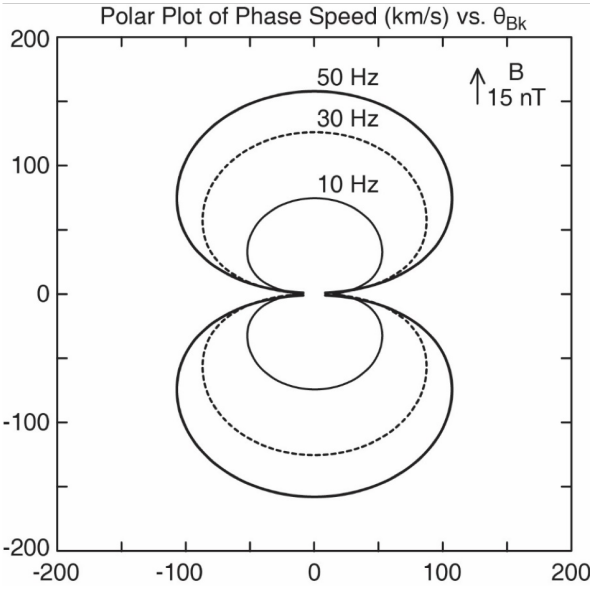

(a) Phase speed of a whister-mode wave.

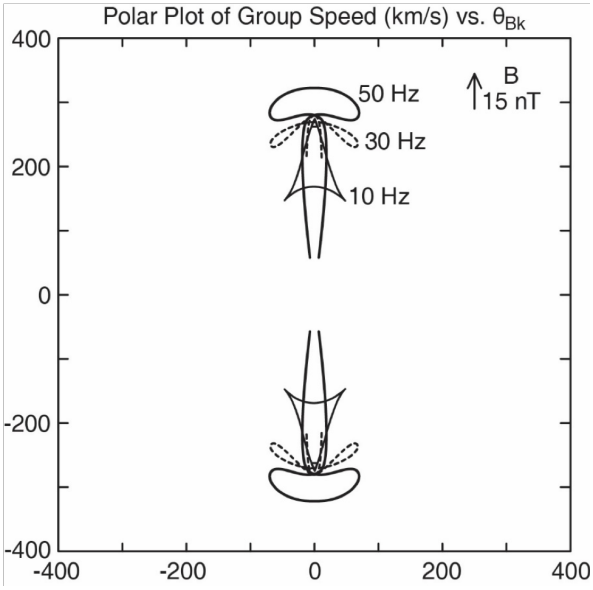

(b) Group speed of a whister-mode wave.

Figure A.14: Polar plots of whistler-mode waves for typical Venus ionospheric conditions (O^+ = 13,500 cm^{-3}; B = 15 nT).

and the evolution of the different wave properties is consistent with passage by a nearby source. This will provide us with enough accuracy for the bin sizes in our statistical study. With a complete set of ionospheric statistics and a corresponding set of whistler origins, we can determine if there is a correlation with geography and/or time or if other atmospheric and external contributors, such as solar EUV, have greater control over lightning production. The comparison of the two sets will also advise us as to whether or not there is an observation bias due to the magnetic field configuration.

Figure A.14a and Figure A.14b show polar plots of the phase speed and the group speed of the whistler-mode waves in typical Venus ionosphere conditions (O^+ = 13,500 cm^{-3}; B = 15 nT). The phase speed is affected by the angle between the propagation vector (**k**) and the magnetic field. The blue color in Figure A.12c and Figure A.13c show that this angle is close to 0° most of the time, but could reach 30° at times (when the bandwidth of the signal narrows). The group speed is the way the energy travels. It is clearly guided by the

magnetic field, so the field direction indicates the direction to the source of the signal. All frequencies are strongly guided by the field but have subtle differences. In our two examples, the event ends when the phase velocity is propagating at a significant angle to the magnetic field.

A.3.3.4 Venus-Earth Comparison

The configurations of the ionosphere magnetic fields are different at Earth and Venus, so the propagation into the ionosphere will differ. We will model the entry of the electromagnetic energy separately into the two ionospheres using the vertical gradient in the index of refraction to calculate the transmitted signal and attempt to compare source strengths in the atmosphere from the energy flux in the ionospheres at the two planets. The well-instrumented DEMETER mission (*Parrot et al.*, 2006) has provided a good comparison set of data for our study.

A.4 Perceived Impact of the Proposed Work on the State of Knowledge

A.4.1 The Venus Express ELF Wave Database

The VEX ELF wave database covers the entire range of altitudes up to the bow shock and was gathered over 9 years. It will be of great value to those studying planetary lightning and those proposing future studies of Venus lightning and atmospheric electricity. It also covers a range of solar activity, over a dozen complete cycles of Venus local time and many phenomena other than lightning-generated signals.

A.4.2 Expected Advance Enabled by this Study

Venus in size and density is close to being Earth's twin, but because it does not have an active magnetic dynamo, there are some differences, such as the lack of a thermosphere and no magnetosphere. These differences affect the ionosphere and upper atmosphere. Currently we do not know the relative strength of the ionospheric heating from the atmosphere and from the sun and solar wind. With the VEX electromagnetic energy flux associated with lightning, we can compare with the earlier Pioneer Venus ionosphere measurements to gauge its ionospheric heating potential relative to other sources. Since lightning produces NO_2 at both planets, comparing the lightning rate is important to understanding the relative amount of NO_2 in the atmosphere.

A.4.3 Impact on the Current State of Knowledge

At present, we poorly understand the lightning process on Venus. This study will provide a basis for determining the ionospheric energy balance associated with lightning activity and provide greater understanding of the nitric oxide production on Venus with lessons for Earth. On Earth, it is now believed (R. Holzworth, personal communication, 2017) that whistler waves in the ionosphere are produced by upward going lightning. If we can find similar evidence in the Venusian ionosphere, it would greatly enhance our understanding of lightning's effect on the ionosphere of both planets.

A.5 Relevance of the Proposed Work to Past, Present and Future NASA Programs

The proposed work enhances our understanding of the Pioneer Venus plasma wave data by providing complementary comprehensive observations of the same phenomena from Venus Express. The PVO plasma wave instrument detected only the one electric component of the

whistler-mode waves in narrow bands at 100 and 700 Hz and only in darkness. The VEX data provide complete coverage of the magnetic oscillations in three components over the entire frequency range from 0 to 64 Hz. This allows calculation of wave power, polarization and direction of propagation (as illustrated in Figure A.6). With a model of the electron density, these measurements can be used to infer the electromagnetic energy flux (from 0 to 64 Hz). While this is an important and large step from the PVO results, VEX covered only the northern polar regions, but complementary to PVO at mid latitudes. Future missions could build on this study in the following ways. A low-altitude mission like the recently proposed VERITAS Discovery mission could use the information provided in this study to design an instrument to map the entire planet and capture the full electromagnetic energy flux in the ELF range and its latitudinal distribution. An atmospheric balloon mission could carry direction finding radio antennas to locate lightning storms based on our estimates of the energy flux (at our lower frequencies). Our estimates may even contribute to understanding the survivability of a balloon in the clouds at different altitudes. The VEGA balloons tested just two altitude and latitude ranges.

A.6 Work Plan, Milestones, Accomplishments

A.6.1 Work Plan

The proposed effort is to form the basis for a dissertation to be written by UCLA EPSS graduate student R.A. Hart, who has assisted with the early phases of this project (see citation *Russell et al.* (2013)), and has set up all the software needed to clean the data, do the wave analysis and interpret the data. The data processing software is in place. He works full-time while pursuing his Ph.D. part-time. If funded, he will be able to complete his degree in the 3 years awarded by this proposal. We envision the following schedule.

First Year:

1. Create an archival data set of all 128 Hz VEX magnetometer data and documentation for use at UCLA and/or for the PSA and PDS archives. Submit the data.

2. Determine the statistical properties of the observed waves. Find the location and duration of each "storm". Calculate model electron densities for all events. Find the average amplitude of the signals as a function of latitude, longitude and altitude in the region covered by VEX. Examine the data for solar cycle and other long-term trends. Write a paper and submit to an appropriate journal.

Second Year:

Use the model densities and the magnetic field strength to convert the wave amplitudes to EM energy flux. Find the statistical properties of the energy flux. Compare with terrestrial estimates. Estimate the production of nitric oxide by lightning at Venus and compare with terrestrial estimates. Compare with Krasnopolsky's data. Write paper and submit to an appropriate journal. Find all events that have potential for geolocating storms. Determine the magnetic and trajectory geometries for these events.

Third Year:

Develop a technique that utilizes a magnetic field model to trace the wave propagation from storms in the atmosphere to VEX in the ionosphere as a function of frequency. Use this program to interpret the dynamic spectra and geo-locate storms responsible for the patterns seen in the dynamic spectra. Write a paper and submit to appropriate journal. Gather results together and write dissertation and/or review paper.

A.6.2 Milestones and Achievements

Year 1.

Submittal of data set to PSA and/or PDS archives. [Target completion, 6 months]

Participate in PDS peer review and resolve any liens that are assigned in that process.

Completion of statistical study. [Target completion, 9 months]

Presentation at DPS meeting or other appropriate venue. [Target completion, 8 months]

Submittal of paper to JGR or other appropriate journal. [Target completion, 12 months]

Year 2.

Test and run electron density model Venus's ionosphere with adjustments for solar conditions. [Target completion, 3 months]

Write paper on nitric oxide production and wave energy fluxes during VEX mission. [Target completion, 7 months]

Submit to appropriate journal, present at appropriate meeting. [Target completion, 8 months]

Year3.

Test and run field-line tracing program. [Target completion, 3 months]

Use program to interpret temporal behavior of waves seen in spectrogram. [Target completion, 6 months]

Write paper, present at meeting, and integrate all results in a dissertation. [Target completion, 12 months]

A.7 Data Management Plan

The proposed effort utilizes data obtained by the Venus Express mission and provided to UCLA by the magnetometer principal investigator, Tielong Zhang, to support the NASA-funded participating scientist investigator, C. T. Russell. These data were submitted to the European Planetary Science Archive (PSA) and are available to all requestors. During the NASA-funded participating scientist investigation, software was developed to improve

the dataset calibration in order to meet the science objectives of the investigation. The participating scientist program ended before the improved data processing was complete. No data were archived with either the PSA or the NASA Planetary Data System (PDS) in the participating scientist activity.

As the first step of this effort, UCLA will produce a PDS4 compliant archive bundle to be archived at the Planetary Plasma Interactions (PPI) node of the PDS (see attached letter from PPI manager R. Walker). The PDS4 archive will consist of data, document, and context (metadata) collections. The data collection will consist of 186 GB of ASCII tables of 128-HZ measurements of the magnetic field. Individual tables contain one day of corrected data created from the two gradiometer sensors on the VEX magnetometer 'boom'. These data have been cleaned of AC noise and an accurate DC value added to the data stream after the AC cleaning. These data can be used by any user without further processing. A complete low resolution dataset is archived in the PSA by the PI, T.L. Zhang. The document collection will contain a single document that briefly describes the instrument, the data processing, and the output format of the data with references to published instrument description and relevant science papers. Data and documentation will be prepared for archive by Richard Hart, the participating graduate student and coordinated with PPI. The effort should take 1 month to generate and iterate with the PPI team prior to PDS peer review. After the review, another one to two weeks of effort may be required to resolve peer review liens to the data or documentation before final archive.[2]

[2]The offset misalignment described in subsubsection 2.2.4.1 was discovered shortly after the start of the SSW grant.

Bibliography

Alexander, R. L., S. O'Modhrain, D. A. Roberts, J. A. Gilbert, and T. H. Zurbuchen (2014). The bird's ear view of space physics: Audification as a tool for the spectral analysis of time series data. *J. Geophys. Res. Space Phys.*, *119*(7), 5259–5271, doi: 10.1002/2014JA020025.

Angelopoulos, V., et al. (2019). The Space Physics Environment Data Analysis System (SPEDAS). *Space. Sci. Rev.*, *215*, 9, doi: 10.1007/s11214-018-0576-4.

Barabash, S., et al. (2007). The Analyser of Space Plasmas and Energetic Atoms (ASPERA-4) for the Venus Express mission. *Planet. Space Sci.*, *55*(12), 1772–1792, doi: 10.1016/j.pss.2007.01.014.

Bauer, S. J., L. M. Brace, H. A. Taylor Jr., T. K. Breus, A. J. Kliore, W. C. Knudsen, A. F. Nagy, C. T. Russell, and N. A. Savich (1985). The Venus ionosphere. *Adv. Space Res.*, *5*(11), 233–267, doi: 10.1016/0273-1177(85)90203-0.

Baum, R. M. (2000). The enigmatic ashen light of Venus: an overview. *J. Br. Astron. Ass*, *110*(6), 325–329.

Bertaux, J. L., et al. (2007). SPICAV on Venus Express: Three spectrometers to study the global structure and composition of the Venus atmosphere. *Planet. Space Sci.*, *55*(12), 1673–1700, doi: 10.1016/j.pss.2007.01.016.

Bortnik, J., U. S. Inan, and T. F. Bell (2003). Frequency-time spectra of magnetospherically

reflecting whistlers in the plasmasphere. *J. Geophys. Res. Space Phys.*, *108*(A1), doi: 10.1029/2002JA009387.

Borucki, W. J., J. W. Dyer, G. Z. Thomas, J. C. Jordan, and D. A. Comstock (1981). Optical search for lightning on Venus. *Geophys. Res. Lett.*, *8*(3), 233–236, doi: 10.1029/GL008i003p00233.

Borucki, W. J., J. W. Dyer, J. R. Phillips, and P. Phan (1991). Pioneer Venus Orbiter search for Venusian lightning. *J. Geophys. Res.*, *96*(A7), 11,033–11,043, doi: 10.1029/91JA01097.

Brace, L. H., H. A. Taylor Jr., T. I. Gombosi, A. J. Kliore, W. C. Knudsen, and A. F. Nagy (1983). The ionosphere of Venus: observations and their interpretation, in *Venus*, edited by D. M. Hunten, L. Colin, T. M. Donahue, and V. I. Moroz, chap. 23, pp. 779–840, University of Arizona Press, Tuscon, AZ.

Brace, L. H., J. M. Grebowsky, and A. J. Kliore (1997). Pioneer Venus Orbiter contributions to a revised Venus reference atmosphere. *Adv. Space Res.*, *19*(8), 1203–1212, doi: 10.1016/S0273-1177(97)00271-8.

Burns, J. A., M. R. Showalter, J. N. Cuzzi, and R. H. Durisen (1983). Saturn's electrostatic discharges: Could lightning be the cause? *Icarus*, *54*(2), 280–295, doi: 10.1016/0019-1035(83)90198-7.

Cardesín Moinelo, A., S. Abildgaard, A. García Muñoz, G.Piccioni, and D. Grassi (2016). No statistical evidence of lightning in Venus night-side atmosphere from VIRTIS-Venus Express Visible observations. *Icarus*, *277*, 395–400, doi: 10.1016/j.icarus.2016.05.027.

Christian, H. J., R. J. Blakeslee, D. J. Boccippio, W. L. Boeck, D. E. Buechler, K. T. Driscoll, S. J. Goodman, J. M. Hall, W. J. Koshak, D. M. Mach, and M. F. Stewart (2003). Global frequency and distribution of lightning as observed from space by the Optical Transient Detector. *J. Geophys. Res.*, *108*(D1), 4005, doi: 10.1029/2002JD002347.

Chum, J., F. Jiricek, O. Santolik, M. Parrot, G. Diendorfer, and J. Fiser (2006). Assigning the causative lightning to the whistlers observed on satellites. *Ann. Geophys.*, *24*, 2921–2929, doi: 10.5194/angeo-24-2921-2006.

Colin, L. and D. M. Hunten (1977). Pioneer Venus experiment descriptions. *Space. Sci. Rev.*, *20*(4), 451–525, doi: 10.1007/BF02186463.

Connerney, J. E. P., J. Espley, P. Lawton, S. Murphy, J. Odom, R. Oliversen, and D. Sheppard (2015). The MAVEN Magnetic Field Investigation. *Space. Sci. Rev.*, *195*, 257–291, doi: 10.1007/s11214-015-0169-4.

Connerney, J. E. P., M. H. Acuña, P. J. Wasilewski, N. F. Ness, H. Rème, C. Mazelle, D. Vignes, R. P. Lin, D. L. Mitchell, and P. A. Cloutier (1999). Magnetic Lineations in the Ancient Crust of Mars. *Science*, *284*(5415), 794–798, doi: 10.1126/science.284.5415.794.

Cook II, A. F., T. C. Duxbury, and G. E. Hunt (1979). First results on Jovian lightning. *Nature*, *280*, 794, doi: 10.1038/280794a0.

Croft, T. A. and G. H. Price (1983). Evidence for a low-altitude origin of lightning on Venus. *Icarus*, *53*(3), 548—551, doi: 10.1016/0019-1035(83)90215-4.

de Bergh, C., V. I. Moroz, F. W. Taylor, D. Crisp, B. Bézard, and L. V. Zasova (2006). The composition of the atmosphere of Venus below 100 km altitude: An overview. *Planet. Space Sci.*, *54*(13–14), 1389–1397, doi: 10.1016/j.pss.2006.04.020.

Dubinin, E., M. Fraenz, T. L. Zhang, J. Woch, and Y. Wei (2014). Magnetic fields in the Venus ionosphere: Dependence on the IMF direction: Venus express observations. *J. Geophys. Res. Space Phys.*, *119*(9), 7587–7600, doi: 10.1002/2014JA020195.

Dwyer, J. R. and M. A. Uman (2014). The physics of lightning. *Phys. Rep.*, *534*(4), 147–241, doi: 10.1016/j.physrep.2013.09.004.

Dyudina, U. A., A. P. Ingersoll, S. P. Ewald, C. C. Porco, G. Fischer, W. S. Kurth, and R. A. West (2010). Detection of visible lightning on Saturn. *Geophys. Res. Lett.*, *37*(9), L09,205, doi: 10.1029/2010GL043188.

Esposito, L. W., R. G. Knollenberg, M. Ya. Marov, O. B. Toon, and R. P. Turco (1983). The clouds and hazes of Venus, in *Venus*, edited by D. M. Hunten, L. Colin, T. M. Donahue, and V. I. Moroz, chap. 16, pp. 484–564, University of Arizona Press, Tuscon, AZ.

Firsoff, V. A., *The Interior Planets*, Oliver and Boyd, Edinburgh, (1968).

Formisano, V., et al. (2007). PFS: The Planetary Fourier Spectrometer. *ESA Special Publication*, *SP 1295*, 1–33.

Fukuhara, T., M. Futaguchi, G. Hashimoto, T. Horinouchi, T. Imamura, N. Iwagaimi, T. Kouyama, S. Y. Murakami, M. Nakamura, K. Ogohara, M. Sato, T. M. Sato, M. Suzuki, M. Taguchi, S. Takagi, M. Ueno, S. Watanabe, M. Yamada, and A. Yamazaki (2017). Large stationary gravity wave in the atmosphere of Venus. *Nature Geosci.*, *10*, 85–88, doi: 10.1038/ngeo2873.

Gokani, S. A., R. Singh, M. B. Cohen, S. Kumar, K. Venkatesham, A. K. Maurya, R. Selvakumaran, and J. Lichtenberger (2015). Very low latitude (L = 1.08) whistlers and correlation with lightning activity. *J. Geophys. Res. Space Phys.*, *120*(8), 6694–6706, doi: 10.1002/2015JA021058.

Goody, R. and T. McCord (1968). Continued search for the Venus airglow. *Planet. Space Sci.*, *16*(3), 343–351, doi: 10.1016/0032-0633(68)90008-1.

Grebowsky, J. M., R. J. Strangeway, and D. M. Hunten (1997). Evidence for venus lightning, in *Venus II: Geology, Geophysics, Atmosphere, and Solar Wind Environment*, edited by S. W. Bougher, D. M. Hunten, and R.J. Phillips, pp. 125–157, University of Arizona Press, Tuscon, AZ.

Grimm, R. E., A. C. Barr, K. P. Harrison, D. E. Stillman, K. L. Neal, M. A. Vincent, and G. T. Delory (2012). Aerial electromagnetic sounding of the lithosphere of Venus. *Icarus*, *217*(2), 462–473, doi: 10.1016/j.icarus.2011.07.021.

Gurnett, D. A., W. S. Kurth, I. H. Cairnsa, and L. J. Granroth (1990). Whistlers in Neptune's magnetosphere: Evidence of atmospheric lightning. *J. Geophys. Res. Space Phys.*, *95*(A12), 20,967–20,976, doi: 10.1029/JA095iA12p20967.

Gurnett, D. A., W. S. Kurth, A. Roux, R. Gendrin, C. F. Kennel, and S. J. Bolton (1991). Lightning and plasma wave observations from the Galileo fly-by of Venus. *Science*, *253*, 1522–1525, doi: 10.1126/science.253.5027.1522.

Gurnett, D. A., P. Zarka, R. Manning, W. S. Kurth, G. B. Hospodarsky, T. F. Averkamp, M. L. Kaiser, and W. M. Farrell (2001). Non-detection at Venus of high-frequency radio signals characteristic of terrestrial lightning. *Nature*, *409*, 313–315, doi: 10.1038/35053009.

Gurnett, D. A., et al. (2004). The Cassini Radio and Plasma Wave Investigation. *Space. Sci. Rev.*, *114*, 395–463, doi: 10.1007/s11214-004-1434-0.

Hansell, S. A., W. K. Wells, and D. M. Hunten (1995). Optical detection of lightning on Venus. *Icarus*, *117*(2), 345–351, doi: 10.1006/icar.1995.1160.

Hart, R. A., C. T. Russell, and T. L. Zhang (2022). Statistical study of lightning-generated whistler-mode waves observed by Venus Express. *Icarus, accepted*.

Häusler, B., M. Pätzold, G. L. Tyler, R. A. Simpson, M. K. Bird, V. Dehant, J. P. Barriot, W. Eidel, R. Mattei, S. Remus, J. Selle, S. Tellmann, and T. Imamura (2006). Radio science investigations by VeRa onboard the Venus Express spacecraft. *Planet. Space Sci.*, *54*(13–14), 1315–1335, doi: 10.1016/j.pss.2006.04.032.

Helliwell, R. A., *Whistlers and Related Ionospheric Phenomena*, Stanford University Press, Stanford, CA, (1965).

Jakosky, B. M., et al. (2015). The Mars Atmosphere and Volatile Evolution (MAVEN) Mission. *Space. Sci. Rev.*, *195*, 3–45, doi: 10.1007/s11214-015-0139-x.

Kimura, I., T. Matsuo, M. Tsuda, and K. Yamauchi (1985). Three Dimensional Ray Tracing of Whistler Mode Waves in a Non-Dipolar Magnetosphere. *J. Geomag. Geoelectr.*, *37*(10), 945–956, doi: 10.5636/jgg.37.945.

Kolmašová, I., M. Imai, O. Santolík, W. S. Kurth, G. B. Hospodarsky, D. A. Gurnett, J. E. P. Connerney, and S. J. Bolton (2018). Discovery of rapid whistlers close to Jupiter implying lightning rates similar to those on Earth. *Nat. Astron.*, *2*, 544–548, doi: 10.1038/s41550-018-0442-z.

Kopparapu, R. K., R. Ramirez, J. F. Kasting, V. Eymet, T. D. Robinson, S. Mahadevan, R. C. Terrien, S. Domagal-Goldman, V. Meadows, and R. Deshpande (2013). Habital zones around main-sequence stars: new estimates. *ApJ*, *765*(131), 16, doi: 10.1088/0004-637X/765/2/131.

Krasnopolsky, V. A. (1980). Lightning on Venus according to information obtained by the satellites Venera 9 and 10. *Kosm. Issled.*, *18*, 429–434.

Krasnopolsky, V. A. (1983a). Lightning and nitric oxide on Venus. *Planet. Space Sci.*, *31*(11), 1363–1369, doi: 10.1016/0032-0633(83)90072-7.

Krasnopolsky, V. A. (1983b). Venus spectroscopy in the 3000-8000 Å region by Veneras 9 and 10, in *Venus*, edited by D. M. Hunten, L. Colin, T. M. Donahue, and V. I. Moroz, chap. 15, pp. 459–483, University of Arizona Press, Tuscon, AZ.

Krasnopolsky, V. A. (2006). A sensitive search for nitric oxide in the lower atmosphere of Venus and Mars: detection on Venus and upper limit for Mars. *Icarus*, *182*(1), 80–91, doi: 10.1016/j.icarus.2005.12.003.

Ksanfomaliti, L. V. (1979). Lightning in the cloud layer of Venus. *Kosm. Issled.*, *17*, 747–762.

Ksanfomaliti, L. V. (1980). Discovery of frequent lightning discharges in clouds on Venus. *Nature*, *284*(5753), 244–246.

Ksanfomaliti, L. V., N. M. Vasilchikov, O. F. Ganpantserova, E. V. Petrovaand A. P. Suvorova, G. F. Filippov, O. V. Yablonskaya, and L. V. Yabrova (1979). Electrical discharges in the atmosphere of Venus. *Sov. Astron Lett.*, *5*(3), 122–126.

Ksanfomaliti, L. V., N. M. Vasilchikov, N. V. Goroshkova, E. V. Petrova, A. P. Suvorov, and V. K. Khondyrev (1982). The low-frequency electromagnetic field in the Venus atmosphere: evidence from Venera 13 and Venera 14. *Sov. Astron. Lett.*, *8*(4), 230–232.

Ksanfomaliti, L. V., F. L. Scarf, and W. W. L. Taylor (1983). The electrical activity of the atmosphere of venus, in *Venus*, edited by D. M. Hunten, L. Colin, T. M. Donahue, and V. I. Moroz, chap. 17, pp. 565–603, University of Arizona Press, Tuscon, AZ.

Lawrence, M. G., W. L. Chameides, P. S. Kasibhatla, H. Levy II, and W. Moxim (1995). Lightning and Atmospheric Chemistry: The Rate of Atmospheric NO Production, in *Handbook of Atmospheric Electrodynamics*, vol. 1, edited by H. Volland, chap. 8, pp. 189–202, CRC Press, Boca Raton, FL, doi: 10.1201/9780203719503.

Lebonnois, S. and G. Schubert (2017). The deep atmosphere of Venus and the possible role of density-driven separation of CO2 and N2. *Nature Geosci.*, *10*, 473–477, doi: 10.1038/ngeo2971.

Leinweber, H. K., C. T. Russell, K. Torkar, T. L. Zhang, and V. Angelopoulos (2008). An advanced approach to finding magnetometer zero levels in the interplanetary magnetic field. *Meas. Sci. Technol*, *19*(5), doi: 10.1088/0957-0233/19/5/055104.

Levin, Z., W. J. Borucki, and O. B. Toon (1983). Lightning generation in planetary atmospheres. *Icarus*, *56*(1), 80–115, doi: 10.1016/0019-1035(83)90129-X.

Levine, J. S. (1968). On the occurrence of the Ashen Light on Venus. *Planet. Space Sci.*, *16*(11), 1417–1418, doi: 10.1016/0032-0633(68)90145-1.

Lorenz, R. D. (2018). Lightning detection on Venus: a critical review. *Prog. Earth Planet. Sci.*, *5*(34), doi: 10.1186/s40645-018-0181-x.

Lorenz, R. D., M. Imai, Y. Takahashi, M. Sato, A. Yamazaki, T. M. Sato, T. Imamura, T. Satoh, and M. Nakamura (2019). Constraints on Venus Lightning From Akatsuki's First 3 Years in Orbit. *Geophys. Res. Lett.*, *46*(14), 7955–7961, doi: 10.1029/2019GL083311.

Luhmann, J. G. (1986). The solar wind interaction with Venus. *Space. Sci. Rev.*, *44*, 241–306, doi: 10.1007/BF00200818.

Luhmann, J. G. and T. E. Cravens (1991). Magnetic fields in the ionosphere of Venus. *Space. Sci. Rev.*, *55*, 201–274, doi: 10.1007/BF00177138.

Luhmann, J. G. and C. T. Russell (1983). Magnetic fields in the ionospheric holes of Venus: Evidence for an intrinsic field? *Geophys. Res. Lett.*, *10*(5), 409–411, doi: 10.1029/GL010i005p00409.

Luhmann, J. G., Y. J. Ma, M. N. Villarreal, H. Y. Wei, and T. L. Zhang (2015). The Venus-solar wind interaction: Is it purely ionospheric? *Planet. Space Sci.*, *119*, 36–42, doi: 10.1016/j.pss.2015.09.012.

Ma, Y. J., A. F. Nagy, C. T. Russell, R. J. Strangeway, H. Y. Wei, and G. Toth (2013). A global multispecies single-fluid MHD study of the plasma interaction around Venus. *J. Geophys. Res. Space Phys.*, *118*(1), 321–330, doi: 10.1029/2012JA018265.

Markiewicz, W. J., et al. (2007). Venus Monitoring Camera for Venus Express. *Planet. Space Sci.*, *55*(12), 1701–1711, doi: 10.1016/j.pss.2007.01.004.

McGouldrick, K., O. B. Toon, and D. H. Grinspoon (2011). Sulfuric acid aerosols in the atmospheres of the terrestrial planets. *Planet. Space Sci.*, *59*(10), 934–941, doi: 10.1016/j.pss.2010.05.020.

McKim, R. J. and R. A. Moore (2007). The Ashen Light of Venus: A century of observations by McEwen and Moore. *J. Br. Astron. Ass*, *117*(5), 265–272.

Means, J. D. (1972). Use of three dimensional covariance matrix in analyzing the polarization properties of plane waves. *J. Geophys. Res.*, *77*(28), 5551–5559, doi: 10.1029/JA077i028p05551.

Meinel, A. B. and D. T. Hoxie (1962). On the spectrum of lightning in the Venus atmosphere. *Comm. Lunar Planet. Lab*, *1*(7), 35–38.

Moore, P., *The Planet Venus*, p. 84, Faber and Faber, London, UK, (1957).

Niemann, H. B., W. T. Kasprzak, A. E. Hedin, D. M. Hunten, and N. W. Spencer (1980). Mass spectrometric measurements of the neutral gas composition in the thermosphere and exosphere of Venus. *J. Geophys. Res.*, *85*(A13), 7817–7827, doi: 10.1029/JA085iA13p07817.

O'Rourke, J. G., J. Buz, R. R. Fu, and R. J. Lillis (2019). Detectability of Remanent Magnetism in the Crust of Venus. *Geophys. Res. Lett.*, *46*(11), 5768–5777, doi: 10.1029/2019GL082725.

Parrot, M., D. Benoist, J. J. Berthelier, J. Błecki, Y. Chapuis, F. Colin, F. Elie, P. Fergeau, D. Lagoutte, F. Lefeuvre, C. Legendre, M. Lévêque, J. L.Pinçon, B. Poirier, H. C.Seran, and P. Zamora (2006). The magnetic field experiment IMSC and its data processing onboard DEMETER- Scientific objectives, description and first results. *Planet. Space Sci.*, *54*(5), 441–455, doi: 10.1016/j.pss.2005.10.015.

Pasko, V. P. (2003). Electric Jets. *Nature*, *423*, 927–928, doi: 10.1038/423927a.

Pérez-Invernón, F. J., N. G. Lehtinen, F. J. Gordillo-Vzáquez, and A. Luque (2017). Whistler wave propagation through the ionosphere of Venus. *J. Geophys. Res. Space Phys.*, *122*(11), 11,633–11,644, doi: 10.1002/2017JA024504.

Piccioni, G., et al. (2007). Virtis: The visible and infrared thermal imaging spectrometer. *ESA Special Publication*, *SP 1295*, 1–27.

Rakov, V. A. and M. A. Uman, *Lightning physics and effects*, Cambridge University Press, Cambridge, doi: 10.1017/CBO9781107340886, (2003).

Rinnert, K. (1995). Lightning within planetary atmospheres, in *Handbook of Atmospheric Electrodynamics*, vol. 1, edited by H. Volland, chap. 9, pp. 203–233, CRC Press, Boca Raton, FL, doi: 10.1201/9780203719503.

Robledo-Martinez, A., H. Sobral, and A. Ruiz-Meza (2011). Space charge effects and arc properties of simulated lightning on Venus. *J. Geophys. Res.*, *116*(A6), A06,313, doi: 10.1029/2010JA015856.

Rodrigues, O. (1840). Des lois géométriques qui régissent les déplacements d'un système solide dans l'espace, et de la variation des coordonnées provenant de ces déplacements considérés indépendamment des causes qui peuvent les produire. *J. Math. Pures Appl.*, pp. 380–440.

Ruf, C., N. O. Renno, J. F. Kok, E. Bandelier, M. J. Sander, S. Gross, L. Skjerve, and B. Cantor (2009). Emission of non-thermal microwave radiation by a Martian dust storm. *Geophys. Res. Lett.*, *13*(13), L13,202, doi: 10.1029/2009GL038715.

Russell, C. T. (1991). Venus Lightning. *Space. Sci. Rev.*, *21*(1), 317–356, doi: 10.1007/BF00177140.

Russell, C. T. (1993). Planetary Lightning. *Annu. Rev. Earth Pl. Sc.*, *21*(1), 43–87, doi: 10.1146/annurev.ea.21.050193.000355.

Russell, C. T. and O. L. Vaisberg (1983). The interaction of the solar wind with Venus, in *Venus*, edited by D. M. Hunten, L. Colin, T. M. Donahue, and V. I. Moroz, chap. 25, pp. 873–940, University of Arizona Press, Tuscon, AZ.

Russell, C. T., M. von Dornum, and F. L. Scarf (1988a). The altitude distribution of impulsive signals in the night ionosphere of Venus. *J. Geophys. Res. Space Phys.*, *93*(A6), 5915–5921, doi: 10.1029/JA093iA06p05915.

Russell, C. T., M. Von Dornum, and F. L. Scarf (1988b). VLF bursts in the night ionosphere of Venus: Effects of the magnetic field. *Planet. Space Sci.*, *36*(11), 1211–1218, doi: 10.1016/0032-0633(88)90074-8.

Russell, C. T., M. von Dornum, and F. L. Scarf (1989a). Source locations for impulsive electric signals seen in the night ionosphere of Venus. *Icarus*, *80*(2), 390–415, doi: 10.1016/0019-1035(89)90148-6.

Russell, C. T., M. von Dornum, and R. J. Strangeway (1989b). VLF bursts in the night ionosphere of Venus: Estimates of the Poynting flux. *Geophys. Res. Lett.*, *16*(6), 579–582, doi: 10.1029/GL016i006p00579.

Russell, C. T., M. von Dornum, and F. L. Scarf (1990). The Ashen Light. *Adv. Space Res.*, *10*(5), 137–140, doi: 10.1016/0273-1177(90)90174-X.

Russell, C. T., T. L. Zhang, and H. Y. Wei (2008). Whistler mode waves from lightning on Venus: Magnetic control of ionospheric access. *J. Geophys. Res. Planets*, *113*(E5), doi: 10.1029/2008JE003137.

Russell, C. T., H. K. Leinweber, R. A. Hart, H. Y. Wei, R. J. Strangeway, and T. L. Zhang (2013). Venus Express observations of ULF and ELF waves in the Venus ionosphere: Wave properties and sources. *Icarus*, *226*(2), 1527–1537, doi: 10.1016/j.icarus.2013.08.019.

Russell, C. T., J. G. Luhmann, and R. J. Strangeway, *Space Physics: An Introduction*, Cambridge University Press, Cambridge, (2016).

Russell, C. T., R. A. Hart, and T. L. Zhang (2022). Venus Express Cleaned High-Resolution 128 Hz Magnetic Field Data Bundle. *PDS Planetary Plasma Interactions Node*, doi: 10.17189/1522415.

Sagdeev, R. Z., V. M. Linkin, R. S. Kremnev, J. E. Blamont, R. A. Preston, and A. S. Selivanov (1986). The Vega balloon experiments. *Science*, *231*(4744), 1407–1408, doi: 10.1126/science.231.4744.1407.

Scarf, F. L. and C. T. Russell (1983). Lightning measurements from the Pioneer Venus Orbiter. *Geophys. Res. Lett.*, *10*(12), 1192–1195, doi: 10.1029/GL010i012p01192.

Scarf, F. L. and C. T. Russell (1988). Evidence of Lightning and Volcanic Activity on Venus: Pro and Con. *Science*, *240*(4849), 222–224, doi: 10.1126/science.240.4849.222.

Scarf, F. L., W. W. L. Taylor, C. T. Russell, and L. H. Brace (1980a). Lightning on Venus: Orbiter detection of whistler signals. *J. Geophys. Res.*, *85*(A13), 8158–8166, doi: 10.1029/Ja085ia13p08158.

Scarf, F. L., W. W. L. Taylor, and P. F. Virobik (1980b). The Pioneer Venus Orbiter Plasma Wave Investigation. *IEEE Trans. Geosci. Remote Sens.*, *GE-18*(1), 36–38, doi: 10.1109/TGRS.1980.350257.

Simões, F., R. Grard, M. Hamelin, J. J. López-Moreno, K. Schwingenschuh, C. Béghin, J. J. Berthelier, J. P. Lebreton, G. J. Molina-Cuberos, and T. Tokanog (2008). The Schumann resonance: A tool for exploring the atmospheric environment and the subsurface of the planets and their satellites. *Icarus*, *194*(1), 30–41, doi: 10.1016/j.icarus.2007.09.020.

Singh, R. N. and C. T. Russell (1986). Further evidence for lightning on Venus. *Geophys. Res. Lett.*, *13*(10), 1051–1054, doi: 10.1029/GL013i010p01051.

Stix, T. H., *Waves in Plasmas*, American Inst. of Physics, (1992).

Takahashi, Y., J. Yoshida, Y. Yair, T. Imamura, and M. Nakamura (2008). Lightning Detection by LAC Onboard the Japanese Venus Climate Orbiter, Planet-C. *Space. Sci. Rev.*, *137*, 317–334, doi: 10.1007/s11214-008-9400-x.

Takahashi, Y., M. Imai, M. Sato, R. D. Lorenz, M. Nakamura, T. Satoh, A. Yamazaki, T. Sato, T. Imamura, Y. Yair, K. Aplin, G. Fischer, and J. Yoshida (2021). An optical flash on Venus detected by the AKATSUKI spacecraft. *PREPRINT (Version 1) available at Research Square*, doi: 10.21203/rs.3.rs-379882/v1.

Taylor, F. W. (2006). Venus before Venus Express. *Planet. Space Sci.*, *54*(13–14), 1249–1262, doi: 10.1016/j.pss.2006.04.031.

Taylor, F. W., D. Crisp, and B. Bézard (1997). Near-Infrared Sounding of the Lower Atmosphere of Venus, in *Venus II: Geology, Geophysics, Atmosphere, and Solar Wind Environment*, edited by S. W. Bougher, D. M. Hunten, and R.J. Phillips, pp. 325–351, University of Arizona Press, Tuscon, AZ.

Taylor, W. W. L., F. L. Scarf, C. T. Russell, and L. H. Brace (1979). Evidence for lightning on Venus. *Nature*, *279*, 614–616, doi: 10.1038/279614a0.

Taylor Jr., H. A., H. C. Brinton, S. J. Bauer, R. E. Hartle, P. A. Cloutier, and R. E. Daniell Jr. (1980). Global observations of the composition and dynamics of the ionosphere of Venus: Implications for the solar wind interaction. *J. Geophys. Res.*, *85*(A13), 7765–7777, doi: 10.1029/JA085iA13p07765.

Taylor Jr., H. A., J. M. Grebowsky, and P. A. Cloutier (1985). Venus nightside ionospheric troughs: Implications for evidence of lightning and volcanism. *J. Geophys. Res. Space Phys.*, *90*(A8), 7415–7426, doi: 10.1029/JA090iA08p07415.

Titov, D. V., et al. (2006). Venus Express: Scientific goals, instrumentation, and scenario of the mission. *Cosmic Res.*, *44*, 334–348, doi: 10.1134/S0010952506040071.

Villarreal, M. N., C. T. Russell, H. Y. Wei, Y. J. Ma, J. G. Luhmann, R. J. Strangeway, and T. L. Zhang (2015). Characterizing the low altitude magnetic belt at Venus: Complementary observations from the Pioneer Venus Orbiter and Venus Express. *J. Geophys. Res. Space Phys.*, *120*(3), 2232–2240, doi: 10.1002/2014JA020853.

von Zahn, U., S. Kumar, H. Niemann, and R. Prinn (1983). Composition of the Venus atmosphere, in *Venus*, edited by D. M. Hunten, L. Colin, T. M. Donahue, and V. I. Moroz, chap. 13, pp. 299–430, University of Arizona Press, Tuscon, AZ.

Zarka, P. and B. M. Pedersen (1986). Radio detection of uranian lightning by Voyager 2. *Nature*, *323*, 605–608, doi: 10.1038/323605a0.

Zhang, T. L., et al. (2006). Magnetic field investigation of the Venus plasma environment: Expected new results from Venus Express. *Planet. Space Sci.*, *54*(13), 1336–1343, doi: 10.1016/j.pss.2006.04.018.

Zhang, T.L., et al. (2007). MAG: The Fluxgate Magnetometer of Venus Express. *ESA Special Publication*, *SP 1295*, 1–10.